

Archive ouverte UNIGE

https://archive-ouverte.unige.ch

Thèse 2017

Open Access

This version of the publication is provided by the author(s) and made available in accordance with the copyright holder(s).

Probing and modelling membrane tension in the context of ESCRT-III regulation

Molinard, Guillaume

How to cite

MOLINARD, Guillaume. Probing and modelling membrane tension in the context of ESCRT-III regulation. Doctoral Thesis, 2017. doi: 10.13097/archive-ouverte/unige:104617

This publication URL: https://archive-ouverte.unige.ch/unige:104617

Publication DOI: <u>10.13097/archive-ouverte/unige:104617</u>

© This document is protected by copyright. Please refer to copyright holder(s) for terms of use.

Probing and modelling membrane tension in the context of ESCRT-III regulation

A DISSERTATION PRESENTED

BY

GUILLAUME MOLINARD

TO

THE DEPARTMENT OF BIOCHEMISTRY

IN PARTIAL FULFILLMENT OF THE REQUIREMENTS

FOR THE DEGREE OF

DOCTOR OF PHILOSOPHY

IN THE SUBJECT OF

BIOCHEMISTRY

University of Geneva Switzerland January 2017 Probing and modelling membrane tension in the context of ESCRT-III regulation

ABSTRACT

A living cell is defined by its separation from the exterior medium. Lipid and proteins form this semipermeable barrier. This boundary is important for the cell to protect itself against biotic or abiotic
stresses, and to regulate exchanges with its environment. However, this membrane, even though fairly
resistant mechanically, is prone to breaking under osmotic stress, which can lead to a damaging stretch
of the membrane. In resting conditions, a cell actively maintains an osmotic pressure differential,
through active regulation of the cytoskeleton, membrane trafficking and ionic channels. Those long
terms (minute-hours) processes have been studied in detail in the previous decades but cannot however account for the short term (second-minute) response to acute osmotic shocks, and thus the processes by which cells cope up with osmotic shock remains elusive. How do cells react immediately to
osmotic stresses before its machinery tries to counter act it?

Osmotic shocks affect 3 essential cell parameters: cell volume, cell area and cell shape. The area changes are the most damaging ones to the cell, as they cause changes of membrane tension which can cause lysis. Membrane tension (σ) is the repelling force created by the stretching of a surface. It scales as the force normalized by the characteristic length (L), typically the edge of the membrane.

This tension constrains the cell to adopt a shape with the least surface area possible. Several assays have been used in order to change membrane tension in cell, from pipette aspiration to cytoskeleton depolymerisation. In this study osmotic shocks were performed while measuring volume, area and membrane tension changes. A linear dependency between the tension and the area, a minimal volume and a linear relationship in between osmolarity changes and volume were observed

This multi-parameter approach allowed us to propose a model to unify and predict a difficult to access variable (σ) through different parameter that are easier to access (Osmotic pressure).

ESCRT-III complex is a multimeric membrane remodelling protein assembly. It acts in membrane scission during HIV budding, ILV formation, abscission. It also participates roles in plasma membrane repair and nuclear membrane sealing. Being a membrane remodeling protein complex, there is a high probability and indirect evidence of its activity being regulated by membrane tension. Probing direct evidence of its reaction to changing (σ) will help us to discriminate between several theoretical models of action. Membrane fission during abscission by ESCRT-III was chosen as the micron-size assembly of the event is accessible by light microscopy and several biochemical components and timing are known.

In this thesis I will describe direct evidence of ESCRT-III activation upon osmotic shocks during abscission and its relation to the cytoskeleton. Those experiments will add on the knowledge of ESCRT field and act as a premise for a better understanding of membrane tension during cytokinesis.

The ultimate part of this work will discuss the results and potential criticism of the methods and conclusion.

Thesis advisor: Aurélien ROUX Guillaume Molinard

Une cellule vivante est définie par son isolation du milieu extérieur. Cette membrane semi-perméable est formée de lipides et protéines. Cette barrière est importante pour la protection de la cellule contre des stress biotique et abiotique ainsi que pour la régulation de ces échanges avec environnement. Bien que cette membrane soit mécaniquement résistante, elle peut se casser sous la contrainte de stress osmotiques. En condition nominale, une cellule maintient de façon active une différence de pression osmotique via une régulation du cytosquelette, un trafic membranaire ainsi que des canaux ioniques. Bien que ces processus au long terme (minutes-heures) ont été étudié en détail dans les décennies précédentes, ils ne peuvent pas être impliqué dans la réponse à court terme (secondes-minutes) à des chocs osmotiques aigus. Ainsi les mécanismes par lesquels la cellule réagit à des chocs osmotiques restent imprécis. Comment la cellule réagit de façon passive à un choc osmotique avant que sa machinerie interne essaye de la contrer ?

Les chocs osmotiques affectent 3 paramètres essentiel de la cellule: le volume cellulaire, la surface cellulaire ainsi que la forme cellulaire. Les changements de surface sont les plus dommageables à la cellule car ils induisent un changement de tension qui peut aboutir à la lyse de la cellule. La tension de membrane (σ) est la force de rappel crée par l'étirement de la surface. Cela évolue avec la force normalisé par la longueur caractéristique (L).

Cette tension contraint la cellule à adopter une forme avec le moins de surface possible. Plusieurs expériences ont été crée afin de perturber la tension de membrane cellulaire: de l'aspiration par micropipette à l'application de drogues dépolymérisant le cytosquelette. Dans cette étude, les chocs osmotiques ont été accomplis tout en mesurant les changements de volume, surface ainsi que la tension de membrane. Une relation linéaire entre la tension et l'aire, un volume minimal ainsi qu'une relation linéaire entre le changement d'osmolarité et le volume ont été observé.

Cette approche multiparamétrique permet de proposer un modèle afin de prédire une variable dif-

ficile d'accès (σ) à travers des variables plus facile d'accès (pression osmotique).

Le complexe d'ESCRT-III est un multimère de protéine permettant le réarrangement de la membrane. Il agit sur la fission de membrane durant le bourgeonnement du VIH, la formation des vésicule intraluminaire et l'abscission. Ce complexe a aussi un rôle dans la réparation de la membrane plasmique ainsi que nucléaire. Etant un complexe permettant de remodeler ma membrane, il existe une grande probabilité théorique ainsi que des preuves indirectes impliquant que son activité est régulé par la tension de membrane. Mesurer de façon directe la réaction de complexe en changeant la tension de membrane (σ) permettra de discriminer entre plusieurs modèles d'action théoriques. La fission de membrane par ESCRT-III pendant l'abscission est un modèle de choix du fait de son diamètre de plus d'un micron impliquent une accessibilité par microscopie optique, de la connaissance des voies de signalisation biochimiques ainsi que de leurs arrangement dans le temps et l'espace.

Dans cette thèse, je vais décrire les indices d'une activation directe d'ESCRT-III déclenché par des chocs osmotiques pendant l'abscission ainsi que ces relations au cytosquelette. Ces expériences vont pouvoir ajouter à la connaissance des ESCRT ainsi que de permettre une meilleure compréhension de la tension de membrane pendant la cytocinèse.

Contents

Intr	RODUCTI	ON	1
1.1	Cell m	embrane and its tension	1
	1.1.1	Biological Membrane and its composition	2
	1.1.2	Elastic description of lipid membrane	4
	1.1.3	Nanotube extrusion	9
	1.1.4	Passive and active dynamics of membrane tension in cell	10
1.2	ESCR	ΓS and its multiple role in cell membrane remodelling	15
	1.2.1	Membrane fission	15
	1.2.2	ESCRTs	17
	1.2.3	ESCRT-III dependent membrane fission	20
Овјя	ECTIVE		22
Тесі	HNIQUES	3	23
3.1	Tube p	ulling	23
3.2	Volum	e, area and sphericity measurement	24
Resu	JLTS		28
4.1	Cell rea	action to osmotic shock	28
4.2	ESCR	ΓS and membrane	48
	4.2.1	Protein activity and membrane tension	48
	4.2.2	ESCRT perturbation in cytokinesis	53
	1.1 1.2 OBJE TECH 3.1 3.2 RESU 4.1	1.1 Cell man 1.1.1 1.1.2 1.1.3 1.1.4 1.2 ESCRT 1.2.1 1.2.2 1.2.3 OBJECTIVE TECHNIQUES 3.1 Tube p 3.2 Volum RESULTS 4.1 Cell results 4.2 ESCRT 4.2.1	1.1.1 Biological Membrane and its composition 1.1.2 Elastic description of lipid membrane 1.1.3 Nanotube extrusion 1.1.4 Passive and active dynamics of membrane tension in cell 1.2 ESCRTS and its multiple role in cell membrane remodelling 1.2.1 Membrane fission 1.2.2 ESCRTs 1.2.3 ESCRT-III dependent membrane fission OBJECTIVE TECHNIQUES 3.1 Tube pulling 3.2 Volume, area and sphericity measurement RESULTS 4.1 Cell reaction to osmotic shock 4.2 ESCRTS and membrane 4.2.1 Protein activity and membrane tension

		4.2.3	Cytokine	esis timei	•	 	 •	 •	•	 •	 •	 •	•	 •	•	 •	•	59
5	Disc	ussion	and Con	CLUSION														64
	5.1	Cell pa	rameters .			 											•	64
	5.2	Cell me	embrane te	ension .		 											•	67
	5.3	ESCRI	Γ			 	 •	 •		 •	 •			 •				68
Re	FEREN	ICES																85
M	ATERIA	ALS AND	METHODS															85
Pτ	BLICA	TIONS																88

Listing of figures

1.1.1	Biological membrane architecture.	2
1.1.2	Presentation of the main classes of lipids	3
1.1.3	Membrane permeability to solutes	3
1.1.4	Membrane deformations examples	4
1.1.5	Lateral extension rate diagram	5
1.1.6	Definition of the principal curvatures of a surface element	6
1.1.7	Membrane tension representation	6
1.1.8	Lipid membrane behavior upon tension	7
1.1.9	Regime of membrane tension: Entropic and enthalpic	8
1.1.10	Nanotube extrusion schematic	9
1.1.11	Water movement through a bilipid layer	12
1.1.12	Water behavior upon osmotic shocks in cells	12
1.1.13	Membrane tension homeostasis.	14
1.2.1	Vesicular exchanges in the cell	16
1.2.2	Membrane fission of a vesicle from a lipid membrane	17
1.2.3	ESCRT complexes	18
1.2.4	Dynamin and ESCRT membrane fission model	18
1.2.5	Endocytic pathway description	19
1.2.6	Multi Vesicular Body structure	20
1.2.7	Models of membrane fission at the ICB	21
3.1.1	Optical tweezer	24

3.1.2	Nanotube Extrusion in mammalian cells and its force evolution	24
3.2.1	GUV calibration	27
4.2.1	CHMP4B-GFP puncta osmolarity response	48
4.2.2	CHMP4B-GFP behaviour upon hyper-osmotic shock	49
4.2.3	CHMPless tubes	51
4.2.4	CHMP4B-GFP puncta energy response	52
4.2.5	Schematic evolution of major protein involved in cytokinesis during telophase	53
4.2.6	CHMP4B-GFP rings	54
4.2.7	Averaging of Jupiter and CHMP4B-GFP	56
4.2.8	Averaging of SirC8 and <i>a</i> -tubulin	57
4.2.9	Cell aspirator	57
4.2.10	CHMPless cells aspirated	58
4.2.11	Cell aspirator survival	59
4.2.12	Cep55 behaviour upon hyperosmotic shock	60
4.2.13	Latrunculin treatment pulled tubes	61
4.2.14	Latrunculin treatment on telophase cells provokes a CHMP4B-GFP recruitment.	62
4.2.15	Cytokinesis timer	62
4.2.16	Cytokinesis timer and CHMP4B-GFP dependency	63
5.1.1	Osmotic pressure ratio and inverse of the volume	65
5.1.2	Evolution of volume upon ATP depletion and osmotic shocks	66
5.2.1	Sea urchin deformation model based on solid elastic gel	67
5.3.1	Analysis of sea urchin egg surface tension (using egg deformation) dynamics dur-	
	ing the first division after fertilization.	69
5.3.2	Mitosis description	70

Listing of tables

	г 1 с	1	11 1 1 1 1 1 1 1 1 1 1 1 1 1 1 1 1 1 1 1	ties	
1 1	Hyamples of me	embrane tencion	ne and hending rigidities.	T100	1 '
	LAGIIIPICS OI IIIV	cilibratic (clision)	is and bending rigidities	100	1.

Acknowledgments

I would like to express my dear thanks to Aurélien Roux for taking a chance in a not so young plant biology graduate to do a membrane biophysics PhD.

I am obliged for the daily support and expertise of Nicolas Chiaruttini.

I truly appreciate the intelligence and availability of Sarah Machado and Emmanuel Derivery.

I am thankfu l for the thesis committee.

I am forever grateful to:

Mathieu Gourgues for transmitting his sparkling interest of science during my bachelor degree. Anna Antmann for hosting a bachelor student in her lab. Christopher Grefen for making me discover that bacteria can clone DNA. Sarah Holec for teaching me how to master molecular biology and plant biology. Laurent Pieuchot for his sceptic eye on data.

Taisuke Nishimura for teaching me his cautious approach to biology and daily observation of plants. Jerzy paszkowski for hosting me in his lab. Marie Mirouze and Mélanie Dapp for their happiness and expertise. Frederic Berger for his understanding, wit and patience with me. The Centre Hospitalier Universitaire Vaudois (CHUV), Marie-Pierre Primi and Céline Leyvraz-Recrosio for their help to train me into *In Vitro* fertilization (IVF) techniques.

The PhD program of the University of Geneva. Stefan Matile's laboratory for their chemical expertise, Giulio Gasparini, Marta Dal Molin, Paola Morelli, Eline and Nicolas Chuard. Ana Joaquina Jimenez and Manuel Théry for his warm welcome in his laboratory.

The microscopy platform : Christoph Bauer and Jérôme Bosset.

The Biochemistry department of the University of Geneva.

Thank you to Scott D. Emr for working on ESCRT protein before I was born.

I would like to thank the Roux lab for his daily dose of input and microscopy challenges. Sandrine, Saleem, Alejandro, Valentina, Annika, Vincent, Margot, Ilaria, Caterina, Joachim, Jorge, Anastasiya, Fred, Byuong-ho.

I would like to thank my parents for allowing me to pursue my studies without question, trusting and supporting me through different town and countries. I will try to remember to be as open as them for my kids.

I am grateful for the daily assistance of Aude Chenu and her help on our life path.

List of Abbreviations

(BAC): Bacterial Artificial Chromosome

(CME): Clathrin mediated endocytosis

(CytoD): Cytochalasin D

(DAPI): 4',6-DiAmidino-2-PhénylIndole

(ER): Endoplasmic Reticulum

(ESCRTs): Endosomal Sorting Complexes Required for Transport

(GUV): Giant Unilamellar Vesicle

(ICB): Inter Cellular Bridge

(ILV): Intra luminal vesicle

(IVF): *In vitro* fertilization

(LatA): Latrunculin A

(MT): Microtubule

(MVB): MultiVesicular body

(OT): Optical tweezer

(PEG): Polyethylene glycol

(PM): Plasma membrane

(PI): Propidium iodide

(RVD): Regulatory Volume Decrease

(RVI): Regulatory Volume Increase

(SM): Sphingomyelin

(A): Area

(V): Volume

 (σ) : Membrane tension

 (Ψ) : Sphericity

Introduction

1.1 CELL MEMBRANE AND ITS TENSION

Biological membranes are acting as a selectively permeable barrier. The scaffolds of a biological membrane consists of a lipid bilayer containing proteins and oligosaccharides. Lipids and protein participate in different proportion to the composition of the plasma membrane while oligosaccharides can be covalently bound to lipids to form glycolipids or to protein to form glycoproteins. The structure of the bilayer is composed of 2 leaflets, that are formed by the spontaneous auto-assembly of the lipids. The bilayer structure buries the hydrophobic acyl chains inside the structure, keeping them away from the water (Fig.1.1.1). In this work, we will mainly focus on lipids and proteins that interact with them. Glycolipids 1 and glycoproteins 2 function and distribution have already been studied, however their role and impact on membrane biophysics remain unknown.

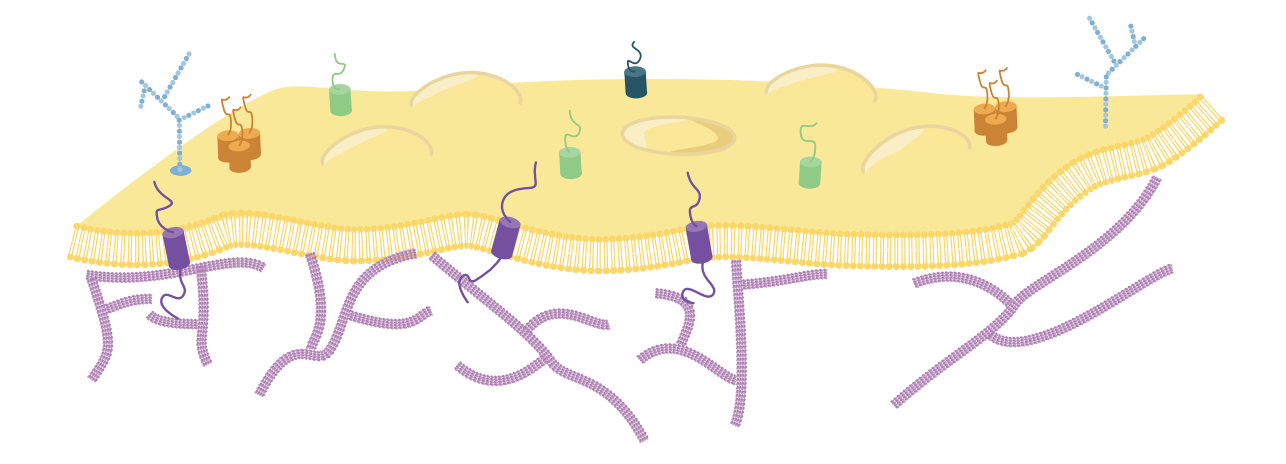


Figure 1.1.1: Biological membrane architecture: A lipid bilayer (yellow) where trans-membrane proteins (purple) are anchored. Glycolipids (light blue) navigate the bilayer in close contact with the cell cytoskeleton cortex (light purple).

1.1.1 BIOLOGICAL MEMBRANE AND ITS COMPOSITION

As seen in Fig1.1.2, lipids can be classified in several families: Sphingolipids, glycerophospholipids and sterols. Their structure are unlike and possess different properties.

Sphingolipids have two saturated or trans-unsaturated hydrocarbon tails which make their hydrophobic core more rigid. Compared to glycerophospholipids, sphingolipids are longer and thus thicken biological membranes. Sphingomyelin (SM) is one of the most abundant sphingolipid in mammalian cells³. Like phosphatidylcholine, SM carries a choline at its hydrophilic head. The plasma membrane, boundary of the cell, is particularly rich in SM. For instance in red blood cell, around 18% of the total lipid weight is due to SM.

Glycerophospholipids are lipids with two hydrocarbon tails and a polar head composed of a glycerol, a phosphate group and a polar group. Phosphatidylcholine (PC) is the major component of most eukaryotic cellular membranes and also functions as a pulmonary surfactant. Whereas PC is globally neutral, phosphatidylserine (PS) has a net negative charge due to the serine group at its polar head. Phosphatidylinositols (PtdIns) and its phosphorylated derivates like phosphatidylinositol 4,5-bisphosphate (PIP₂) are quite rare (<1%) in biological membranes. However they play a significant role in membrane trafficking and signalling pathways⁴.

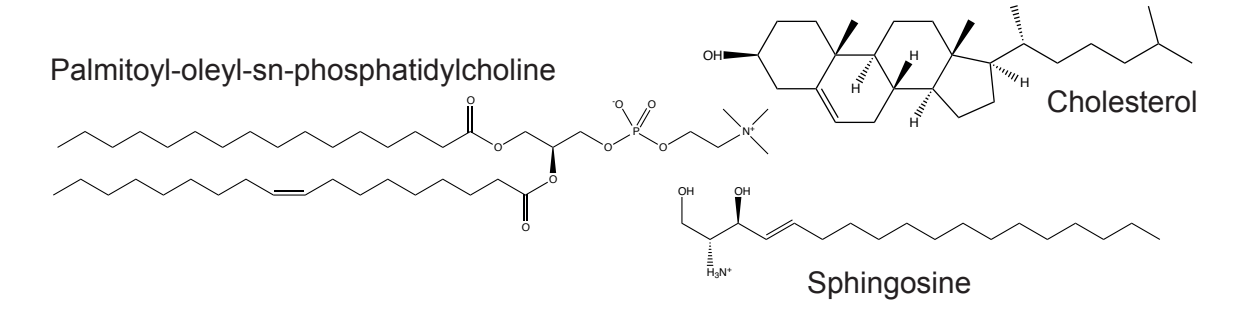


Figure 1.1.2: Presentation of the main classes of lipids. Palmitoyl-oleyl-sn-phosphatidylcholine (POPC), a classical glycerophospholipids used in *in vitro* membrane reconstitution. Sphingosin, the primary part of sphingolipids. Cholesterol, an essential lipid for membrane integrity and fluidity.

Sterols are apolar lipids with a single hydrocarbon tail. They do not form bilayers by themselves but insert within membranes at the upper part region of hydrophobic chains. Cholesterol (see Fig.1.1.2) is the major sterol in mammalian cells. Like sphingomyelin, cholesterol is enriched in plasma membranes. It represents 23% of the total lipid weight in red blood cells plasma membranes.

A lipid bilayer is a semi permeable barrier depending on the solute (Fig. 1.1.3).

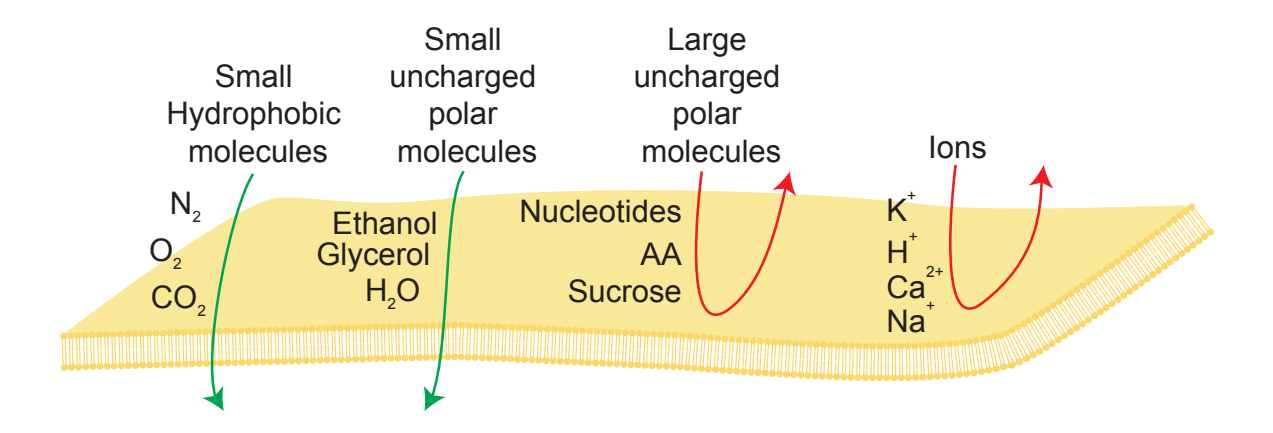


Figure 1.1.3: Membrane permeability to solutes. AA: Amino acids

1.1.2 ELASTIC DESCRIPTION OF LIPID MEMBRANE

Membranes can be modeled as a thin homogeneous fluid sheets. Generally, the thickness of this sheet (a few nm) is negligible compared to its surface (a few μ m). If that previous characteristic is respected and the membrane is isotropic, all membrane deformation can be decomposed into three elementary ones: shearing, stretching and bending (See Fig1.1.4).

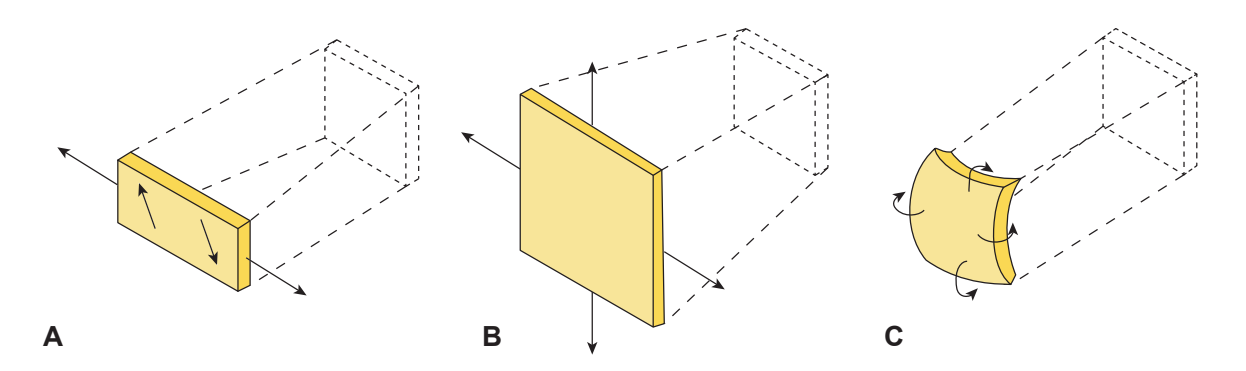


Figure 1.1.4: Membrane deformations examples. Arrows represent deformation directions. **A**) Shearing. **B**) Stretching. **C**) Bending. Inspired by [1].

Shearing is a deformation in which parallel internal surfaces slide past one another while maintaining the surface area. In a viscous sheet, the shearing energy per unit area is:

$$E_{\mathit{Shearing}} = rac{1}{2}\mu(\lambda^2 + \lambda^{-2} - 2)$$

where μ is the shear modulus in $J.m^{-2}$ and λ is the lateral extension rate $\lambda = \frac{L_0 + \Delta L}{L_0}$ (as seen in Fig1.1.5).

Due to the high fluidity of lipid membrane, shearing deformations are negligible compared to stretching and bending and will be ignored afterwards.

Stretching is a deformation that modifies the membrane area A by either extending or compressing it. The tension associated with a relative change in area $\frac{\Delta A}{A}$ is:

$$\sigma = rac{dE_{Stretching}}{dA}$$

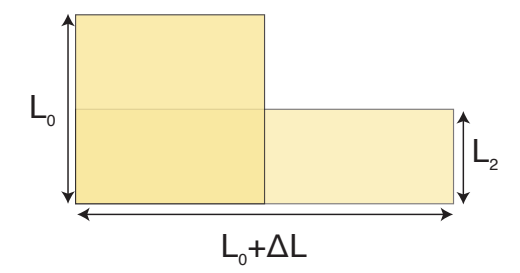


Figure 1.1.5: Lateral extension rate diagram. L_0 square represents

for a finite membrane undergoing stretching from A to $A+\Delta A$ and having an elastic response, the tension follows a Hooke's law:

$$\sigma = \chi rac{\Delta A}{A}$$

where χ is the compressibility modulus of the lipid membrane. In this case the energy of stretching per unit surface writes as follow:

$$E_{Stretching} = rac{1}{2} \chi (rac{\Delta A}{A})^2$$

This is only applicable in a case where the membrane does not have access to an infinite reservoir. The stretching force will be balanced by the membrane tension, a concept that will be developed later in this thesis.

If the membrane is connected to an infinite reservoir of surface, typically if one considers a small portion of a very large membrane, σ can be considered as constant towards an area increase. In this case the stretching energy is:

$$E_{Stretching} = \sigma \Delta A$$

Bending is a deformation that modifies the membrane curvature at constant area. The bending energy derives from the membrane curvature. At any point of a surface, one can define two radii of curvature R_1 and R_2 (See Fig1.1.6). The inverse of these radii are the two principal curvatures c_1 and c_2 . The mean curvature J is the sum of the principal curvatures $J = c_1 + c_2$. The Gaussian curvature K is the product of the principal curvatures $K = c_1 \cdot c_2 \cdot c_3 \cdot c_4 \cdot c_5 \cdot c_5$

$$E_{bending} = \frac{1}{2}\kappa(J-c_{o})^{2} + \kappa_{G}K$$

where κ is the bending rigidity modulus and κ_G the gaussian bending rigidity modulus and c_o the spontaneous curvature.

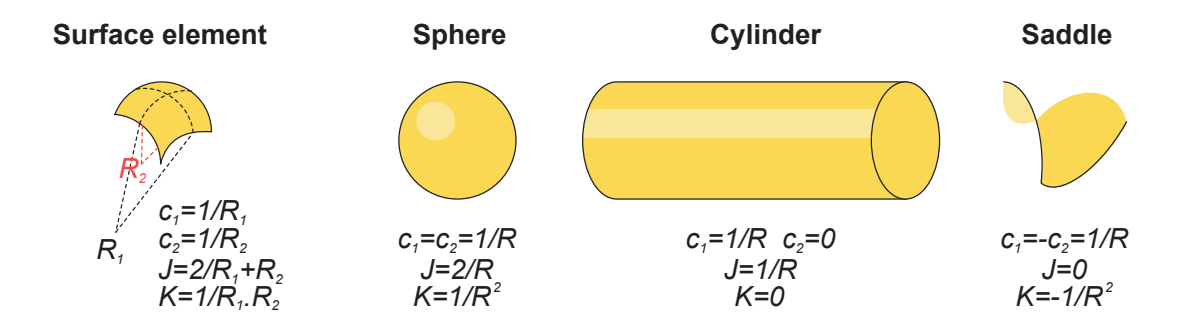


Figure 1.1.6: Definition of the principal curvatures of a surface element. Examples of Gaussian curvatures $(K = c_1.c_2)$ and mean curvatures $(J = c_1 + c_2)$ of a sphere, a cylinder and a saddle.

In the case of a membrane connected to a reservoir, the free energy of the membrane including contribution of bending and stretching is 5,6 :

$$F = \int_A ds \{ \frac{1}{2} \kappa (J - c_o)^2 + \kappa_G K + \sigma \}$$

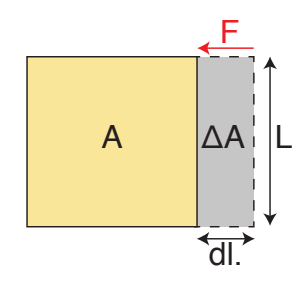


Figure 1.1.7: Membrane tension representation

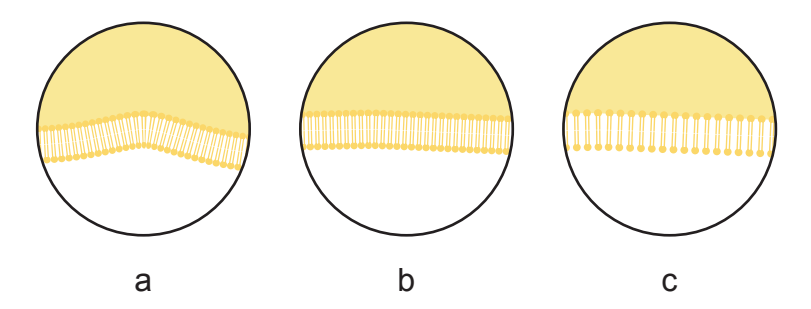


Figure 1.1.8: Lipid membrane behavior upon tension. a) The membrane is not tensed and is under thermal fluctuation: entropic regime. b) The membrane folds are fully unwrapped. c) The lipids are stretched apart in enthalpic regime.

There are two regimes of tension in lipid bilayers which differ by the relationship between tension and projected area: The entropic and enthalpic regime (Fig.1.1.8).

In the entropic regime, at low tensions, the surface of a membrane fluctuates due to thermal agitation. Stretching a membrane results first in the unfolding of the area stored in the thermal fluctuation of the membrane. Whether biological membranes can be in a state of an entropic regime remains unknown. However observation of these fluctuations is accessible *in vitro* in Giant Unilamellar Vesicle (GUV).

Using the Canham-Helfrich Hamiltonian^{5,7,8}, one can calculate the variance of the fluctuations of the vertical displacement of the membrane (u) for low σ values (typically below 10⁻⁵ $N.m^{-1}$)

$$< u^2 > \propto \frac{k_B T}{\sigma} ln \frac{L}{a}$$

where k_B is the Boltzmann constant, T the temperature, L is the macroscopic length scale of the membrane (\simeq 10 μ m) a its microscopic length scale (\simeq 1 nm, typically, the size of a lipid). We can observe in this equation that the membrane tension (σ) tends to reduce the amplitude of the fluctuations. In detail, the relationship between membrane tension and excess area can be calculated from fluctuations spectrum analysis:

$$\frac{\Delta A}{A} = \frac{k_B T}{8\pi\kappa} ln \frac{\frac{\pi^2}{a^2} + \frac{\sigma}{\kappa}}{\frac{\pi^2}{L^2} + \frac{\sigma}{\kappa}}$$

For low tensions, when the condition $\frac{\kappa\pi^2}{L^2}\ll\sigma\ll\frac{\kappa\pi^2}{a^2}$ is satisfied, the relationship simplifies:

$$\frac{\Delta A}{A} = \frac{k_B T}{8\pi\kappa} ln \frac{\kappa \pi^2}{\sigma a^2}$$

In the enthalpic regime, after all excess area stored in membrane folds has been unfolded (See Fig.1.1.9)), the membrane behave following the Hook's law defined above:

$$\frac{\Delta A}{A} = \frac{\sigma}{\chi}$$

As the entropic contribution to tension is negligible at high tension values as well as the enthalpic contribution to tension is negligible as low tension values. The two terms can be summed up to give:

$$\frac{\Delta A}{A} = \frac{k_B T}{8\pi\kappa} ln \frac{\kappa \pi^2}{\sigma a^2} + \frac{\sigma}{\chi}$$

This equation allows to fit experimental data of σ vs ΔA over a very large range of tension values. This model has been tested *in vitro* in GUV⁹, however it is unknown whether a living cell with its complex composition and architecture behaves accordingly to this theory or from a specific derivation of it.

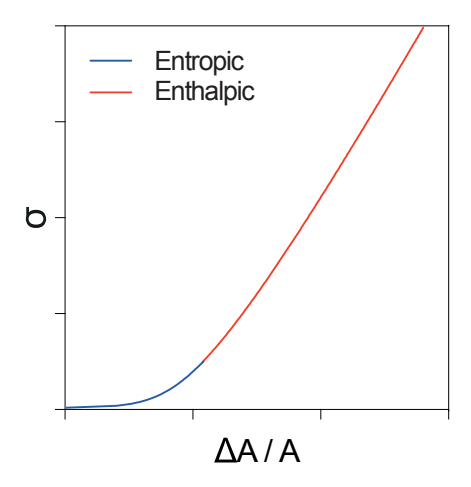


Figure 1.1.9: Regime of membrane tension. Non linear entropic (blue) and linear enthalpic (red). Schematic representation with no real values.

1.1.3 NANOTUBE EXTRUSION

Nanotube extrusion is the method of choice to monitor σ . When a local force is exerted on a lipid membrane, a nanotube is formed. This deformation is characteristic of fluid bilayer, in opposite to a conical shape from the deformation of an elastic solid surface (eg rubber balloon). By stretching the surface, σ increases and the system minimizes the energy by reducing the surface of the deformation. A perpendicular line to the plane would be the minimal surface to adopt, however this would imply a infinite curvature of the membrane. The nanotube is indeed the result of the balance between $E_{bending}$ and $E_{stretching}$

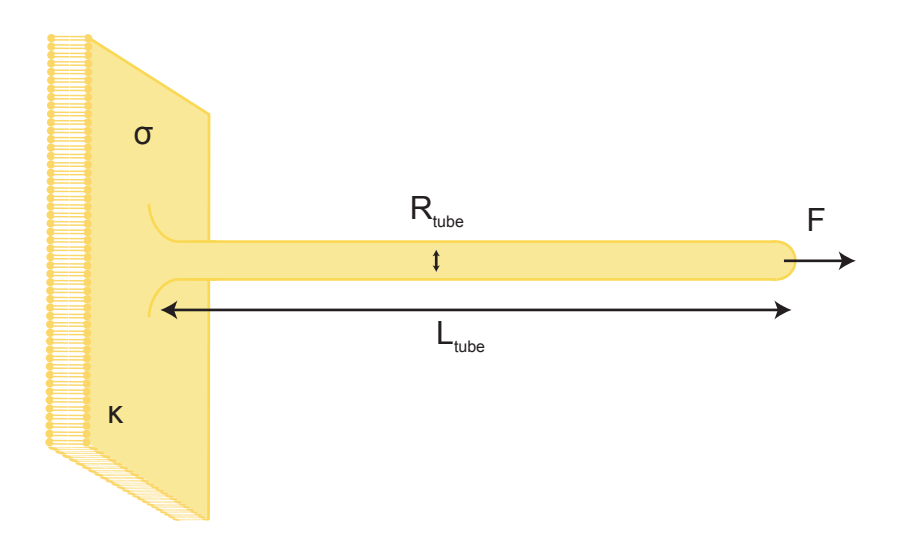


Figure 1.1.10: Nanotube extrusion. R_{tube} the tube radius, L_{tube} the tube length, κ the membrane

Using Canham-Helfrich Halmitonian, the free energy of the system *F* is:

$$F = \{rac{\kappa}{{}_2R_{tube}^2} + \sigma\}$$
2 $\pi R_{tube}L_{tube} - fL_{tube}$

with R_{tube} the nanotube radius, L_{tube} the nanotube length, f the force applied to extrude the nanotube and κ the bending modulus of the membrane.

Minimizing the energy against the tube radius R_{tube} , we can obtain the tube radius at equilibrium R_{\circ} :

$$R_{\rm o}=\sqrt{\frac{\kappa}{2\sigma}}$$

Minimizing the energy against the tube length L_{tube} , we can obtain the force f_o necessary to maintain the tube at equilibrium:

$$f_{\rm o} = 2\pi\sqrt{2\kappa\sigma}$$

Those theoretical predictions were experimentally validated in 1996 in vitro 10 and in vivo 11.

1.1.4 PASSIVE AND ACTIVE DYNAMICS OF MEMBRANE TENSION IN CELL

The theory of Canham and Helfrich is not *per se* applicable in living cells, because it is an out-of equilibrium and inhomogeneous system, however it is the best model so far. Nonetheless this method has been used in various cellular contexts (Table 1.1.1). These measurements helped shed a light on the wide range of tension present (from 3·10⁻² mN·m⁻¹ in epithelial cell bleb to 15·10⁻² mN·m⁻¹ in melanoma cell). Indeed the lipid composition is highly variable in between cell types ¹², and the deformability ¹³ also. Moreover, having access to the bending modulus of the studied membrane remains challenging. Indeed only two studies ^{11,14} have succeeded to measure the radius of the nanotube extracted from the cell.

The presence of cytoskeleton in extruded membrane tether is still a question that remains elusive. It is absent in certain membrane tethers ¹⁵ although it has been shown to be present in other studies ^{16, 17}. Exploring whether a true plasma membrane tether is extracted or whether it results from an extended filopodia may shed light on this discrepancy.

Membrane tension response to modification of osmolarity has been previously partially observed in neurons ²³, endothelial cells ³¹, epithelial ³² and *C.elegans* sperm cells ²². However a basic theory describing the relationship between osmolarity, membrane tension, volume and area remains to be described.

Rapid cell volume variations are mostly due to water exchange. Indeed, cells are highly permeable to water in both directions. This transfer of water is mediated by proteins (Aquaporins) or through the lipid bilayer³³ (Fig. 1.1.11).

Table 1.1.1: Examples of membrane tensions and bending rigidities

	Membrane tension	Bending modulus
	$(mN \cdot m^{-1}) = (dyn \cdot cm^{-1})$	$(N \cdot m)$
SOPC 18, 19	-	1.1 · 10 ⁻¹⁹
SOPC/CHOL ^{18,8,20}	-	$2.6 \pm 0.5 \cdot 10^{-19}$
SM/CHOL ¹⁸	-	5.5 · 10 ⁻¹⁹
Red Blood cell ²¹	-	1.8 · 10 ⁻¹⁵
Keratocyte 14	1.5 to 4.5 · 10 ⁻²	$1.4 \pm 0.1 \cdot 10^{-19}$
Chicken neuron 11	$3.1 \cdot 10^{-3}$	2.7 · 10 ⁻¹⁹
C.elegans sperm cell ²²	1.5 to 4.5 · 10 ⁻²	-
Molluscan neuron 23	2 to 12 · 10 ⁻²	-
Protoplast ²⁴	1.2 · 10 ⁻²	-
Neutrophil ²⁵	6.9 to $10.3 \cdot 10^{-2}$	-
Melanoma cell bleb 26	1.1 · 10 ⁻²	-
Epithelial cell bleb 26	3 · 10-3	-
Melanoma cell ²⁷	1.8 to $15 \cdot 10^{-2}$	-
Outer hair cell ²⁸	3.71 to 4.57 · 10 ⁻³	-
HeLa ²⁹	0.2 to 1.6 (surface tension)	-
Water at RT 30	72 (surface tension)	-

The osmotic pressure (Π) of a diluted solution of osmolytes at a solute concentration C can be derived from the equation of Van't Hoff.

$$\Pi = C \cdot R \cdot T$$

where *R* is the ideal gas constant and *T* the absolute temperature.

Media used to grow cells in culture have typically an osmotic concentration in the range of C=250-350 mOsm/l and an associated pressure of $\Pi=300\cdot8.3\cdot300\simeq7\cdot10^5$ Pa. A wide variety of factors influence the osmotic concentrations of the medium but their net contribution to the final osmotic concentration varies greatly. In cell culture medium ions are the major contributor to the osmotic concentrations.

Another potential source of net water flux through the plasma membrane arises from the cell surface tension γ which can generate a hydrostatic pressure difference ΔP between the inside and the outside of the cell. Using the Laplace law, this difference is computed as follows:

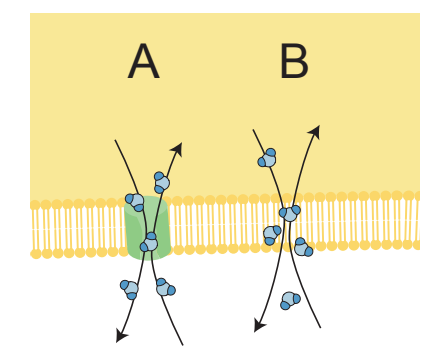


Figure 1.1.11: Water movement through a bilipid layer. A) Aquaporin B) Diffusion

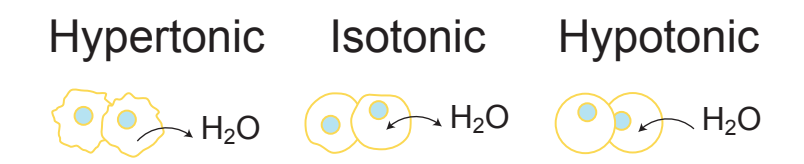


Figure 1.1.12: Water behavior upon osmotic shocks in cells.

$$\Delta P = rac{2\gamma}{r}$$
 with $\gamma = \sigma + \gamma_{cortex} \simeq \gamma_{cortex}$

with r the cell radius (if approximated as a sphere), γ_{cortex} the surface tension of the cortex located underneath the plasma membrane σ the surface tension of the plasma membrane (which is negligible compared to γ_{cortex}) ³⁴.

In animal cells, a hydrostatic pressure differential between the inside and the outside of the cell can arise from contractions of the actomyosin cortex, which is associated to the plasma membrane by ERM (ezrin, radixin, moesin) proteins. When the differences in hydrostatic pressure ΔP and in osmotic pressure $\Delta \Pi$ across the plasma membrane do not equilibrate, a net water flux J_{H_2O} is generated. This water flux (assuming a linear response approximation) can be defined as follows:

$$J_{H,o} = k(\Delta P - \Delta \Pi)$$

with k the water permeability of the plasma membrane.

The hydrostatic pressure differential generated by the cell cortex can reach 10³ Pa, given a cell radius of 5 μ m and a surface tension of $\gamma=2.5\cdot 10^{-9}$ nN/ μ m³⁵. This value is 100 times lower than

the osmotic pressure of a standard cell culture medium. Thus, reorganistation of the actomyosin cortex contributes little in generating a net water flux though the plasma membrane 36,37 . Therefore, the outside and the inside of the cell are always osmotically at equilibrium and the main variable to net water flux and changes in cellular volume is the difference in osmolarity. By assuming a cell at osmotic equilibrium and neglecting ΔP , the volume of a cell V_{Cell} that contains $n_{osmolytes}$ moles of osmolytes and surrounded by a medium of osmotic pressure Π_{med} can be approximated as:

$$V_{Cell} \simeq rac{n_{osmolytes}RT}{\Pi_{med}}$$

All of that is valid for cells with lipidic semi-permeable membrane. However for other cell types, another term should be added in order to take into account the pressure formed by cell walls (such a the peptido-glycan envelope of bacteria or cellulose-based wall of plant cells) as it constrains the cell volume.

The membrane shape can also be altered in order to adapt/respond to changes in tension and/or osmolarity. Indeed a cell able to quickly adapt to a change in its environment would be positively selected. A living cell is an enclosed environment with set ranges of values for protein and salt concentrations in order to function properly. By expanding or reducing the volume, those concentrations change and could deregulate or stop many enzymatic processes. Moreover a hole in this lipid membrane could potentially lead to cell lysis.

Several membrane reservoirs are available in the cell to respond to an osmotic shock ^{38, 39}: Caveolae, endocytosis, blebbing, osmolite release, microvilli (Fig. 1.1.13). The size of those reservoirs can be measured using membrane tether ⁴⁰.

The adjustments of the endocytosis/exocytosis rate can explain the regulation of tension and osmotic pressure in the range of minutes/hours⁴¹.

Caveolae, latin for little caves, were first described in 1974 in skeletal muscle cells⁴². While remaining elusive for numerous years, its functions are getting clearer by the years. Their flask-shaped structures have a distinct lipid composition (sphingolipids and cholesterol) and are rich in proteins.

Recently they have been shown to regulate membrane tension upon hypo-osmotic shock 31 . By flattening upon increase in hypo-osmotic shock they release plasma membrane area to buffer the increase. Interestingly, the resting membrane tension is two times smaller in caveolin depleted cells ($Cav1^{-/-}$) compared to the control 31 .

A bleb is a spherical protrusion of the plasma membrane uncoupled from the cytoskeleton. Blebbing is also a hallmark of membrane tension release. It is mainly observed in apoptosis, however it has been reported to be used in HeLa cell for furrow positioning⁴³. It has also been observed during spreading and retracting⁴⁴.

Microvilli are microscopic plasma membrane protrusions present at the surface of epithelial cell in the intestine. This increases the surface area of the cell while minimizing any increase in volume. This reservoir of membrane can be used for spreading, locomotion or resistance to shock^{45, 46}.

An indirect way for the membrane to cope with membrane tension variations is the release of osmolites. Osmolites can be released in the cytoplasm⁴⁷ or in the external medium⁴⁸.

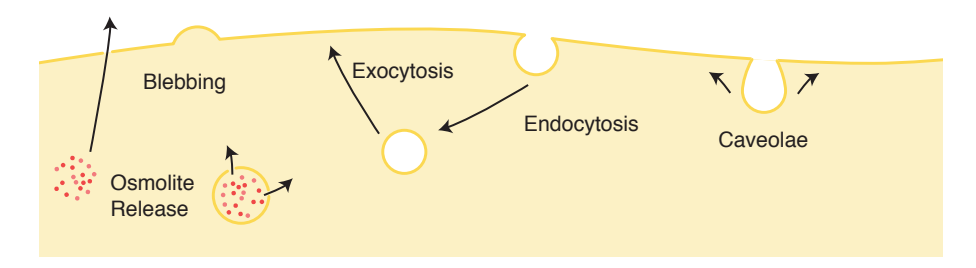


Figure 1.1.13: Membrane tension homeostasis.

Either linked to the plasma membrane via lipids ¹⁵ or connected via ezrin, radixin, moesin (ERM) proteins, the cytoskeleton plays an important part in setting membrane tension. The combined activity of F-actin and myosin motors produces a cortical tension that can be critical for events such as mitosis rounding. However the combined pressure of the osmolarity and the cortex is roughly equivalent to the exterior medium of an animal cell. Its depolymerisation leads to a 10% increase in volume and allows accessibility to a membrane reservoir ⁴⁰.

On the other hand, in prokaryotes and plants, disruption of the cell wall can lead to the cell lysis due to the great difference between internal and external pressure ⁴⁹. The stiffness of the acto-myosin cortex has been showed to protect *Dictyostelium discoideum* cell shape and motility against hyperosmotic shocks ⁵⁰.

Upon osmotic shocks, a regulatory volume increase (RVI) or decrease (RVD) has been observed. Those regulatory mechanisms works through the activation of ionic channels 51 . Na $^+/H^+$ and Cl $^-/HCO_3^-$

ion exchangers participate in RVI by pumping Na^+ and K^+ inside the cell while removing HCO_3^- . Conversely, RVD is performed by the cell through Ca_2^+ activated channel that pumps Cl^- , K^+ and organic osmolites in the extracellular medium.

Polymers have a notably higher contribution to osmotic pressure than monomers at an equal concentration, because of their large gyration radius and entropic constrains on water molecules. Protein polymers (such as microtubules, actin and intermediate filaments) have the capacity to change their osmolarity by rearranging themselves from polymers to monomers ^{52,53}. However this "defense mechanism" was not yet observed *in vivo*. Interestingly, inhibition of actin polymerisation led to a drastic drop in membrane tension ¹⁴. The organisation of the acto-myosin network seems to be more important that its own osmolarity.

The intricate relationship between the plasma membrane tension, the osmolarity and the cytoskeleton remains quite unclear despite numerous reviews 54, 55.

Moreover, contradictory results on the link between membrane tension and osmotic shocks suggest that this matter owes to be studied in a more exhaustive approach 14, 31, 56.

1.2 ESCRTS AND ITS MULTIPLE ROLE IN CELL MEMBRANE REMODELLING

1.2.1 MEMBRANE FISSION

Membrane fission is the basis for dynamic exchanges between cell compartments. The basic principles of vesicular transport are conserved regardless of the donor organelle to the target destination ⁵⁷.

From the endoplasmic reticulum (ER) to the Golgi (COPII⁵⁸), from the Golgi to the ER (COPI⁵⁹), from the exterior medium to the endosomes (Clathrin Mediated endocytosis (CME)⁶⁰) and from the endosome to the lysosome (ESCRT), numerous protein complexes achieve this membrane fission procedure (Fig. 1.2.1).

The fission event is the critical step to release a vesicle inside the cytoplasm or into the external medium. A classical example of membrane fission is the CME. Triskelions of clathrin assemble and deform the membrane in a bulb-like shape. However this deformation is not sufficient in order to separate this vesicle from the donor membrane. A polymer of dynamin assembles on the tube link-

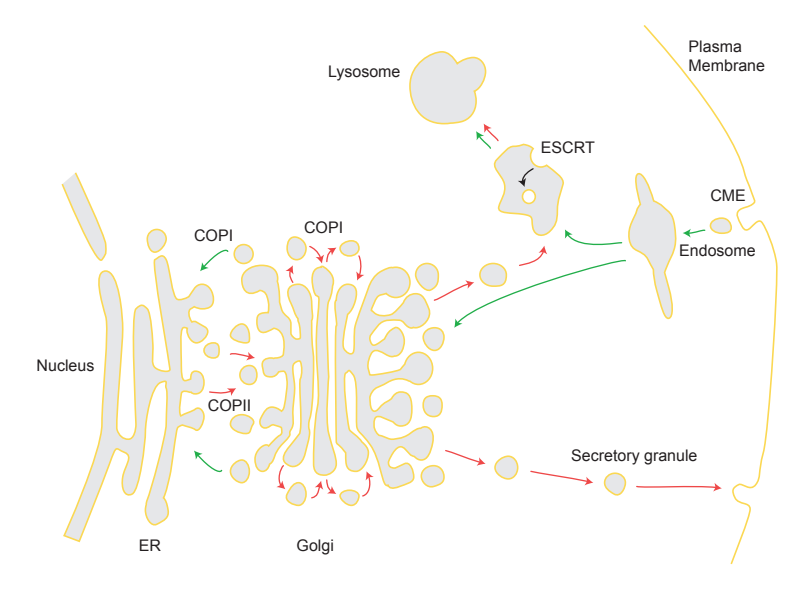


Figure 1.2.1: Vesicular exchanges in the cell. Different examples of membrane fission from the nucleus to the plasma membrane.

ing the clathrin-coated pits to the plasma membrane. Upon GTP hydrolysis, the polymer of dynamin contracts and shrinks the tube to the point where the energy of fission is only provided by the thermal fluctuation ^{61, 62}. The membrane fission mechanism *in vivo* can be summarized with a membrane deformation of the donor membrane (*via* lipids or a coat of proteins) followed by fission (Fig. 1.2.2). A consumption of energy (ATP or GTP) is required for effective membrane fission and/or coat recycling.

Genetic deletion was a leading tool in discovering the proteins involved in these mechanisms, however *in vitro* assays helped the recent understanding of associated biochemical and biophysical properties of both lipids and proteins that take part to these mechanisms. Indeed curvature and phase-induced membrane fission was shown possible *in vitro* ⁶³ ⁶⁴ ⁶⁵ and lipid composition of the membrane affects the fission event independently of its binding role to the proteins in COPII (Melero et al., Unpublished) and ESCRT ⁶⁶.

On a greater scale, membrane fission is not only involved in vesicular trafficking, it is also involved in organelle division 67 and cell division 68,69 . Indeed, mitochondria division is carried by a Dynamin-like protein in a conformation close to the CME, FtsZ a bacterial protein similar to tubulin can induce

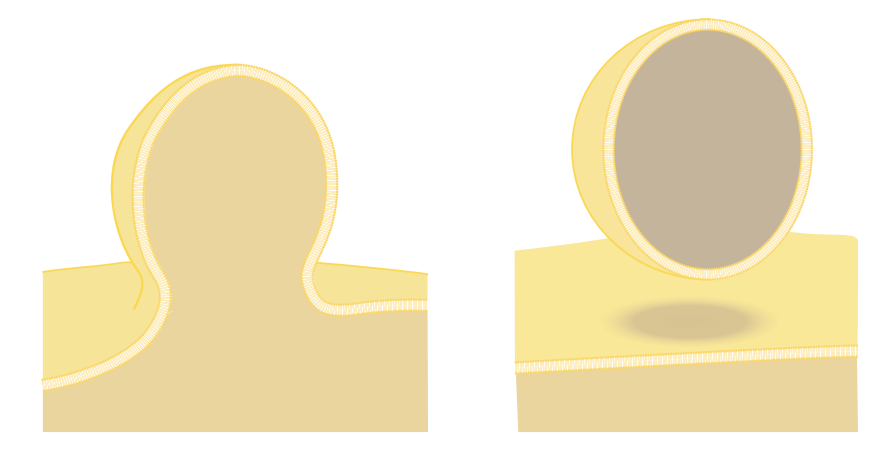


Figure 1.2.2: Membrane fission of vesicle from a lipid membrane. Deformed vesicle before fission (left). Pinched-off vesicle after membrane fission (right).

liposome fission and ESCRT-III is the main actor in the animal cell membrane fission.

In the following parts focus will be brought on a particular membrane fission protein complex: The endosomal sorting complexes required for transport.

1.2.2 ESCRTs

The endosomal sorting complexes required for transport (ESCRTs) discovery was pioneered in the 2013 Nobel prize winner Randy Schekman's lab by Scott Emr⁷⁰. A screen designed to screen for secretory pathway mutants revealed the class E compartments, a hallmark phenotype of ESCRT dysfunction in yeast.

ESCRT is composed of cytoplasmic protein complexes. Known as ESCRT-O, ESCRT-I, ESCRT-II and ESCRT-III, they sequentially enable membrane remodelling (Fig. 1.2.3). Together with accessory proteins they are present from archaea to metazoans ⁷¹.

As opposed to the dynamin-mediated membrane fission which is a constriction of the membrane neck from the outside, ESCRT-mediated membrane fission is a constriction of the membrane from the inside (Fig. 1.2.4). This different conformation involves a new understanding of how it is theoretically possible to cut from the inside, and a modelling of the forces and constraints required to perform this

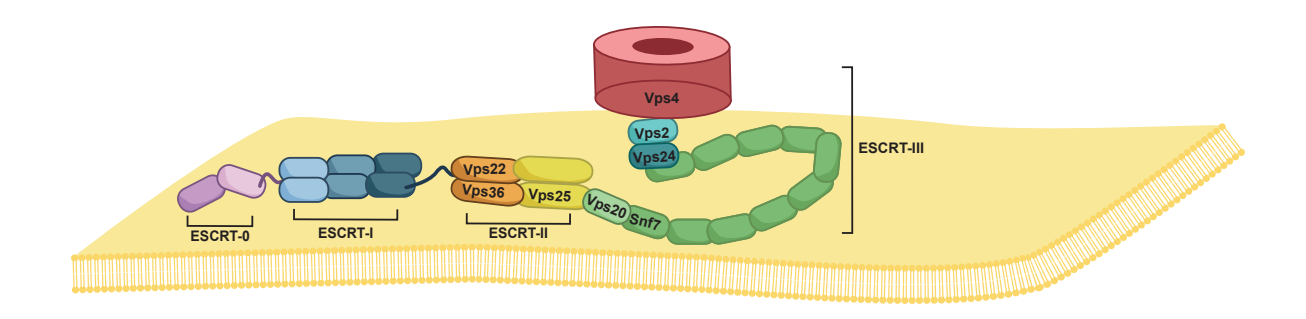


Figure 1.2.3: ESCRT complexes and proteins.

fission event.



Figure 1.2.4: Dynamin and ESCRT membrane fission model. Membrane in yellow, Dynamin polymer in red ESCRT-III polymer in green.

In this thesis we will focus on the ESCRT-III complex, the active membrane remodelling family.

ESCRT-III is a versatile system for the cell and even for extra-cellular objects. Cytokinesis $^{7^2,7^3}$, intraluminar vesicle formation (ILV) 74 , plasma membrane wound repair 75 , autophagy 76,77 , nuclear envelope sealing 78,79 , neuronal pruning 80 , nuclear pore assembly 81 and HIV release 82,83 are ESCRT-III dependent processes.

One of the most studied phenomenon is the multi vesicular body formation (MVB). ESCRT-III has been showed to be involved in the formation of ILV in MVB both by biochemical 84,74,85 and genetic assays 86,87 (Fig.1.2.5).

However, in order to observe membrane fission with a good resolution, the most accessible event is the abscission. Although many biochemical pathways are combined to regulate its timing ⁸⁸, it pos-

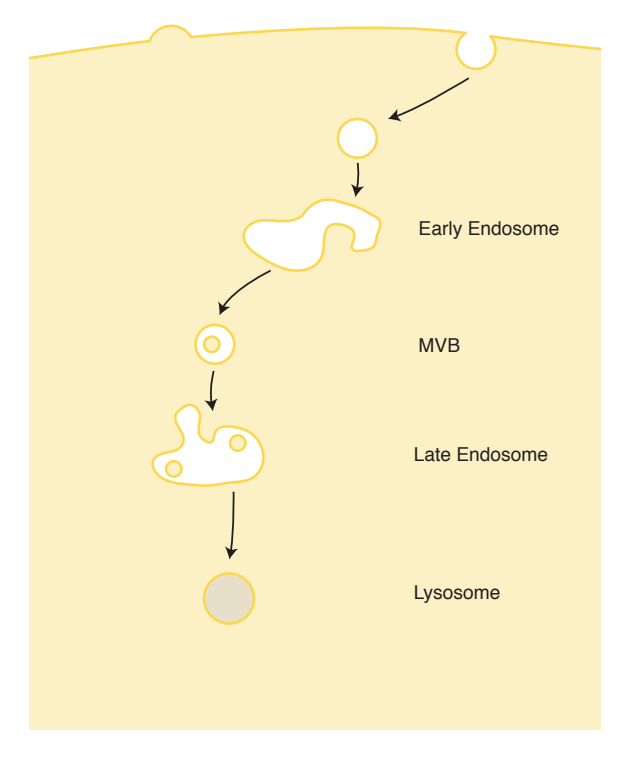


Figure 1.2.5: Endocytic pathway description.

sesses the greatest diameter combined with a physically accessible membrane. The abscission event occurs once per cell cycle, but the diameter of constriction starts at 1 µm. For mass quantification and genetic testing, HIV release or MVB biogenesis would be a wise readout. However, plasma membrane is accessible mechanically and is sensitive to osmotic shocks as compared to endosomes. Moreover the ESCRT components are in a native configuration and not hijacked by viral particle like in the HIV-release case. On top of that, MVB can not be resolved by photonic microscopy and have to be observed in a fixed state via electron microscopy (Fig. 1.2.6). Overall, abscission during cell division seems to represent an interesting readout in order to explore the underpinnings of membrane fission relative to membrane tension.

Nevertheless, the observation of abscission event is not straightforward and requires to overcome

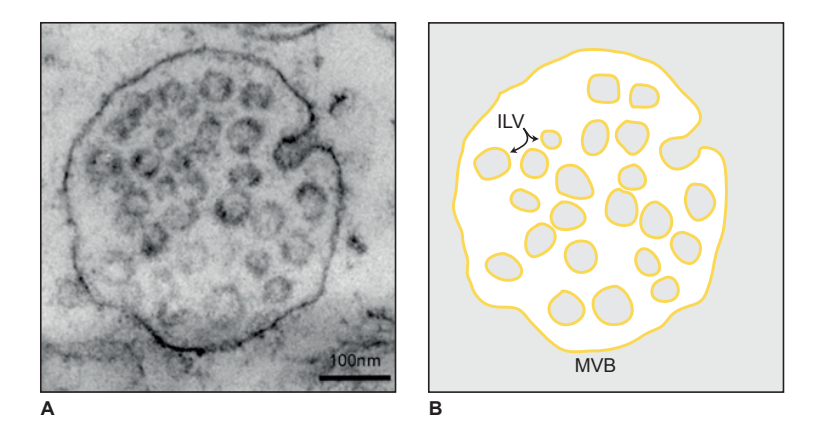


Figure 1.2.6: Multi Vesicular Body structure. A) Electron micrograph from a neuron of the CA1 region of the adult rat hippocampus. Taken from ⁸⁹. B) Scheme of a MVB with IntraLuminal Vesicles (ILV).

numerous difficulties. The cell is particularly sensitive to manipulation and microscopic observation at this stage. The membrane fission event is rapid (seconds) however it is hard to predict and/or to induce. Laser ablation of the inter-cellular bridge (ICB) were shown to increase the speed of fission ⁹⁰ as well as CHMP4C and ULK3 down-regulation too ^{91,92}.

This event is rather critical, for example a failure of cytokinesis can lead to various chromosomal abnormality that lead to cancer 93, 94.

Moreover, most of the studies assert that microtubule fission are concomitant to the membrane fission. However preliminary results showed that the two could be uncoupled and nanotube, membrane remnants could connect the two daughter cells 95, 96.

1.2.3 ESCRT-III DEPENDENT MEMBRANE FISSION

Different models of ESCRT-mediated fission ^{97, 98, 99} have been proposed along the years (Fig1.2.7). Some argue for a polymer of ESCRT working as a lasso loop to cut the membrane ⁸⁵. A more popular model is that the polymer of ESCRT-III has a preferred radius of curvature and an affinity to the membrane, that would lead to spiralling. However, the rings smaller than the preferred radius of curvature

would be under constraints. This energy could be released by buckling the membrane in a mechanism similar to the event where the wound-up spring of a watch jumps out of its socket when sufficiently disturbed ⁹⁹.

Other models support a massive fusion of vesicle with or without a combination of the ingression mechanism of the ESCRT-III polymer ¹⁰⁰. Those events could happen sequentially and/or in a simultaneous fashion.

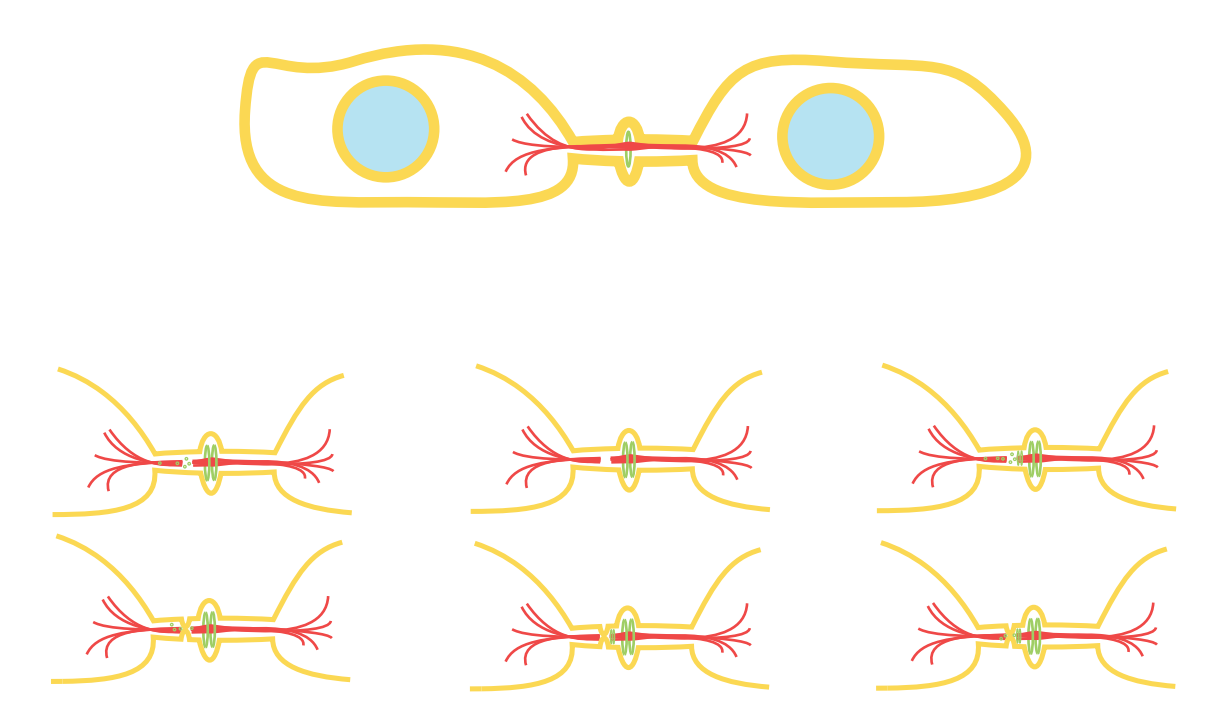


Figure 1.2.7: Models of membrane fission at the ICB. A purely vesicle fusion-driven model (Left) An ESCRT only driven model(Middle) A combinatory model (Right). Nucleus in blue, membranes in yellow, microtubule in red and ESCRT polymer and vesicles in green

In order to understand in detail the mode of function of a protein complex, all the parameter available must be analyzed. Shedding light on certain important parameter and quantitatively measure (σ) and other variables would lead to better modelling capabilities.

2 Objective

The aim of my thesis is to study the visco-elastic response of cell membranes upon osmotic stresses, and to determine how membrane tension changes associated with those osmotic stresses could impact the ESCRT-III dependent membrane fission reaction.

3 Techniques

3.1 Tube pulling

Currently, in order to access the membrane tension of a biological object, only few tools are developed. This thesis will focus on the tether extrusion by optical tweezers (OT). Magnetic tweezers used a similar approach where light is replaced by magnetism ¹⁰¹. Recently interferometry has been shown to be a non invasive method ²⁷ to measure membrane tension.

Derived from Nobel winning tools, OT were created after the discovery of optical scattering and gradient forces on micron-sized particles at the Bell's lab ¹⁰². The first uses in biology was the trapping and manipulation of viruses and bacteria ¹⁰³. Using a highly focused laser beam, an OT can provide an attractive force that depends on the refractive index mismatch between an object and the medium surrounding (See Fig. 3.1.1).

Nanotube extrusion is one way of monitoring membrane mechanics. Using either IgG or Con-

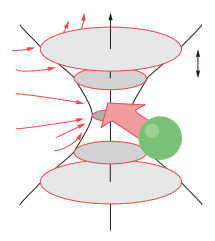


Figure 3.1.1: Optical tweezer.

canavalin A coated beads and/or electrostatic interaction, a thin membrane tube is extruded from the plasma membrane. As a pulling force is applied on a lipid membrane, a nanotube is formed. This shape deformation is intrinsic to lipid bilayer as discussed previously.

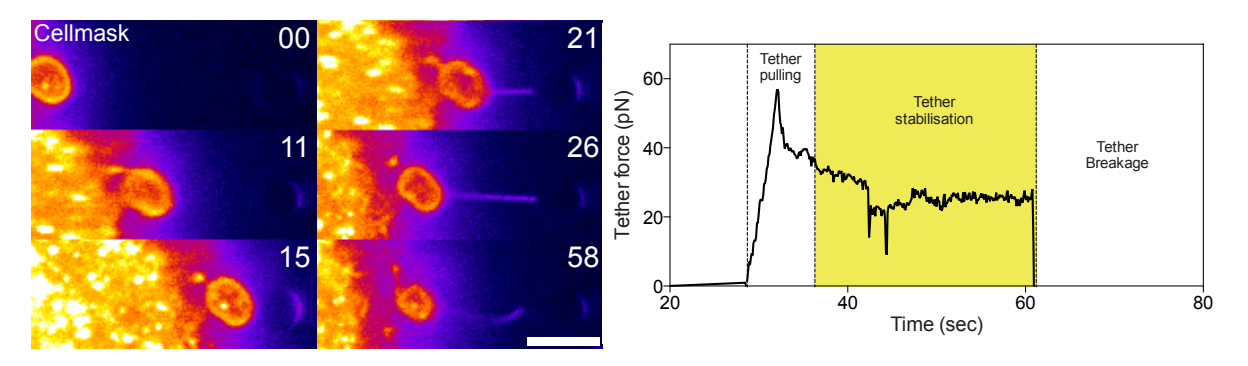


Figure 3.1.2: Nanotube Extrusion from HeLa cell. Tube break at time 58 sec. Scale bar is 5 μm . Time frame are in seconds (left). Force evolution during nanotube extrusion in mammalian cells (right).

3.2 VOLUME, AREA AND SPHERICITY MEASUREMENT

Raw material required for the cell metabolism can only enter the cell through its plasma membrane. Cell volume is therefore physically limited to a certain size following square-cube law¹⁰⁴, whereby the growth rate of a cell is proportional to the square of its typical size while its upkeep cost is proportional

to its cube. Indeed cells need a high surface area to volume ratio to be efficient in passing food and waste across the cell membrane. Larger cells have a lower surface area to volume ratio and cells will divide rather than grow larger. Moreover the membrane shape will help the cell to modify its surface area.

The volume of the cell varies along the cell cycle in a quite linear fashion, except at the nuclear envelope breakdown ^{105, 106}. At this particular step nucleus osmolites are released into the cytoplasm creating an effect similar to an internal hyper-osmotic shock in the cell.

In order to access key parameters of the cell, several techniques were developed. Membrane tension can be accessed via OT, however multiple tools were available for area and volume measurements, depending on the cell type and conditions.

Volume measurement is available through different approaches: Resistance of a small chamber 107 , coulter counter $^{108, 109}$ or electrophysiology $^{110, 111}$. Those techniques use the resistance (R) of the cell which is proportional to its volume.

Laser light scattering ¹¹² can also be used to determine the particle size and distribution in a medium. The drawbacks from this technique is that only cells in suspension can be measured and that the sphericity of the particle must be assumed. Non-spherical particle measurement has been developed however only rods have been able to be measured so far ¹¹³. Although adherent cells are accessible through Reflection interference contrast microscopy (RICM) ¹¹⁴, this technique also poses a shape-dependent bias unfit for our study.

Assuming a cytoplasmic dye concentration as an absolute number of dye is constant relative volume can be inferred ¹¹⁵. The drawbacks of this techniques is that the absolute volume remains out of reach.

Another technique such as Atomic force microscopy (AFM) ³⁶ are physically invasive for the cell. Optical and electron microscopy ¹¹⁶ would not allow for a live imaging and would require computing power and software unavailable.

An absolute volume of the cell can be extracted though negative imaging in epifluorescence microscopy ^{117, 105}. The cell is imaged in a small chamber, surrounded by a fluorescently-labelled medium that the cell cannot internalize. Once the proper calibration is carried out, this technique allows for a quick and absolute measurement of the cell volume.

This technique was used in combination with a volume reconstruction by software ³¹.

Historically, area measurement have been difficult to access. Area has been quantified via perimeter

measurement in fixed cell 118. However this method has a bias by rounding-up the cell and most of the structure smaller than the slicing are removed.

Area has also been measured with plasma membrane marker (FM1-43¹¹⁹ or DiIC12¹²⁰) in living cell. However those protocols require ice-cold solution and have a steady state amount of dye. A variation in *A* could be measured *in lieu* of exocytosis (a dye-contaminated vesicle could bring more dye to the surface than area) or through exosome. On top of that the behaviour of most of the dyes are unknown in term of fluidity, phase separation. Some dye could be excluded from certain membrane areas.

Confocal microscopy, spinning-disc microscopy or lattice light sheet microscopy ¹²¹ can be used to acquire the thinnest and quickest slice of the cell membrane. However a reconstruction of the surface would then need to be executed by an algorithm assuming various parameters.

Finally, cells were imaged in a chamber filled with a fluorescently-labelled solution and reconstructed with a software. This allowed the volume (V), area (A) and sphericity (Ψ) to be measured.

Primarily designed to measure rock particles sphericity 122 , a sphericity index Ψ can be used to compare cell sphericity.

$$\Psi = \frac{\pi^{\frac{1}{3}} (6V_p)^{\frac{2}{3}}}{A_p}$$

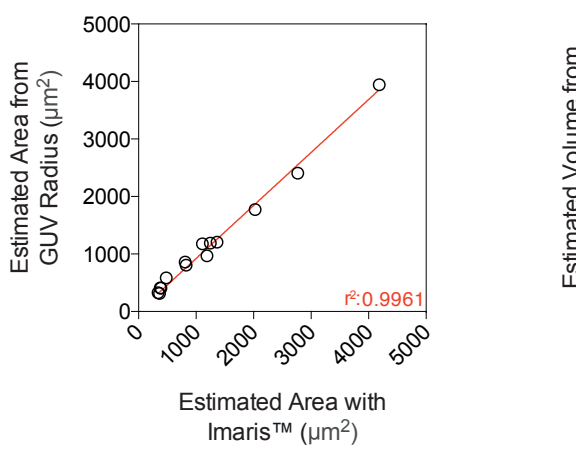
with A_p the surface area of the particle and V_p the volume of the particle. Any particle which is not a sphere will have a sphericity lower than 1.

In order to obtain cell measurements for various parameters, the cell volume was reconstructed using IMARIS (Biplane, Belfast, UK). The cell exterior was smoothed by 1 μ m.

Giant Unilamellar Vesicle (GUV) composed of DOPC were imaged in a fluorescent dextran solution. The volume of the GUV was measured first with extrapolation from the GUV radius. Then the inverse of the fluorescent dextran media picture was reconstructed in IMARIS. To finish, the two volume were compared in Fig. 3.2.1.

Imaris and extrapolation from the radius are consistent with each other.

HeLa Kyoto cells were chosen as a model for this study due to its numerous advantages. Indeed, a wide range of stable cell line are available in this background through bacterial artifical chromosome



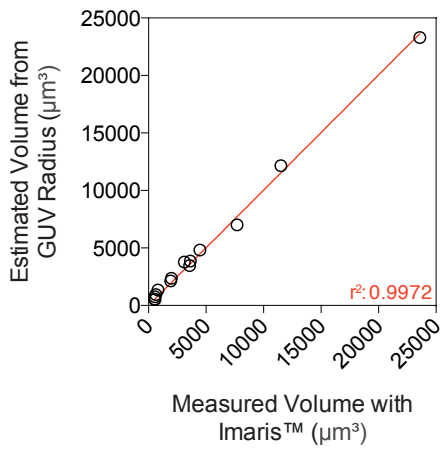


Figure 3.2.1: GUV calibration.

(BAC) transformation 123, mitosis has been well characterized in these cells 90 and their and their ease of cultivation are a plus.

Results

4.1 CELL REACTION TO OSMOTIC SHOCK

Visco-Elastic response of fibroblastic cells to osmotic shock

Guillaume Molinard, Martin Lenz, Aurelien Roux

Abstract

Osmotic shocks are common cellular stresses in particular for unicellular organisms such as yeast or protists. Such cells live in environment which humidity varies dramatically according to weather changes. As well, epithelial and endothelial cells which form barriers between multicellular organisms and their environment are subjected to changes of the osmolarity of their environment. Historically, osmotic shocks have been useful to study the response of cells to changes of membrane tension. However, the quantitative mechanical response of cells to osmotic shocks has not been studied, notably the link between membrane tension and changes in osmolarity, mostly because of the difficulty of measuring simultaneously changes of volume, area and membrane tension. By measuring at the same time membrane tension changes, volumes and area changes, we show that the mechanical response of cells to osmotic shocks is highly asymmetric: for hypotonic shocks, the membrane tension changes very little even for volume changes up to 1.5 time. For hypertonic shocks, membrane tension dwindles to very small values even for limited changes in the osmolarity. However, cell volume never shrinks below 50% of the initial volume, suggesting that cells have a minimal volume (or a maximal compressibility Poisson factor). By considering that cells adapt their volume to equilibrate the osmotic pressure of their cytoplasm to the environmental osmotic pressure, we can predict volume, area and tension changes. We further discuss the role of ATP in the recovery from hypotonic shocks. Using a physical model, we are able to describe the important parameters governing the cell responses to osmotic shocks and predict membrane tension from previous data.

Introduction

Lipid membranes are auto-assembled viscoelastic bilayers that separate cells and organelles from their environment. The elastic properties of lipid bilayers are unique, as they are very easy to bend but quite resistant to stretching. These properties strongly affect all cellular processes that require membrane remodeling. In particular, membrane tension is a critical parameter highly regulated during numerous cell processes including membrane traffic, cell motility (1, 2) and cell division . In the case of plasma membrane (PM) – the outer envelope of the cell – membrane tension changes may arise from the required cell volume and shape changes occurring during cell division or cell motility (3). Also, many cells, such as unicellular organisms or epithelial cells, are subjected to acute osmotic changes of their environment, which may cause volume changes and membrane tension increase leading to lysis.

Cells have thus evolved to respond to changes of membrane tension (4). The genetic response to osmotic stress has been studied extensively_(5), but its timeline is in order of minutes, and cannot account for immediate resistance to stretch. Caveolin were shown to be an important structure that provides immediate buffer of hypo-osmotic shock (6) as they are proposed to disassemble upon stretch and release a membrane reservoir. The link between the genetic and caveolae response to membrane tension changes could be through TORC2, as it was recently shown that plasma membrane tension increase leads to activation

of TORC2 through eisosomes, yeast specific structures that could play the same role than caveolae (7). The acto-myosin contractile cortex is also an essential regulator of membrane tension (8, 9).

However, the membrane tension response to cell volume and shape changes has not been studied quantitatively, mostly because of the technical difficulty to measure these three values at the same time (10). As a consequence, even though osmotic shocks are commonly used to study the role of membrane tension in many cell processes, how osmotic shocks quantitatively change cell membrane tension is not known. Simple estimates using the Laplace law give unrealistic values, far above the lysis tension, even for very small osmotic changes of a few tens of milliOsmoles.

Moreover, the impact of cytoskeleton has been probed a handful of times in a non-systematic manner (2, 11). The conclusion being that the membrane reservoir is affected, but the membrane tension might be unaffected.

To have a quantitative description of the relationship between the membrane tension, area, volume and osmotic shocks, we performed live membrane tension measurements coupled with 3D imaging.

Results

Osmotic shocks affect membrane tension on short time scale

To measure in real-time, changes of cell membrane tension during osmotic shocks, membrane tubes were extruded from the plasma membrane of HeLa Kyoto cells using concanavalin A-coated beads held in optical tweezers (Fig1A). The force applied onto the bead by the tube is a direct measurement of membrane tension (see Methods). While holding the tube, an osmotic shock was applied on the cell and the force was measured instantaneously (Fig 1B). To apply hypertonic shocks, we directly added 0.5 ml of cell culture media containing 0 to 0.5M of Sucrose to the 0.5 ml of buffer present in the petri dish. For hypotonic shocks, cell culture media was diluted up to 4 times in double distillated water. Changes of the force along with osmotic shocks are almost instantaneous (1, 6), and correlated to the intensity of the shocks. We thus measured the tube force averaged over the 5 minutes before the shock (f_0) and over the 5 minutes immediately following the shock (f) (Fig1B). We then calculated the relative change of the tube force $((f-f_0)/f_0)$ for various shocks (Fig1C). A striking observation is that membrane tension decreases by almost 60% even in mild hypertonic shock, whereas tension hardly changed upon hypotonic shocks, with a maximum of 40% in the strongest hypertonic conditions texted (75% water). These results show that hyper and hypotonic shocks have a direct impact on membrane tension in HeLa cells on a short time scale, but that the cellular response to the shocks is very asymmetric, as cells seems to control better tension upon hypotonic shocks.

We then measured the osmotic pressure of all solutions (Π) , and plotted the relative change of membrane tension $((\sigma-\sigma_0)/\sigma_0)$ – calculated from $(f-f_0)/f_0$ – as a function of the osmotic ratio, $\frac{\Pi}{\Pi_0}$ where Π_0 is the initial pressure of the cell media (**Fig1D**). We observed a continuous non-linear relation between the relative change of membrane tension with the osmotic ratio, which seemed to saturate rapidly around 0.9 for $\frac{\Pi}{\Pi_0} \geq 2$ (hypertonic

conditions) whereas it did not seem to saturate for values $\frac{\Pi}{\Pi_0} \leq 1$ (hypotonic conditions. Since the trend of this relation was robust, we wondered how we could explain it.

Cell volume and surface changes upon osmotic shocks have different dynamics

During osmotic shocks, volume, shape and surface of cells change. To understand how membrane tension is coupled to osmotic differences, we thus ought to measure volume, sphericity and surface of cells during and after osmotic shocks of various intensities. We used a fluorescence exclusion imaging (12, 13) followed by 3D reconstruction (See methods) to measure area, sphericity and volume of cells (Fig2.A). Cells were first incubated 5min with fluorescent dextran, and then the shadow of cells was imaged with time-lapsed 3D Spinning Disk confocal. For each image stack, the cell volume was reconstructed using IMARIS, which allowed a direct estimation of volume, surface and sphericity of single cells. On average, we obtained volumes of 3727±1980 um³, surfaces of 1825±736 um² and sphericity values of 0.71±0.11 (SD). We validated this method on Giant Unilamellar vesicle (GUV), for which volume and surface can be estimated directly from the radius (see Suppl. figure 1) with a r² of 0.9961 and 0.9972 for area and volume measurements respectively. However, we point out that the real surface value is largely underestimated, as the photonic resolution cannot resolve membrane folds below a few hundred nanometers.

Strikingly, as seen for membrane tension, the volume response to osmotic shocks was also very asymmetric: - for hypertonic shocks above 1568 mOsm, the volume changed rapidly and reduced by about half (37% \pm 11%). The volume did not recover for the 20 min of observation. Intriguingly, for osmotic shocks ratio values above 2, the volume change was constant, showing that the cell volume could not be compressed more than approximately 2 times. This suggested the existence of a minimal volume V_{min} .

For hypotonic shocks, as seen for tension, the maximum was obtained two minutes after the shock and a rapid recovery was following (Fig2B). Both the volume maximum and the duration of the recovery phase were correlated to the intensity of the shock. To describe better the coupling between volume changes and osmotic difference, we averaged the volume value during the 5 minutes prior to the shock (V₀) and during the 5 minutes following the shock (V), thus containing the peak value. We then plotted $\Delta V/V_0$ as a function of $\frac{\Pi}{\Pi_0}$ and found a continuous – but not linear – relation between volume and osmotic pressure ratio (Fig2C). The relation was very similar to the one we found for tension and osmotic pressure ratio. It suggested that the essential process driving membrane tension was volume change. It is expected that volume changes would change membrane tension proportionally to the change of cell area A. Indeed, we found that $\Delta A/A_0$ was following the exact same relation to $\frac{\Pi}{\Pi_0}$ than tension and volume (Fig 2D and E). We also noted that $\Delta A/A_0$ could take values up to 50%, which is probably coming from two factors: the underestimation of the cell area because of the photonic resolution, and because of the important buffering reservoir of membrane in fibroblastic cells (6, 11). Thus, our results suggested that osmotic shocks would induce a volume change, probably to equilibrate osmotic pressure outside and inside the cell. This change would then drive a change of membrane tension by changing the cell area. A corollary to this hypothesis is that in cases where membrane tension increases (hypotonic shocks) a rounding up of the cells (followed by an increase of the sphericity) should be observed, as well as the reverse in hypertonic conditions. We observed this predicted sphericity change (see suppl. figure **Sup2**), supporting further our hypothesis.

Because of the known role of cytoskeleton in controlling cell volume, membrane tension and shape, we next wondered if the fast response (within 5 min after shock) of the cell was passive, and /or regulated by components of the cytoskeleton.

The short-term response to osmotic shocks is passive and cytoskeleton-independent.

First, the role of actin in the cell response to osmotic shocks was assessed, using Cytochalasin D (CytoD). Cells were treated with 1 uM CytoD for 30 min, before osmotic shock was applied. CytoD-treated cells were observed to have a rounder aspect ratio compared to untreated cells, which may be due to the fact that the volume of cells increased during CytoD treatment (Sup3). However, no impact on the short-term response of CytoD-treated cells to osmotic shocks was observed for area and volume (Sup4A). This was further confirmed by using another actin blocking drug latrunculin A, showing that actin did not play a significant role in the short term response of cells to osmotic shocks (Sup4B).

The fast increase in volume observed upon CytoD treatment can be attributed to a release of the acto-myosin cortex tension applied on the plasma membrane (**Sup3**). Moreover, we can observe that the volume is stable 5 min after CytoD treatment, suggesting that perturbing the cytoskeleton does not break the cell equilibrium but rather shifts it.

Interestingly, the rapid recovery phase of volume, tension and area observed during the 20 minutes following hypotonic shocks was not abolished in actin-drug treated cells (see **Sup6**). This does not support an active role of the actin cortex in allowing cells to recover from hypotonic shocks.

We then assessed the effect of the Microtubule depolymerizing drug nocodazole (Noc). Cells were treated for 30 min with 0.5 uM of nocodazole, and then cells were subjected to osmotic shocks. As observed for actin, no significant changes of the tension, volume and area was observed in the short-term response to osmotic shocks (**Sup4C**). The recovery phase was in this case untouched, suggesting that microtubules did not actively participate in the recovery phase following hypotonic shocks (**Sup6**).

Although actin and microtubule network do not seem to play an important role in the short-term response of the cell to osmotic shocks, we wondered if any other source of energy consumption could play a role in the short-term response. Cells were depleted of ATP by treating them with 2-Deoxyglucose and azide for 60 min (see methods) and were subsequently exposed to osmotic shock. No significant difference in area, sphericity or volume was observed between control and ATP-depleted cells on a short time scale (Sup5). This strongly supported that the initial response to osmotic shocks of fibroblastic cells was passive. However the recovery of volume in hypotonic conditions was fully abolished upon ATP depletion (Sup5).

Our results indicate that the immediate, fast response of cells to acute osmotic shocks is passive and does not require actin. The response to osmotic shocks should thus essentially

involve only membrane as an elastic counter player to volume changes. To verify this assertion, we developed a simple mathematical model to describe our quantitative findings.

Quantitative coupling of cell membrane tension to osmotic shocks.

Based on our experimental results, we built a physical model to quantitatively described the short term response of fibroblastic cells to osmotic shocks: since no active process nor cytoskeletal elements had been implicated, we first postulated that the volume and area changed to equilibrate the osmotic pressure inside the cell to the one of the outside solution. The volume change will concentrate or dilute osmolites inside the cell to equilibrate the inner osmotic pressure with the new external osmotic pressure. Indeed, by plotting the ratio of volume changes along the ratio of osmotic pressure ratio, $\frac{V}{V_0}$ is linear with $\frac{\Pi}{\Pi_0}$ up to a certain osmolarity ($\frac{\Pi}{\Pi_0}$ =2) (Fig3A). Above this value, the volume ratio stays constant, indicating that the cell cannot shrink below a minimal volume V_{min} . Taking into account the proportionality law and V_{min} , we can write the expected dependence law of $\frac{V}{V_0}$ with $\frac{\Pi}{\Pi_0}$:

$$\frac{\pi}{\pi_0} = \frac{1-\varphi}{\lambda^3 - \varphi} \tag{1}$$

Where $\frac{V}{V_0} = \lambda^3$ and $\varphi = \frac{V_{min}}{V_0}$, and is valid only for $\lambda^3 > \varphi$. By plotting $\frac{V}{V_0}$ with $\frac{\Pi}{\Pi_0}$, and fitting with equation one, we found that $\varphi = 0.53$ (see fig.3A).

To compute tension from this volume change, we have to make two postulates: first, we considered cells to be almost spherical shapes, which is not correct since we are using fibroblastic adherent cells, but is a fairly good approximation since cells have on average a high sphericity coefficient ($\varphi_{Average} = 0.71$). Second, we postulated that tension has linear (Hook's law) dependence to area stretching $\sigma = \chi \Delta A/A_0$, where χ is an adimensional compressibility modulus. Combining the two postulates, we obtained:

$$\frac{\sigma}{\sigma_0} = (1 + \chi \left(\frac{A}{A_0} - 1\right)) \tag{2}$$

By plotting the tension ratio $\frac{\sigma}{\sigma_0}$ with the area ratio $\frac{A}{A_0}$, and fitting with equation 2, we find a fairly good agreement and χ = 0.3 (Fig 3B). Interestingly, even though the amplitude of stretching is large (Δ A/A₀ up to 50%), the dependence of tension towards area change is linear, which is the simplest elastic behavior.

Using equation (1) and (2), we can deduce the following law to couple membrane tension changes to osmotic pressure ratios:

$$\frac{\sigma}{\sigma_0} = 1 + \chi \left(\left[\frac{1 + \varphi\left(\frac{\pi}{\pi_0} - 1\right)}{\frac{\pi}{\pi_0}} \right]^{2/3} - 1 \right) \tag{3}$$

We then superimposed the experimental results with equation (3), setting χ and ϕ values to the ones extracted from fits to eq. (2) and (1) respectively. The agreement was good, and fits of the data with (3), leaving χ and ϕ as free parameters, gave similar values. Altogether, the good agreement between experiment results and the simple model, show that membrane tension changes result primarily from a stretch of the membrane driven by a volume change, itself driven by the osmotic shock.

To yield a more quantitative description of this hypothetical frame work, let us consider a spherical cell of volume V_0 and area A_0 (with $V_0=2\pi$ V $_0=2\pi^{-0.5}A^{1.5}$) which adapts its volume and area upon external osmotic changes to equilibrate the external and internal osmotic pressure. The cell contains a concentration C_0 of osmolites having a osmotic pressure Π_0 , and subjected to an osmotic shock changing the external osmotic pressure to Π_0 , which will results in a change of the osmolites concentration to C. Because C changes linearly with Volume V, these considerations give the following relation between V, V_0 , Π_0 and Π : $\Pi = \Pi_0 * V_0/V$

Interestingly, when plotting the volume ratio $\frac{\nu}{\nu_0}$ with the osmotic pressure ratio $\frac{\Pi}{\Pi_0}$ (**Fig3A**) we find a linear relationship with a slope of approximately 0.6 until $\Pi/\Pi_0=2$. This is fairly good agreement with the equation above. However, above $\Pi/\Pi_0=2$, the volume does not change anymore and stay at its minimal value of $V_{min}=2/3$ V_0 . This strongly suggests that the cell cannot compress more than this minimal volume. Moreover, our hypothesis postulates that membrane tension σ change is the direct elastic response to area change. As described in the introduction, in this case, membrane tension ratio σ σ_0 is expected to follow a classical elastic Hook's law towards A/A₀:

$$\frac{\sigma}{\sigma_0} = (1 - \chi(\frac{A}{A_0} - 1))$$

$$\sigma/\sigma_0$$
= (1 - $\chi(A/A_0$ - 1) $\approx \Delta\sigma/\sigma_0$ = - $\chi(A/A_0)$

where χ is the compressibility modulus of the membrane.

By plotting the ratio $\Delta\sigma/\sigma_0$ towards $\Delta A/A_0$, we find a fairly linear relation (**Fig3B**), again confirming that quantitatively, our theoretical framework is valid. However, the slope is $\chi = 0, 3$.

To further test our model, we ought to see if membrane tension followed the expected relation with changes of osmotic pressure. By using the two previous equations and using the sphericity of the cell to calculate the volume from the area, we find that:

By plotting $\Delta\sigma/\sigma_0$ towards Π/Π_0 and fitting with the previous equation, we find a pretty good agreement with low values of Π/Π_0 , but not so good for values of $\Pi/\Pi_0 \geqslant 2$. We reasoned that his could be due to the fact that the cell cannot compress below a minimal volume V_{min} , and in this case, it is expected that the drop of tension would be higher than in the case where volume can adapt continuously.

$$\sigma/\sigma_0 = 1 + \chi((1+\phi(\Pi/\Pi_0-1)/\Pi/\Pi_0)^{2/3}-1)$$

where $\phi = V_{min}/V_0$.

Using this previous equation to fit data of Fig3C (orange), leaving φ and χ as free fitting parameters, we obtain a better fit, with $\chi=1,8$ and $\varphi=0,4$. The value of φ is in very good agreement with the minimal volume we observed in **Fig3A**. The value of χ increases from 0.7 to 1,8 indicating that setting a minimal volume implies a higher elastic parameter. It would be interesting to compare this elastic modulus to known biologic or artificial elastic modulus. Overall, our simple theory of volume adaptation to equilibrate osmotic pressures inside and outside the cell as the instantaneous response of the cell to osmotic shocks, with the limit of a minimal, incompressible volume describes quantitatively our results.

The plasma membrane and actin cortex behavior upon osmotic shock was monitored using fluorescent dyes (Cell Mask Orange and SiR-Actin) (**Fig4**). This led to the observation of localized membrane detachments of the plasma membrane from the cortex in hypotonic conditions. Even though the volume increase approaches 20%, the actin cortex is dynamic enough to follow the membrane and only localized detachment is observed, similar to blebs(14).

DISCUSSION:

A systematic, dynamic, live membrane tension measurement during osmotic shocks was never achieved yet in the literature. Although theories and partial experiments could be used to extrapolate a cell reaction to osmotic shocks, a detail theory was missing.

Historically the relationship between volume and osmolarity were measured in muscle cell (15). Those measurements prompted to postulate a linear relationship between osmotic pressure and volume. Other studies argued for a non-linear relationship (16, 17). In this study, we could confirm that the relationship between volume and osmotic was linear until a certain limit (Fig3A).

The model that was assembled, even though simple, is able to extrapolate membrane tension variation only from osmotic pressure variation. Indeed, cell volume is an accessible parameter. The incorporation of the minimal volume in the equation brought a finer behavior in the extreme range of hypertonic conditions (**Sup7**). Although microtubule and actin do not seem to play an important part in the short-term response, the nucleus or the intermediate filaments might be the potential actors for the non-linearity of volume and osmolarity relationship. This in contradiction of a poro-elastic model, that contains a highly important cytoskeleton cortex (*18*). Moreover, the global diffusion hydrophilic properties of proteins in the cytoplasm might be responsible for the minimal volume observed, even though no difference of diffusion coefficient of cytoplasmic GFP in *E.Coli* under osmotic stress (*19*).

The compressibility modulus for phosphatidylcholin (PC) bilayers is 250 mN.m⁻¹(20) and between 95 and 195 mN.m⁻¹-in red blood cells (21). In our results the compressibility modulus of 34 mN.m⁻¹ for HeLa cells is observed. This is in the range of previously calculated

cells.

Our theory present itself with some limitations. First of all, it assumes a conservation of the cell shape. However, it was observed that the cell increases its sphericity in hypotonic shock (**Sup2**). Morever, this model derives only from one typical cell (HeLa Kyoto), as different cells can present different membrane tension(22) and membrane composition(23).

To conclude, we were able to measure membrane tension and volume variation upon osmotic shocks and construct a model containing few parameters.

Materials and methods.

HeLa Kyoto cells were cultured in Minimum Essential Media supplemented with 10% Fetal Bovine Serum and 1% Penicillin Streptomycin (Life Technologies, Carlsbad, CA, USA) 5% CO₂ incubator (Thermo Scientific, Waltham, MA, USA).

Microscopy: Two setup were used for imaging.

The first is composed of an inverted Nikon Ti-E system, a Yokogawa CSU-X1 Confocal ScannerUnit, a iXon camera (Andor, Belfast, NIR, UK), a Laser stack by Intelligent Imaging Innovatios Inc (Denver, CO, USA), a 37°C incubator (Life Imaging service, Basel, Switzerland), 2 micro-manipulator MP-285 (Sutter, Novato, CA, USA) and a home-made optical tweezer with a 1A Manlight laser.

The second is composed of an inverted Nikon Ti-E system, a Yokogawa CSU-W1 ConfocalScanner Unit, an Evolve camera (Photometrics, Tucson, AZ, USA) a Laser stack by IntelligentImaging Innovations, Inc (Denver, CO, USA), a 37°C incubator (Life Imaging service, Basel, Switzerland), a 37°C incubator (Life Imaging service, Basel, Switzerland), an H301 CO₂ incu-bator (Okolab, Pozzuoli, NA, Italy) and MP-285 (Sutter, Novato, CA, USA).

All images were acquired Slidebook software (Denver,CO, USA) and processed using ImageJ soft-ware (Public Domain).

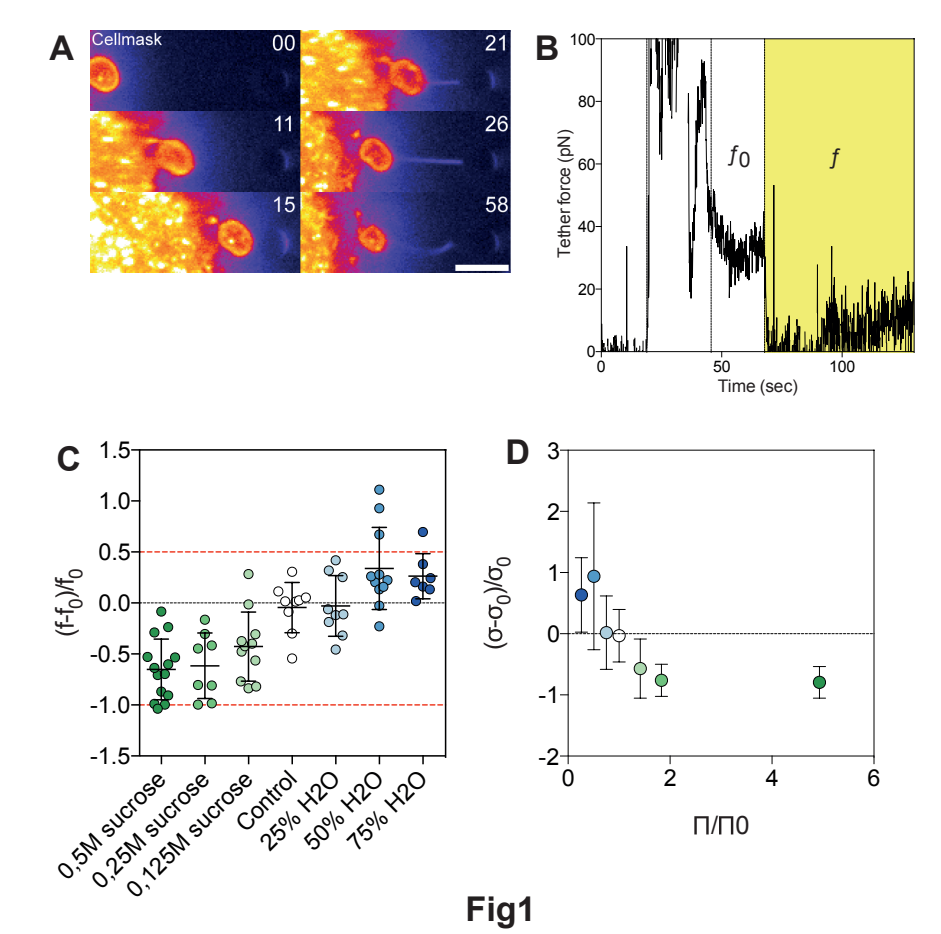
Membrane integrity measurement: HeLa Kyoto cells were incubated for 5 min with Propidium Iodide 160 μ g/mL then observed. 1% Saponin was used as a positive control.

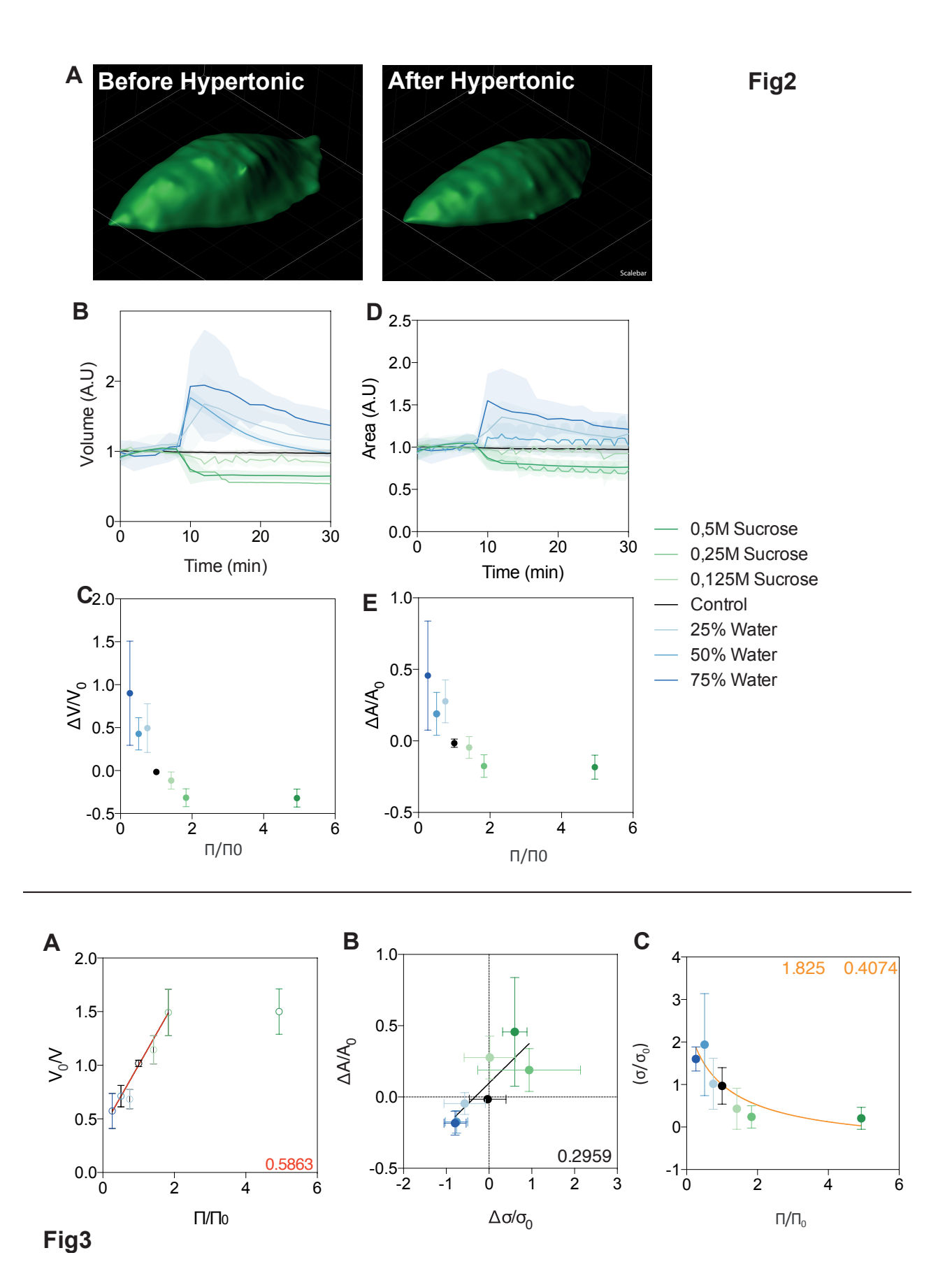
References

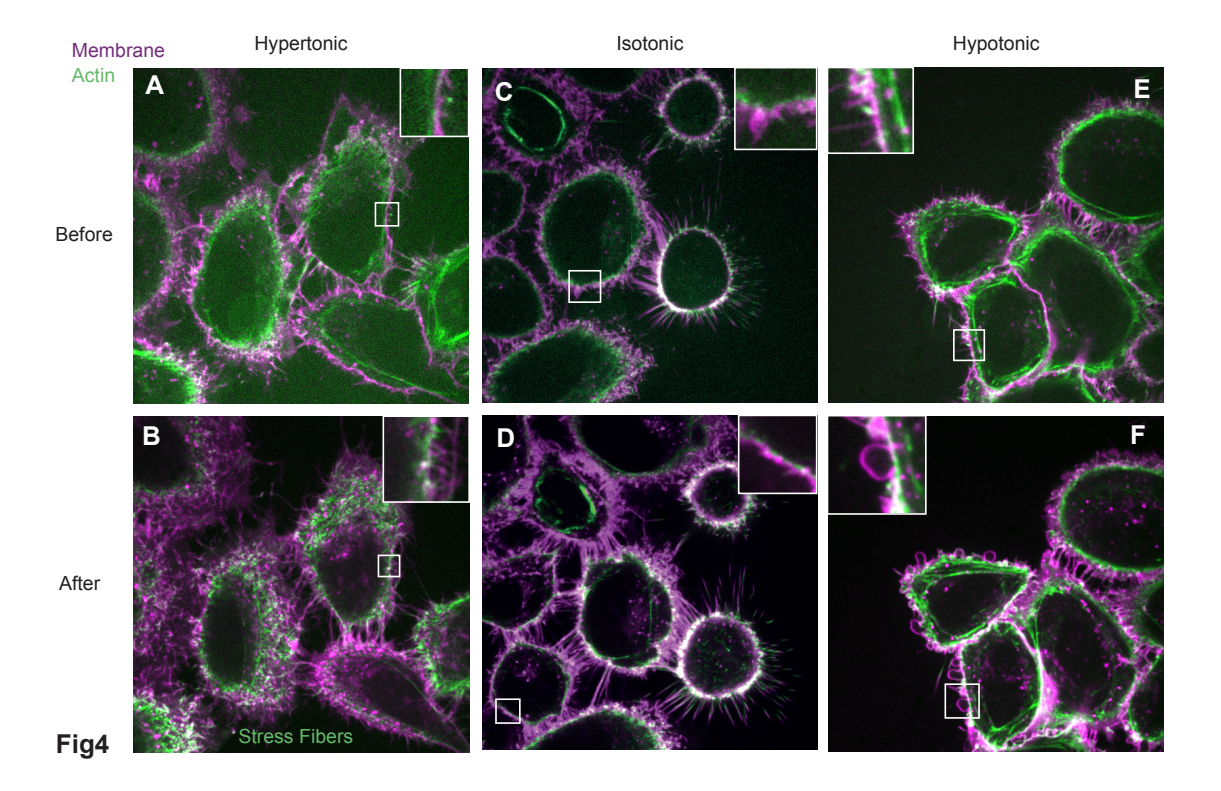
 A. D. Lieber, S. Yehudai-Resheff, E. L. Barnhart, J. A. Theriot, K. Keren, Membrane Tension in Rapidly Moving Cells Is Determined by Cytoskeletal Forces. *Current Biology*. 23, 1409–1417 (2013).

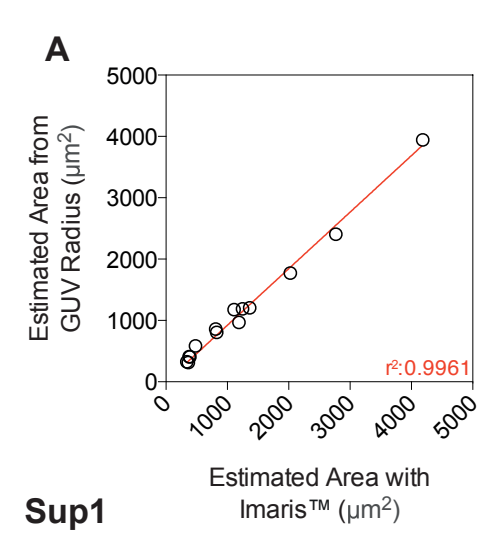
- C. Gabella et al., Contact Angle at the Leading Edge Controls Cell Protrusion Rate. Current Biology. 24, 1126–1132 (2014).
- 3. S. J. Singer, G. L. Nicolson, The fluid mosaic model of the structure of cell membranes. *Science*. **175**, 720–731 (1972).
- 4. H. Yu, J. K. Mouw, V. M. Weaver, Forcing form and function: biomechanical regulation of tumor evolution. *Trends in Cell Biology*. **21**, 47–56 (2011).
- E. K. Hoffmann, I. H. Lambert, S. F. Pedersen, Physiology of cell volume regulation in vertebrates. *Physiol. Rev.* 89, 193–277 (2009).
- B. Sinha et al., Cells Respond to Mechanical Stress by Rapid Disassembly of Caveolae. 144, 402–413 (2011).
- D. Berchtold et al., Plasma membrane stress induces relocalization of SIm proteins and activation of TORC2 to promote sphingolipid synthesis. Nature Cell Biology. 14, 542–547 (2012).
- 8. J. Dai, M. P. Sheetz, Mechanical properties of neuronal growth cone membranes studied by tether formation with laser optical tweezers. *Biophysj.* **68**, 988–996 (1995).
- 9. N. C. Gauthier, T. A. Masters, M. P. Sheetz, Mechanical feedback between membrane tension and dynamics. *Trends in Cell Biology*. **22**, 527–535 (2012).
- 10. A. Diz-Muñoz, D. A. Fletcher, O. D. Weiner, Use the force: membrane tension as an organizer of cell shape and motility. *Trends in Cell Biology*. **23**, 47–53 (2013).
- 11. D. Raucher, M. P. Sheetz, Characteristics of a Membrane Reservoir Buffering Membrane Tension. *Biophysj.* **77**, 1992–2002 (1999).
- 12. E. Zlotek-Zlotkiewicz, S. Monnier, G. Cappello, M. Le Berre, M. Piel, Optical volume and mass measurements show that mammalian cells swell during mitosis. *The Journal of Cell Biology*. **211**, 765–774 (2015).
- 13. M. L. Gray, R. A. Hoffman, W. P. Hansen, A new method for cell volume measurement based on volume exclusion of a fluorescent dye. *Cytometry*. **3**, 428–434 (1983).
- 14. G. T. Charras, A short history of blebbing. Journal of Microscopy. 231, 466–478 (2008).
- 15. J. R. BLINKS, INFLUENCE OF OSMOTIC STRENGTH ON CROSS-SECTION AND VOLUME OF ISOLATED SINGLE MUSCLE FIBRES. J. Physiol. (Lond.). 177, 42–57 (1965).
- 16. M. DYDYNSKA, D. R. WILKIE, THE OSMOTIC PROPERTIES OF STRIATED MUSCLE FIBERS IN HYPERTONIC SOLUTIONS. *J. Physiol. (Lond.).* **169**, 312–329 (1963).
- 17. J. P. REUBER, E. LOPEZ, P. W. BRANDT, H. GRUNDFEST, MUSCLE: VOLUME CHANGES IN ISOLATED SINGLE FIBERS. *Science*. **142**, 246–248 (1963).
- 18. H. Jiang, S. X. Sun, Cellular pressure and volume regulation and implications for cell

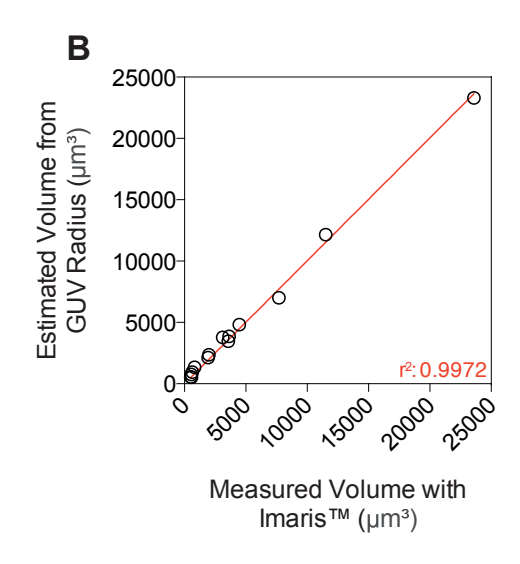
- mechanics. Biophys. J. 105, 609-619 (2013).
- 19. K. A. Sochacki, I. A. Shkel, M. T. Record, J. C. Weisshaar, Protein diffusion in the periplasm of E. coli under osmotic stress. *Biophys. J.* **100**, 22–31 (2011).
- 20. W. Rawicz, K. C. Olbrich, T. McIntosh, D. Needham, E. Evans, Effect of chain length and unsaturation on elasticity of lipid bilayers. *Biophysj.* **79**, 328–339 (2000).
- 21. E. A. Evans, R. Waugh, L. Melnik, Elastic area compressibility modulus of red cell membrane. *Biophysj.* **16**, 585–595 (1976).
- 22. J. Dai, M. P. Sheetz, Membrane tether formation from blebbing cells. *Biophysj.* **77**, 3363–3370 (1999).
- 23. X. L. Guan *et al.*, Biochemical membrane lipidomics during Drosophila development. *Developmental Cell.* **24**, 98–111 (2013).

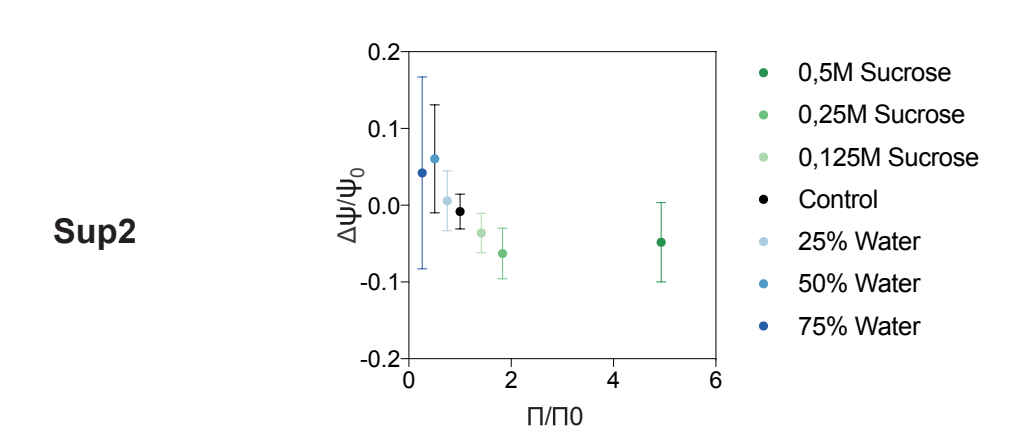


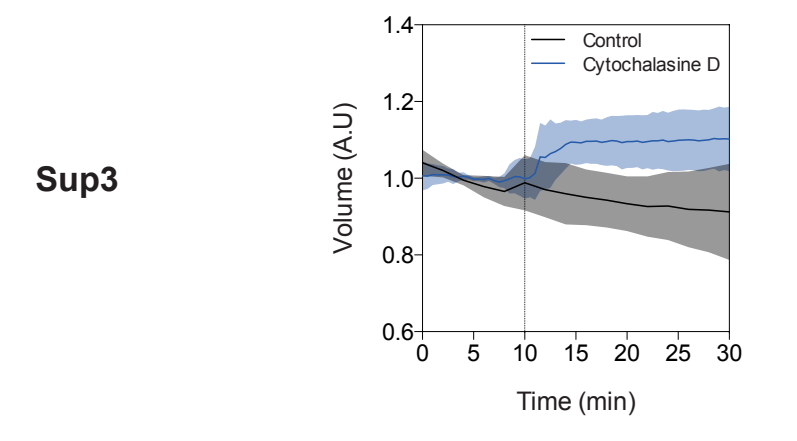


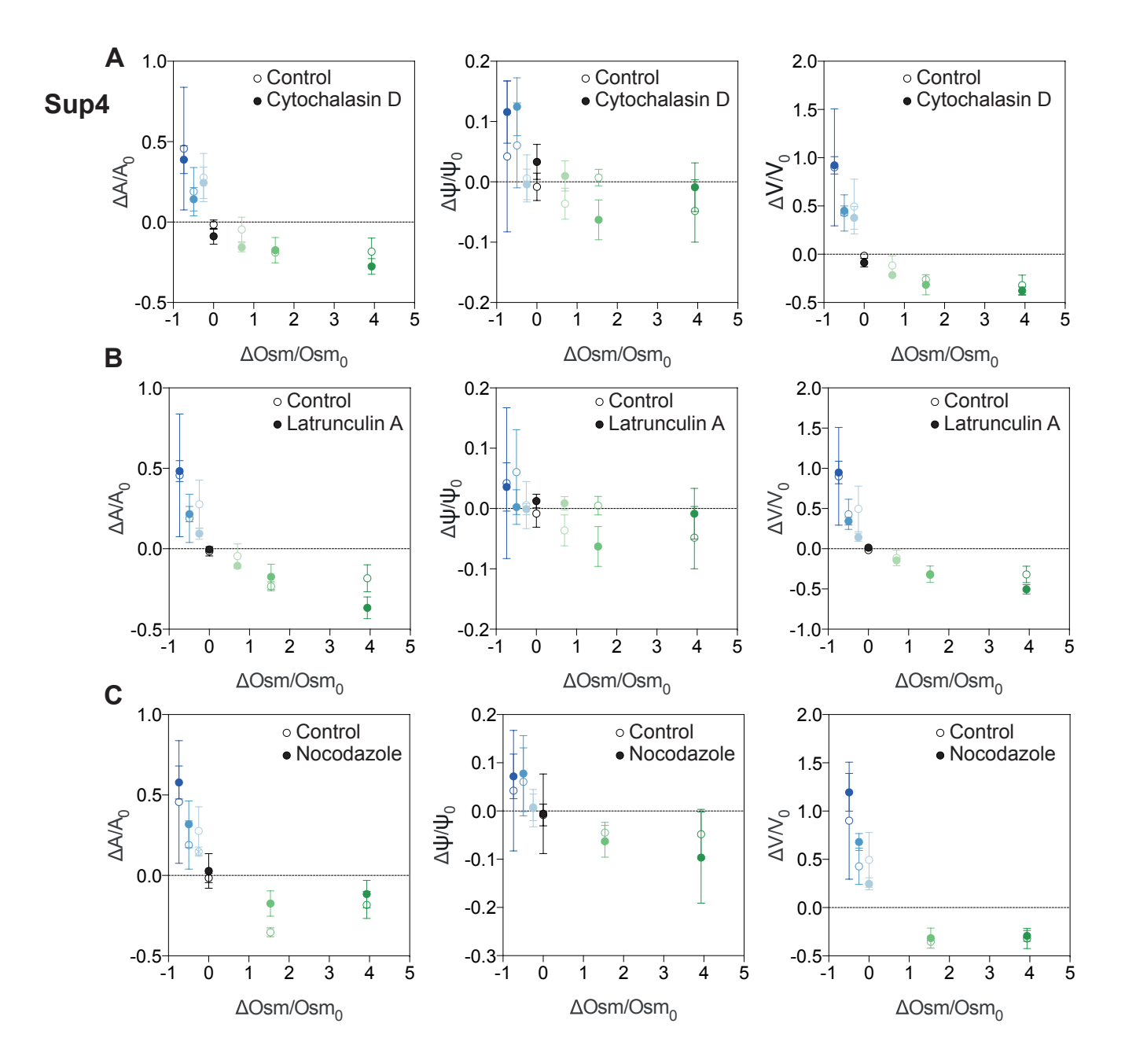


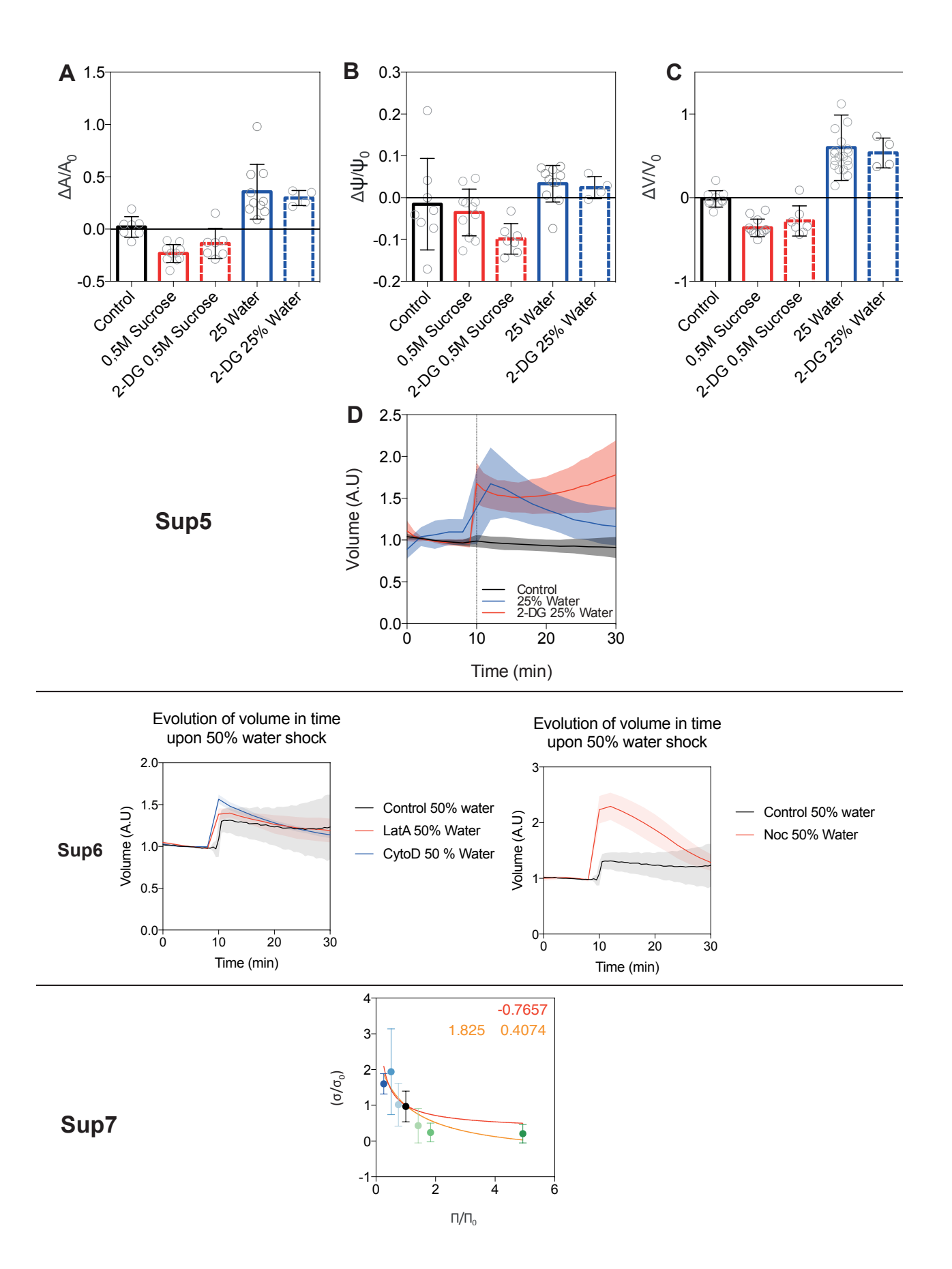












4.2 ESCRTS AND MEMBRANE

4.2.1 Protein activity and membrane tension

As mentioned in the introduction, membrane tension (σ) can influence protein activity ^{61,124}.

In the interest of exploring the relationship between osmotic pressure and CHMP4B-GFP behaviour a wide range of osmotic shocks were performed on HeLa Kyoto cells. CHMP4B-GFP punctae number was measured using the "Analyze particle" tool in ImageJ software. In Fig. 4.2.1, on the one hand we can observe that hypotonic shocks bear no impact on this recruitment. On the other hand we can find out that hypertonic shock have a meaningful impact at around 600 mOsm.

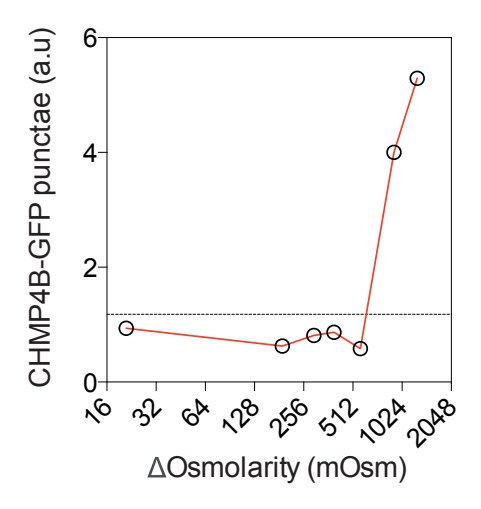


Figure 4.2.1: CHMP4B-GFP puncta osmolarity response.

Indirect evidence suggested that ESCRT-III might be regulated by membrane tension ^{90, 91}. However ESCRT-mediated membrane fission remains elusive and the best evidence for it remains cryoelectron-tomography ¹²⁵, as *in vitro* studies brilliantly dissect the biochemical structures and binding properties but have failed to replicate membrane fission so far.

The main protein subunit of the ESCRT-III complex is charged multivesicular body protein 4b (CHMP4B). A stable cell line transformed with this protein fused to the reporter green fluorescent

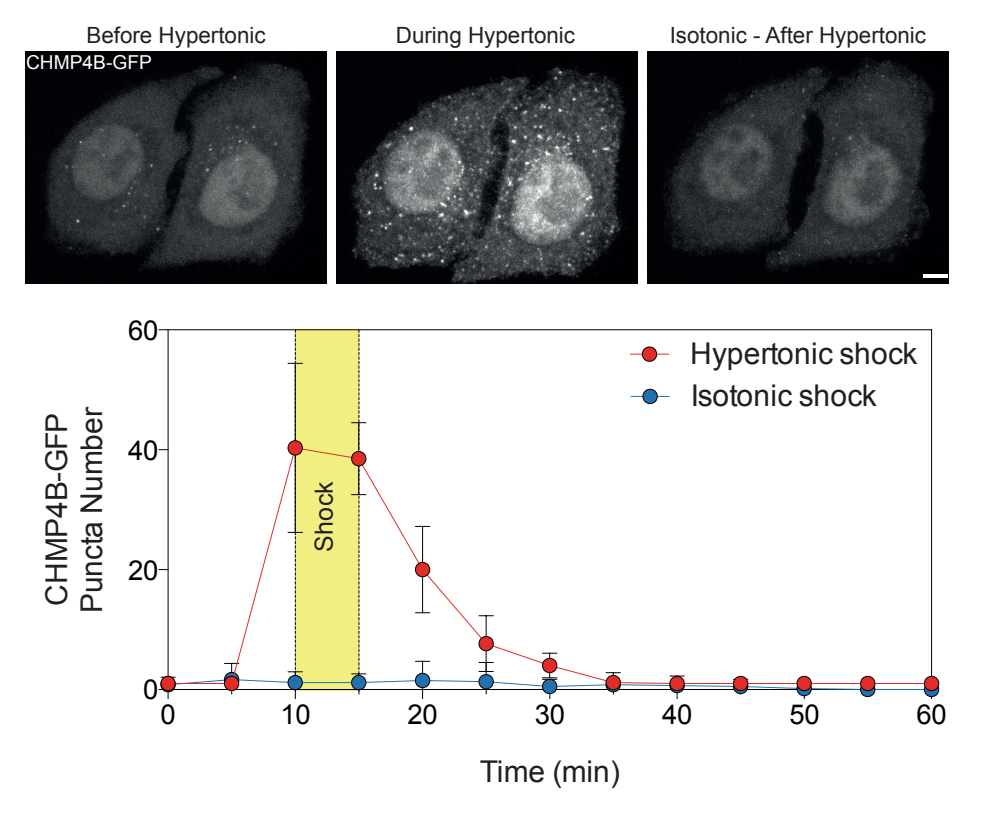


Figure 4.2.2: CHMP4B-GFP HeLa Kyoto cells upon hyper-osmotic shock. Scale bar is 5μ m (top). Quantification of the puncta phenotype (bottom).

protein (GFP) in its chromosomal environment in a bacterial artificial chromosome (BAC) was developed by the Hyman laboratory and kindly provided by the Piel laboratory. Indeed a slight increase or decrease in ESCRT-III subunits concentrations in the cell leads to tubulation or unfit cells due to the numerous roles of ESCRTs in the cellular processes.

CHMP4B-GFP basal expression present a diffuse cytoplasmic signal with sparse puncta in the cytoplasm. Interestingly, the nucleus signal is particular as the chromatin is staining in a specific pattern. The CHMP4B-GFP signal in the nucleus resembles to a nucleolus staining. Indeed CHMP proteins were classified as chromatin modifying protein (CHMP) later changed to charged multivesicular body protein due to evidence of its role in membrane traffic.

Curiously, puncta number was increased in the cytoplasm of HeLa Kyoto cells (Fig. 4.2.2), but not

in a proportional manner. As the main activity of ESCRT-III complex in interphase cells is the MVB formation, it is not surprising that the protein signal is enhanced in a endosomal-like pattern. On top of that, this effect is transient as the flushing of isotonic media reversed this behaviour in 15 min. This is an indirect indication that those CHMP4B puncta are not simply protein aggregate.

As it was previously shown that hypertonic shocks affects plasma membrane tension and cell volume, it is possible to postulate that by reducing the volume of the cell, cytoplasmic concentration of solutes (ions and proteins) increases thus imposing an hyper-tonic shock on cytoplasmic compartments. Therefore early, late endosomes and MVB might behave in a similar fashion as the cell. That would imply a decrease in $\sigma_{endosome}$ and $V_{endosome}$.

CHMP4B-GFP can be recruited *in vivo* in the cytoplasm by hypertonic shock. This effect is rapid and dose-dependent.

CHMP4B-GFP or its yeast counterpart Snf7 has been shown *in vitro* to polymerise on bare membrane and preferentially on curved membrane ^{126, 127}. However, the influence of membrane tension on CHMP4B polymerisation has not yet been reported. Certain proteins polymerisation were shown to be mainly curvature-dependent *in vitro* ¹²⁸.

In order to check if negative membrae curvature could trigger CHMP4B polymerisation *in vivo*, membrane tethers were pulled from HeLa Kyoto cells stably expressing CHMP4B-GFP. Plasma membrane was stained with Cell Mask. After several attempts and repetition no visible recruitment of CHMP4B-GFP was observed in the tube or at the base of the membrane (Fig. 4.2.3). The number of CHMP4B-GFP protein present at the membrane vicinity or in the tube might not be enough to visualize in live-cell imaging. In the direction of cumulating curvature and tension, observing the presence of CHMP4B-GFP at the base of the tube during hyper tonic shock would be a good experiment to perform.

Plasma membrane bending by tether extraction is not sufficient to polymerise CHMP4B-GFP. Curvature is not sufficient to induce CHMP4B-GFP polymerisation, contrary to membrane tension.

During an hypertonic shock, the volume of the cell is reduced therefore the cytoplasmic protein concentration increases. Similarly, Snf7 (the *Saccharomyces cerevisiae* homolog of CHMP4B) nucleation rate and radial growth speed has been shown to be concentration dependent *in vitro* 99. To assess

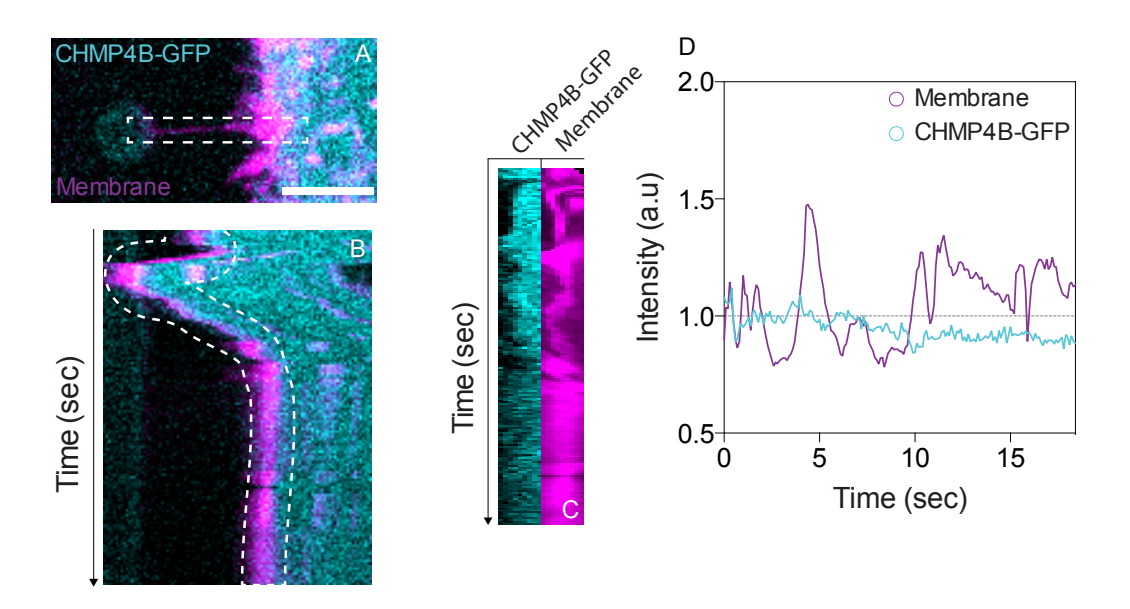


Figure 4.2.3: CHMPless tubes. A) Still image of a tube pulled using optical tweezer. B) C) Straightified along the membrane edge D) Evolution of CHHMP4B-GFP signal at the tube base along time

the nature of those CHMP4B-GFP puncta and to rule out an observation of aggregates, an ATP depletion experiment was performed (Fig. 4.2.4). Indeed, if those puncta were to be aggregates, they would have no particular relationship to ATP, contrary to polymers of ESCRT-III.

Firstly, ATP was partially depleted from the cell for 15 minutes using 2-DG and sodium azide as previously described. Then a mild hypertonic shock was applied on the cells in an ATP-depleted media. To conclude, isotonic conditions were restored and the inhibition of ATP-production was removed. This experiment (Fig. 4.2.4 top) led to the previously observed polymerisation of CHMP4B-GFP in the cell during the osmotic shock and its disappearance after the shock is passed. This shows that the polymerisation is not ATP-dependent.

On a second experiment (Fig. 4.2.4 bottom), ATP-depletion is performed before, during and after the hyper-osmotic shock. In these conditions, the CHMP4B-GFP puncta remains present even after isotonic conditions have been restored. This experiment show that the depolymerisation of osmotic shock induced CHMP4B-GFP puncta is ATP-dependent. Since Vps4p, the yeast homolog of the mammalian AAA ATPase VPS4, is involved is normal endosome function ¹²⁹. Moreover VPS4

ATP use is postulated to be either the driving force of membrane fission via the polymerisation of the ESCRT-III polymer, or a more unique recycling property ¹³⁰. To confirm this theory a knock-down of VPS4 via the use of siRNA could be performed. However contrary to the ATP-depletion, a siRNA knock-down is a long-term experiment that could have numerous long-term and across the cell consequences.

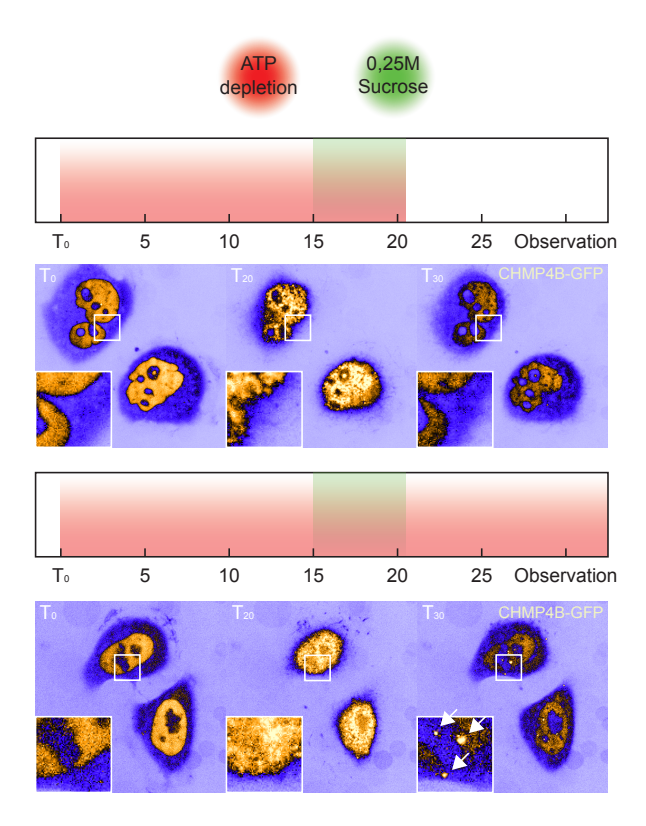


Figure 4.2.4: CHMP4B-GFP polymerisation (top) and depolymerisation (bottom) dynamics, ATP and osmotic-dependency.

ATP depletion does not affect the polymerisation ability of CHMP4B-GFP *in vivo*. However its depolymerisation competencies are greatly affected suggesting that osmotic shocks induce native ESCRT-III complex polymerisation and not aggregates.

4.2.2 ESCRT PERTURBATION IN CYTOKINESIS

In the interest of testing the dependency of CHMP4B-GFP to membrane tension in an other cellular context than endocytosis, cytokinesis was observed. Indeed ESCRT has been shown to be involved in cytokinesis in manner similar to retroviral budding 73,131 and CHMP1B an ESCRT subunit was shown to be critical for the timing of Aurora B-mediated abscission checkpoint 91 . Moreover, the size of the intercelullar bridge diameter ($\approx 2~\mu m$) allows for a detailed observation in light microscopy. On top of that ESCRT-III is regulated by different protein complexes might shed a light on its regulation, if it is membrane tension independent.

To confirm the hypothesis that CHMP4B-GFP reacts to a lowering of membrane tension, osmotic shocks were performed on HeLa Kyoto cells not at interphase but during late telophase.

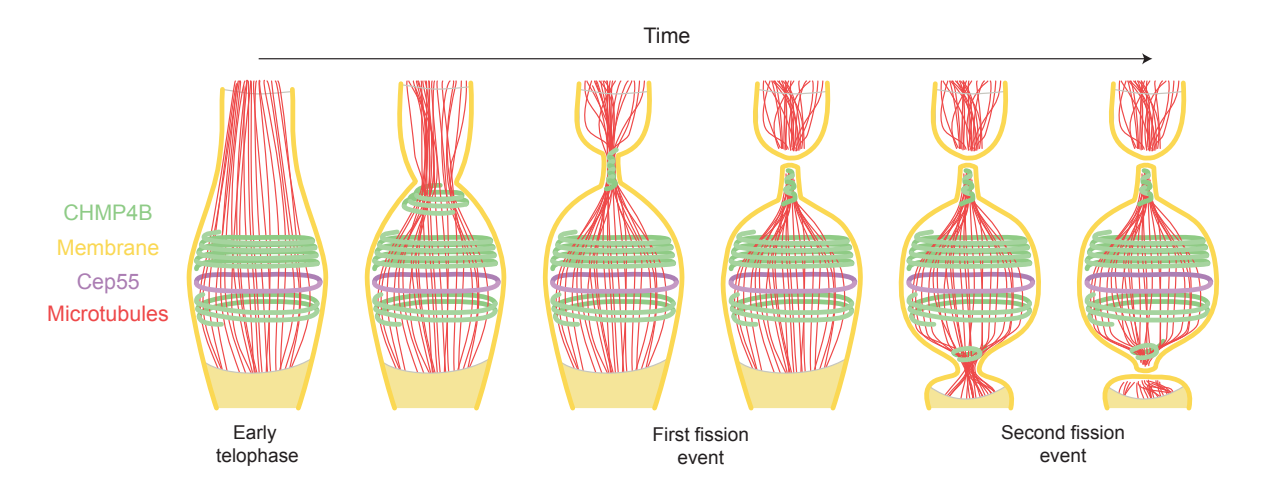


Figure 4.2.5: Schematic evolution of major protein involved in cytokinesis during telophase in the inter-cellular bridge.

Hyper-osmotic shocks were performed on a CHMP4B-GFP Jupiter-mCherry HeLa Kyoto cell line. Jupiter is a microtubule associated protein (MAP) ¹³² that binds to microtubules. The Jupiter gene has been cloned from *Drosophila melanogaster*. Because it is a MAP, Jupiter-mCherry allow the visualization of microtubule structures in cells, and because it is from *Drosophila* origin does not perturb the microtubules dynamics nor the recruitment of its partners (other MAPs), in mammalian cells.

In Fig. 4.2.6 the absence of CHMP4B-GFP polymer at the abscission bridge (early telophase),

an hypertonic shock triggers the recruitment and/or polymerisation of CHMP4B-GFP at the midbody (right). However this recruitment is different from the 2 rings observed in regular telophase (top left). Indeed CHMP4B-GFP are present in the middle of the midbody. This mis-localisation is unprecedented so far, even upon mutation and/or knock down of the ESCRT components.

Moreover, in late telophase, when the two characteristic rings of CHMP4B-GFP flanks the midbody, and hypertonic shock trigger a collapse of those 2 rings in one compared to a classic cyotkinesis (Fig. 4.2.5).

This striking phenotype was never observed to our knowledge. Indeed, the protein density observed in electronic microscopy and the difficulty to stain midbody components using antibody promote a space-deprived environment ¹³³. Moreover the recruiting platform does not assemble in this fashion as seen in Fig. 4.2.5.

An explanation for the space could be hinted by the rapid disassembly of the microtubules at the midbody.

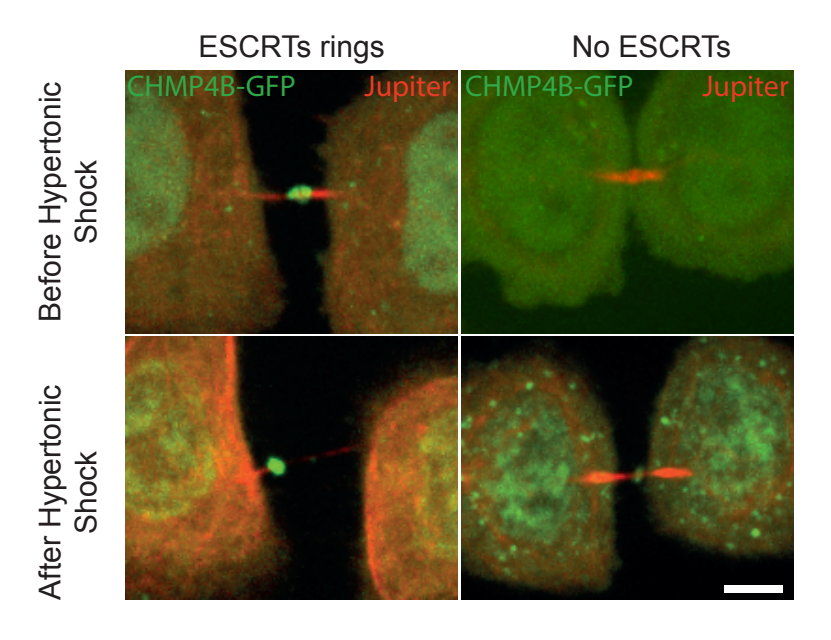


Figure 4.2.6: CHMP4B-GFP rings behavior before and after hyperosmotic shock in early and late telophase. Scale bar is 10 microns

Indeed microtubule behavior, visualised by Jupiter-mCherry in this experiment, is greatly influ-

enced by hypertonic shocks: a rapid disappearance is observed in the midbody. Moreover, the midbody diameter is thinning during this shock.

Kymograph

Kymograph, derived from the greek kuma (wave) and graphō (to scratch) was a mechanical device invented by Thomas Young in 1807 ¹³⁴. Nowadays it is a mode of graphical representation that allow us to represent and analyze a one-dimension sample along time. However due to the movement of the daughter cells and the biologic nature of the abscission bridge, its evolution could not be monitored by a simple straight line kymograph. A 5 points, 3 lines kymograph was designed in order to follow it, with the help of Emmanuel Derivery. The central point was fixed on the midbody, while the others followed the curvature and the movement of the two half bridges.

In Fig. 4.2.7 Jupiter mCherry, a microtubule reporter fluorescence signal along the intercellular bridge, centered on the midbody was averaged along the time among several cells. This averaging led to a clean and smooth representation of the hypertonic shock phenotype on microtubule. Indeed, before the osmotic shock, the maximum signal intensity can be observed at the midbody (center). After osmotic shock (red dotted line) a clear profile inversion can be remarked. MT reporter fluorescence is slowly going down in the midbody and increase in the bridge.

On the other hand CHMP4B-GFP is absent before shock and recruited right after it (Fig. 4.2.7 (right)). The dynamics of those two proteins being different indicate a rather indirect link between the two, through other protein partners.

In order to rule out any bias coming from the Jupiter-mCherry reporter of microtubules, 2 other microtubule reporters were tested in hyper-osmotic shock condition. Firstly SirC8 (SiR-Tubulin), a docetaxel-bound compound that a silicon-rhodamine moiety that fluoresces in the far-red spectrum to polymerised tubulin only ¹³⁵. Secondly, *a*-tubulin-RFP was tested.

In Fig. 4.2.8, both probes labelling microtubule behave in a similar fashion as the Jupiter-mCherry reporter, with a profile inversion. Microtubule reporter leave the midbody and extend outwards to the daughter cells.

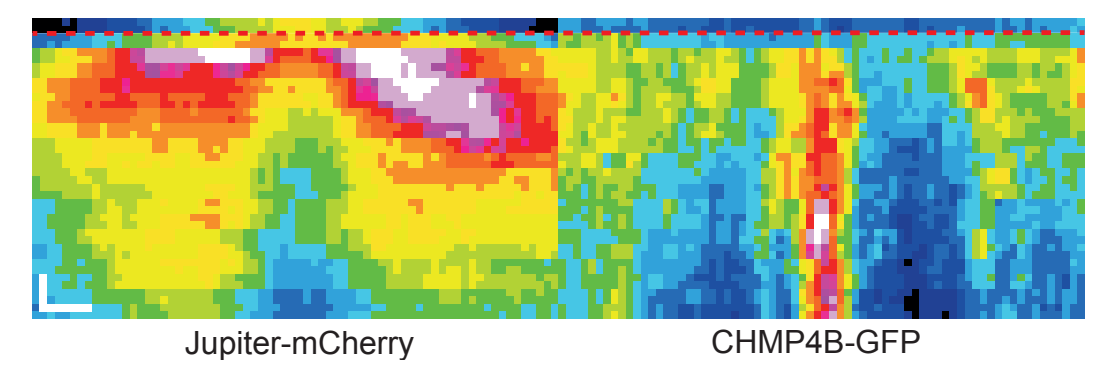


Figure 4.2.7: Averaging of Jupiter-mCherry (left) and CHMP4B-GFP (right) in time. Hyperosmotic shocks at the dotted red line. Time scale bar (vertical) represents 5 min, space scale bar (Horizontal) represents 1 micrometer.

Kymograph averaging of both microtubule and CHMP4B reporter helped for quantitative analysis. The rapid recruitment of CHMP4B-GFP and the disappearance of microtubule from the midbody could be assessed clearly with this method.

Surely, as formerly described, ESCRT-III have a great impact on cytokinesis at the late telophase stage.

In order to test for a direct membrane perturbation on CHMP4B-GFP and cytokinesis, a cell aspirator was designed (Fig. 4.2.9).

Indeed, the use of micro-pipettes has already been used to modulate cell tension ^{136, 137}. The challenges for holding a pair of dividing cell were numerous. As the set-up was designed no CO₂ was available in order to buffer the pH of the growth medium. However the 37°C implied a high evaporation rate. A constant flow of fresh and sterile Leibovitz medium was not sufficent to remedy this difficulty. The evaporation problem was circumvented using Ovoil™, a paraffin oil used in human IVF technique. It allowed to eliminate completely any evaporation whilst remaining non-toxic (most mineral oil are toxic for cell culture)

The tip of the pipettes was fire forged in order to smoothen its surface of contact to the cell ¹³⁸. That allowed to decrease the inner radius of the pipette while having a constant outer radius. This shape was similar as the pipette holding the ovula during IVF.

Bending of the pipette gave rise to the final design as seen in Fig 4.2.9. A tight control of the aspi-

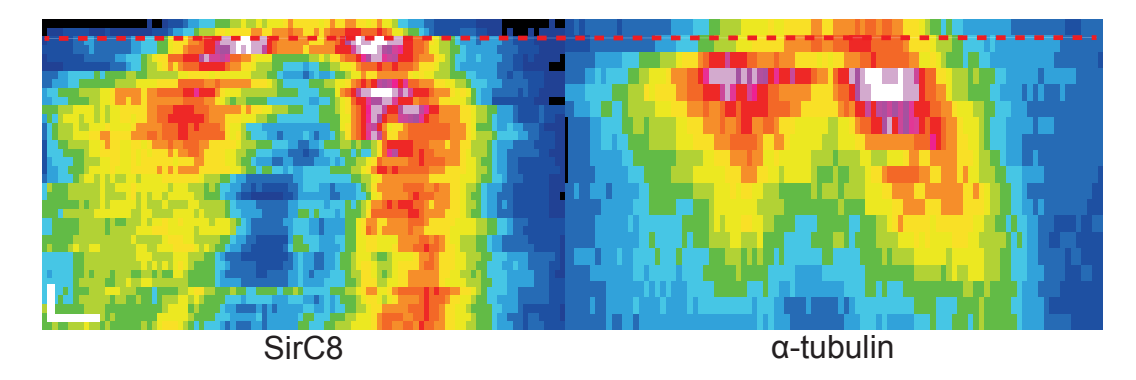


Figure 4.2.8: Averaging of SirC8 (left) and α -tubulin (right). Hyper-osmotic shocks at the dotted red line. Time scale bar (vertical) represents 5 min, space scale bar (Horizontal) represents 1 micrometer.

ration negative pressure was achieved using MFCS-VAC (microfluidic pressure controller) instead of the traditional water tank mounted on Zaber™actuator.

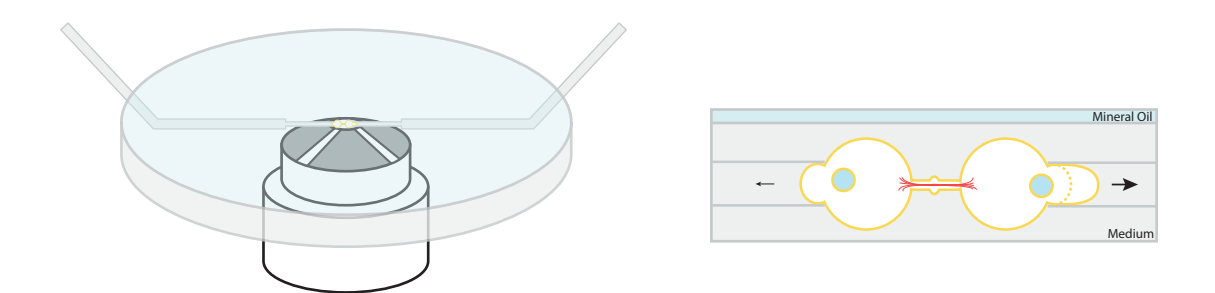


Figure 4.2.9: Cell aspirator.

Nevertheless, no recruitment of CHMP4B-GFP was observable. Besides, no breaking of microtubules (MT) could be detected in Fig. 4.2.10, even when cells where pulled apart (Data not shown).

Putative increase in membrane tension and cell stretching had no positive impact on CHMP4B-GFP recruitment. On the contrary it seemed to inhibit it.

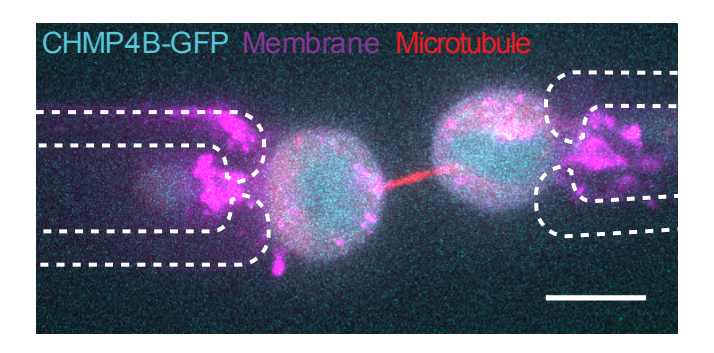


Figure 4.2.10: CHMPless cells aspirated. Pipettes outlined in white. Scale bar is 10 microns

Controls

Centrosomal associate protein 55 (Cep55) discovered in a bioinformatics screen is a mitotic phosphoprotein that paly an essential role in abscission by recruiting the ESCRT machinery and endobrevin, a protein involved in membrane fusion 139. Cep55 is phosphorylated by the mitotic kinase Cdk1 (Cyclin-dependent Kinase 1) and ERK2 (Extracellular signal-regulated kinase 2) and its stability is thightly regulated throughout the cell cycle 140. Defects in the expression or the phosphorylation of Cep55 lead to mitotic failure and multi-nucleate cells 141. Being an ESCRT-recruiting platform and having a telophase localisation in the midbody, observing its behaviour under hyper-osmotic stress is crucial. Stably BAC-transformed HeLa Kyoto expressing Cep55-GFP were observed upon hyperosmotic shock (Fig. 4.2.12). The localisation of Cep55-GFP remains constant after applying a 0,5M Sucrose shock. It does not disappear in a similar fashion as the microtubules, that behave here as a positive control of the shock (thinning and disappearing). Moreover, the sudden recruitment of CHMP4B-GFP is not associated with a de novo recruitment of Cep55-GFP. On top of that, the complex movement of both CHMP4B-GFP and microtubules do not provoke a flushing mechanism on CEP55-GFP. Further analysis of Cep55 phosphorylation state upon those osmotic shocks and the dependency of CHMP4B-GFP recruitment to Cep55 via siRNA or CRISPR-Cas9 cells could be characterised in order to describe this complex pathway.

Cep55-GPF localisation is not affected upon osmotic shocks and its fluorescence does not increase.

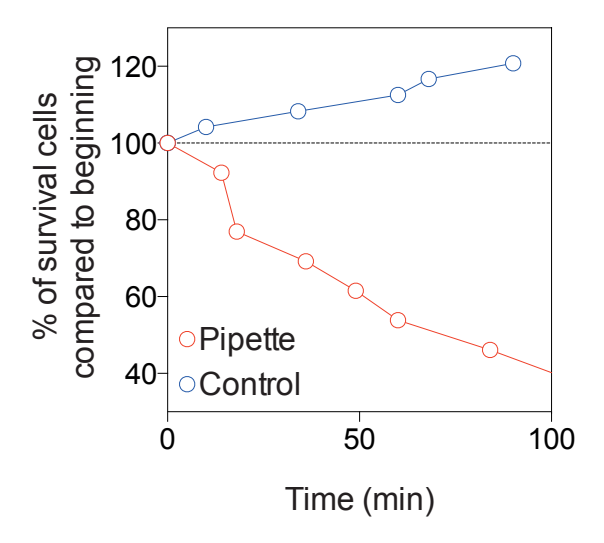


Figure 4.2.11: Cell aspirator survival.

Interestingly, LatA treatment affects membrane tether force in various ways (Fig4.2.13):

In some cases the value increases while other ones decrease. How those these cases differ remains unknown, however a mild LatA treatment on HeLa-Kyoto CHMP4B-GFP stable cell line in late telophase induced a recruitment of CHMP4B-GFP in a similar fashion as the hyper-osmotic shocks although slower (Fig4.2.14). In this experiment the characteristic disappearance of the microtubules is not striking, despite the clear changes in microtubule bundles in the inter-cellular bridge connecting the two daughter cell.

LatA treatment provokes the recruitment of CHMP4B-GFP to the midbody in a similar fashion as the osmotic shocks and microtubule rearrangement.

4.2.3 CYTOKINESIS TIMER

Mammalian cell synchronization can be performed by chemically inhibiting DNA synthesis or mitotic spindle formation and growth factor removal ¹⁴². However those techniques are known to create some bias, especially if the cytoskeleton has to be observed.

In order to synchronize movies of different times a cytokinesis timer was designed, based on the

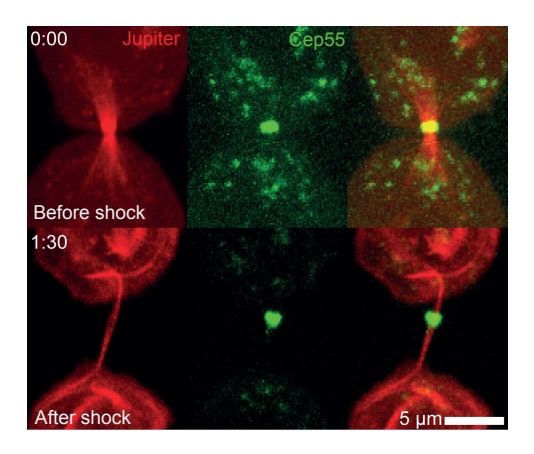


Figure 4.2.12: Cep55 behaviour upon hyperosmotic shock.

midbody size parameters. Prior tools have been developed in *Drosophila melanogaster* using the midbody as a reference point and the microtubules as an axis and timer, however they were not applicable to mammalian cell line ¹⁴³.

Indeed the midbody is the remains of the acto-myosin ring that segregate the mother cell into two daughter cells. The timing and speed of its contraction is critical for mitosis success. It contracts at the equatorial plane of the cell from metaphase to telophase. A ratio of the minimum bridge diameter and midbody diameter was used to time cytokinesis (Fig. 4.2.15). As expected the relationship between the bridge diameter and the midbody diameter is perfectly linear in the anaphase (Fig. 4.2.15 A). However during the telophase, the linear relationship is conserved but faint (Fig. 4.2.15 B).

In the right part of Fig. 4.2.15, no statistically relevant difference can be drawn in between bridge ratio prior to CHMP4B-GFP recruitment (blue), during CHMP4B-GFP recruitment (red) or after CHMP4B-GFP recruitment (green).

Averaging data depending on the presence or absence of CHMP4B-GFP on the bridge in Fig. 4.2.16 show the linear progression of the ratio from the absence (red), to the recruitment (blue) and to the complete recruitment (green). However the noise is too great for drawing any precise timing from those ratio.

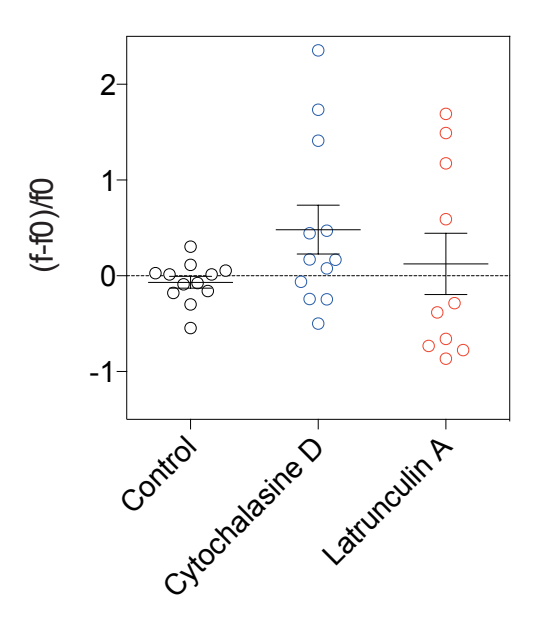


Figure 4.2.13: 2 μ M Latrunculin A and 1 μ M Cytochalasin D treatment on pulled tubes.

Midbody and inter-cellular bridge diameter ratio is a good tool for anaphase timing however it is not precise enough to be adopted as a telophase clock.

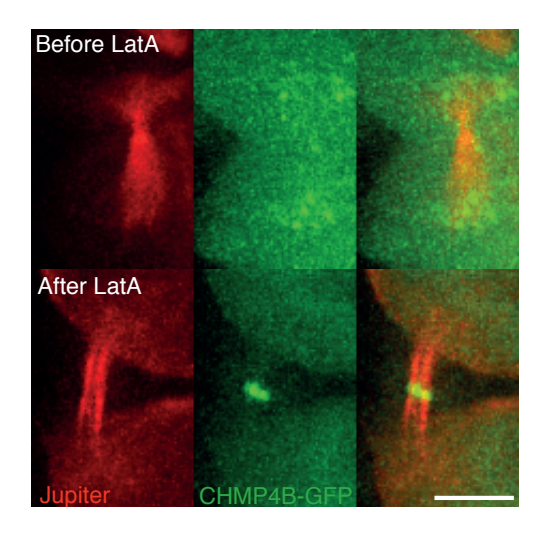


Figure 4.2.14: 2 μ M Latrunculin A treatment on telophase cells provokes a CHMP4B-GFP recruitment and microtubule rearrangement. Scale bar is 5 μ m

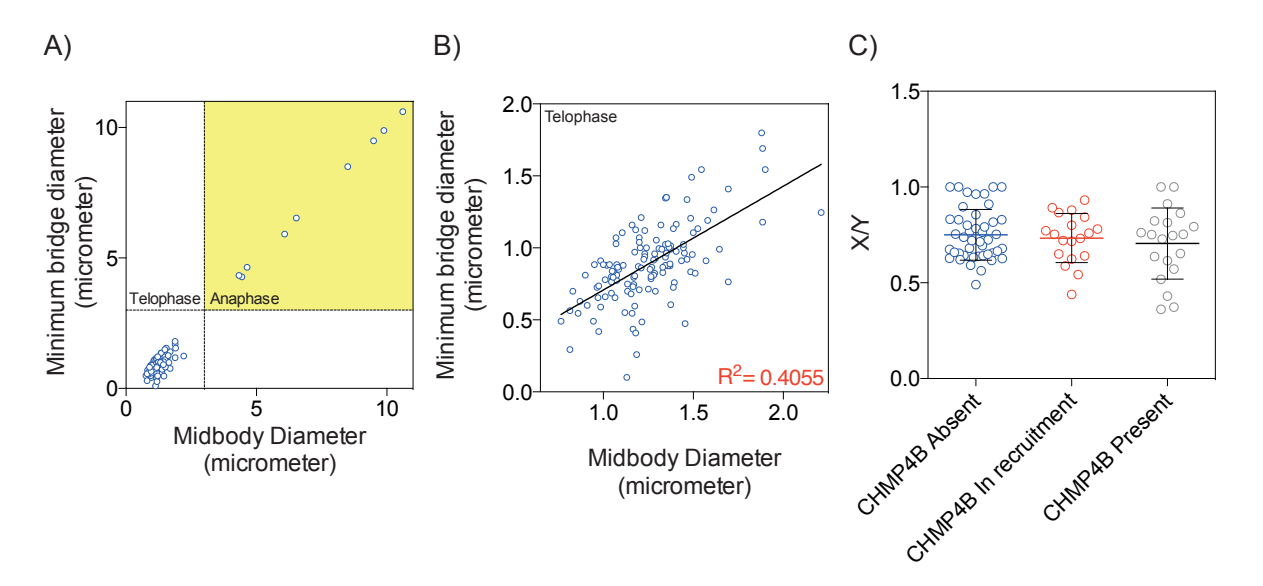


Figure 4.2.15: Cytokinesis timer. A) Plot of midbody diameter relationship to the minimum bridge diameter in telophase and anaphase cells. B) Detailed view of telophase cells measurements. C) Values of the ratio of diameters depending on the presence of CHMP4B-GFP.

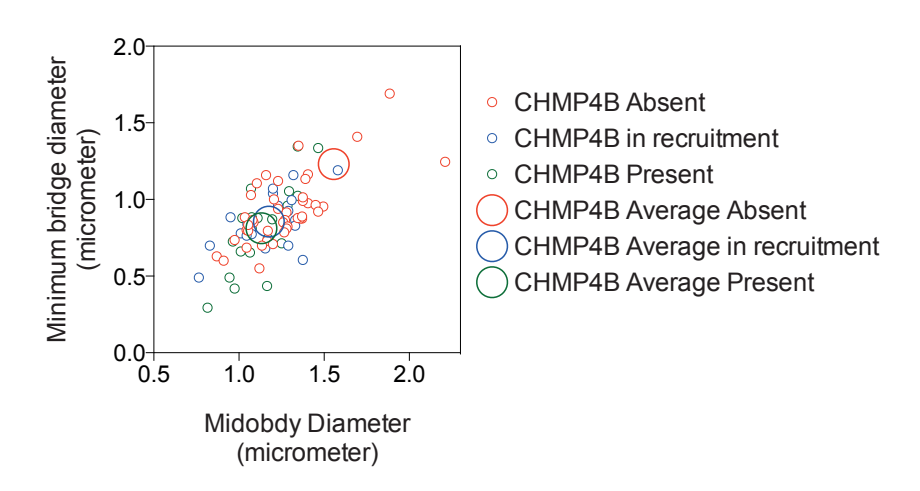


Figure 4.2.16: Cytokinesis timer and CHMP4B-GFP dependency.

5

Discussion and Conclusion

Prior to this study, cells parameters such as area, volume, sphericity or membrane tension were scattered amongst different cell type and not measured in a combined and calibrated fashion 51, 144.

5.1 CELL PARAMETERS

Cell volume response response to hypertonic and hypotonic shocks is linear until a V_{max} or Π_{max} is reached (Fig. 5.1.1). This response is a very good tool to infer volume changes from osmotic changes as the time resolution and osmotic shock range are unprecedented.

Historically the relationship between volume and osmolarity were measured in muscle cell ¹⁴⁵. In these measurements, the volume change induced by osmotic shock was proportional to the osmotic pressure difference. Other studies were in support of a more complex relationship between volume and osmotic pressure ^{146, 147}. The results obtained in this thesis (Fig. 5.1.1) bring another piece of

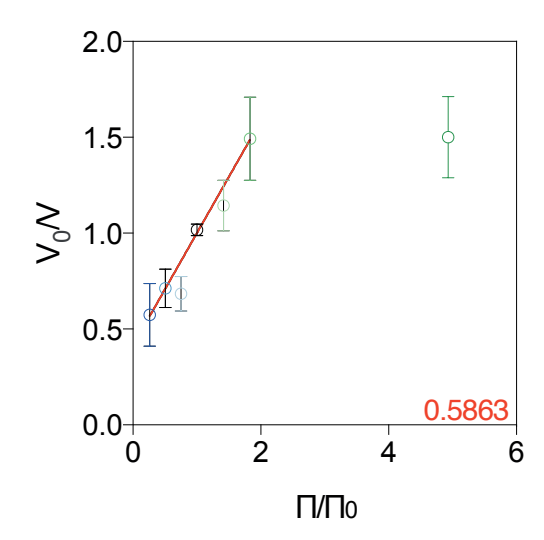


Figure 5.1.1: Osmotic pressure ratio and inverse of the volume linear fit on $\frac{\Pi}{\Pi_o}$ < 2 (red) with a 0.5863 slope.

evidence for HeLa Kyoto cells.

The discrepancy of timing between RVD and RVI remains to be better understood. Whether the cytoskeleton, the membrane shape, the lipid composition is the main factor determining the speed of recovery remains to be clarified.

Indeed, in the ATP-depleted cells, the RVD response is abolished (Fig. 5.1.2). Whether the amount or availability of energy required for pumping solutes or water in or out is different remains to be investigated. Another explanation for the difference of recovery speed would be the concentration of protein inside the cytoplasm. Although more dilute in hypo-osmotic condition, proteins and co-factors are still freely available. On the other hand, in the collapsed state of hypertonic shock, the HeLa Kyoto cell could be in a frozen mode, where some protein might be polymerizing in an non-controlled fashion or having co-factors and water inaccessible. Indeed, cytoskeleton and actin more particularly have been shown to be involved in cell volume regulation. F-actin content was shown to be changed during osmotic shocks 148 while Rho activity is increased in hypertonic condition 149.

Moreover, in hypertonic shocks, the area decreases, so the absolute values of ion channels or aquaporin channel could also decreases by internalization. This could lead to a certain variability in aqua-

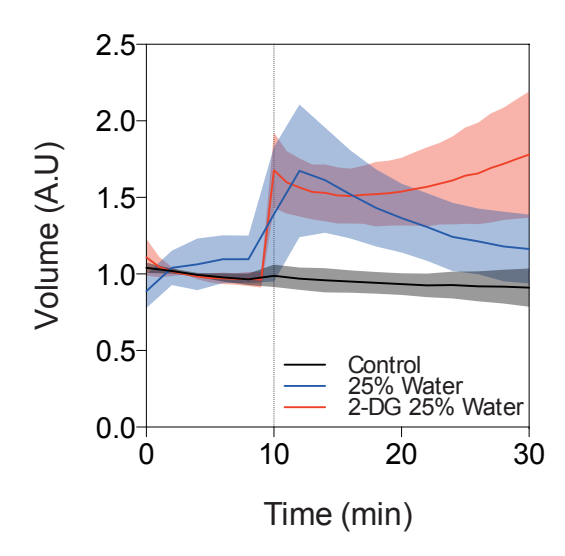


Figure 5.1.2: Evolution of volume and ATP depletion. Control (-) 25% Water (-) and 2-DG 25% Water (-). Osmotic shock applied at t=10 min.

porin density and membrane water permeability. For example cells can adapt their membrane to be less water permeable in order to resist osmotic shocks ¹⁵⁰.

On a the membrane level, lipid re-localisation has been observed upon osmotic shocks. Indeed PhosphoLipase 2 (LPA2) inhibition by Melittin hampered the release of amino acid by the NIH₃T₃ cells and critically disrupted the cell volume recovery upon hypo-osmotic shock ¹⁵¹. The release of Lysophosphatidic acid (LPA) and Arachidonic acid upon LPA2 activation might also induce changes in the membrane properties.

The sphericity of the cell might need to be studied in a more systematic approach. The presence or absence or bleb upon drug treatment and osmotic treatment has to be assessed on available data. For example, blebs form after ATP depletion in correlation with the loss of spectrin ¹⁵². Moreover membrane pearling has also been reported upon cytoskeletal rearrangement ^{153, 154}.

The volume increase after hypotonic shocks scales in a similar fashion in NRK-49F and MDCK cells ¹⁰⁷. The response seems to be conserved, however mechano-sensitive channels do not regulate regulatory volume decrease in all cell type. The drug GsMTx4 ¹⁵⁵ does not change the RVD in MDCK cells although it does it significantly in NRK-49F.

A wider range of drugs could also be tested in order to refine our knowledge. Brefeldin A¹⁵⁶ could have been used to show the impact of exocytosis on the osmotic shocks.

5.2 CELL MEMBRANE TENSION

Easier to access than membrane tension, the surface tension of cell has been studied since 1891 ¹⁵⁷. In 1926 it was explored *via* gravity cell deformation ¹⁵⁸ (Fig 5.2.1). Interestingly, one year before, two Dutch scientists measured the thickness of a lipid bilayer of a red blood cell ¹⁵⁹. This data would be critical in order to propose a model of lipid membrane behaviour. The surface tension was also assessed with a gold fiber compression in 1932 on sea urchin egg ¹⁵⁹. It was then measured using a cell "elastimeter" in 1954 ¹⁶⁰.

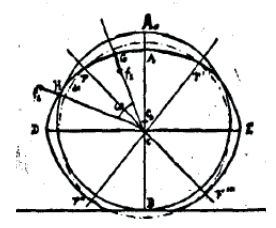


Figure 5.2.1: Sea urchin deformation model based on solid elastic gel¹⁵⁸.

Only very recently, the relationship between osmotic pressure and lipid membrane tension was measured *in vitro* 161 . Results showed that GUV cannot resist to high $\Delta\Pi$ in contrast to the cell. This might be due to the presence of cholesterol that increases the line tension of pores and prepores $^{162, 163}$ and thus antagonizes the opening and enlargment of such pores and thus prevents membrane rupture. Mechanosensitive channels would also help by opening upon membrane stretching $^{164, 165}$. Finally as previously stated, cell structure such as caveaole would dampen some effect.

For the future modeling, a variation in the bending modulus (κ) could be taken into account. Indeed κ does change with sucrose concentration *in vitro* in SOPC GUV¹⁶⁶, it decreases as the sucrose concentration increases.

Surprisingly, several studies do not observe cell tension changes upon hypo-osmotic shocks or through TOR activation ²⁵.

The experiment set-up with an indirect volume measurement of membrane tension *via* membrane tether can also be considered to give an incomplete picture of the cell membrane tension. Indeed, the formation of bleb at the membrane has been shown to change membrane tension, moreover only local measurement can be performed on small time scale. A better tool such as interferometry ²⁷ could provide finer data. On top of that emergent technology such as twisted push-pull probes ¹⁶⁷ imaging with Fluorescence-lifetime imaging microscopy could increase the resolution of membrane tension in a spatial manner, over longer period of time.

5.3 ESCRT

The rapid recruitment of CHMP4B-GFP remains to be explained, although some partners have already been involved in osmotic response. Indeed, Increase sodium tolerance (IST1), discovered in a salt tolerance screen ¹⁶⁸ is an ESCRT-III partner specifically at the cytokinesis bridge. Its relation with Vps4 ¹⁶⁹ and spastin, a microtubule severing protein is rather interesting. A behaviour analysis of IST1-GFP upon hyper-osmotic shock could reveal its recruitment prior to CHMP4B-GFP. Moreover the delay observed in between CHMP4B-GFP recruitment and microtubule disappearance could be explained by the sequential recruitment of spastin and its limited rate of microtubule severing and the amount of microtubule to cut.

The fact that microtubule removal can be uncoupled from membrane abscission argues against microtubule as a marker for the abscission. 170, 125.

Although the inhibition of abscission and/or recruitment of CHMP4B-GFP by pipette was a crafty, time consuming experiment, it helped to confirm a theory that an increase in membrane or bridge tension does not lead to membrane fission. Moreover, an hypotonic shock would not have been relevant as the RVD kicks in in 5 min. The use of drugs such as Lysophosphatidic acid (LPA) could have helped to confirm the relationship between σ and abscission.

The fact that no membrane fission was observed upon hyper-osmotic shock (data not shown), indicates that the ectopic recruitment of CHMP4B-GFP is not sufficient to induce membrane fission. Indeed ESCRT-mediated membrane fission remains elusive. *In vitro* reconstitution assay have been failing to replicate controversial results ¹⁷¹. FIP3 vesicle fission have been proposed to help bringing membrane reservoir at the inter-cellular bridge ¹⁷². More recently, 3 modes of fission have been proposed that accounts for 3 different microtubule behaviour ¹⁷³. Different mode of fission is a way for

the cell to cope with an ever-changing environment. Indeed some organism such as *Dictyostelium discoideum* possess as much as 4 radically different means for cytokinesis ¹⁷⁴. On top of that osmotic changes in polymersome was shown to lead to shape changes and near-fission events ¹⁷⁵. Those result shows that even in *in vitro* system osmotic pressure can drive fission event. This is a piece of evidence that was proposed to be important for the proto-cell. Indeed, the relationship between osmotic pressure and membrane tension might have an impact for the Darwinian evolution of the proto-cell ¹⁷⁶.

Finally an increase in tension at the metaphase followed by a drop at telophase was already observed in sea urchin egg in 1926^{158} in Fig 5.3.1 while membrane shape changes and midbidy movement was observed in 1968^{177} (Fig. 5.3.2).

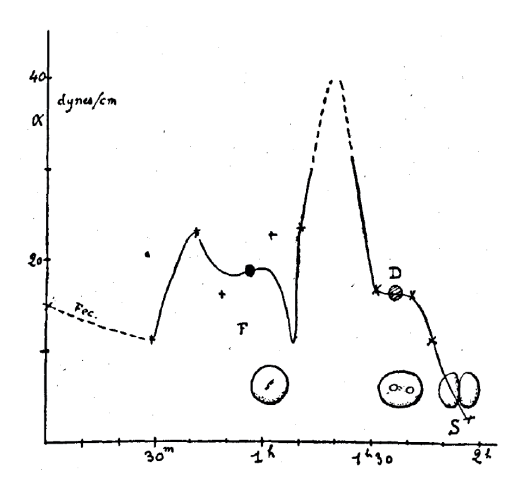


Figure 5.3.1: Analysis of sea urchin egg surface tension (using egg deformation) dynamics during the first division after fertilization.

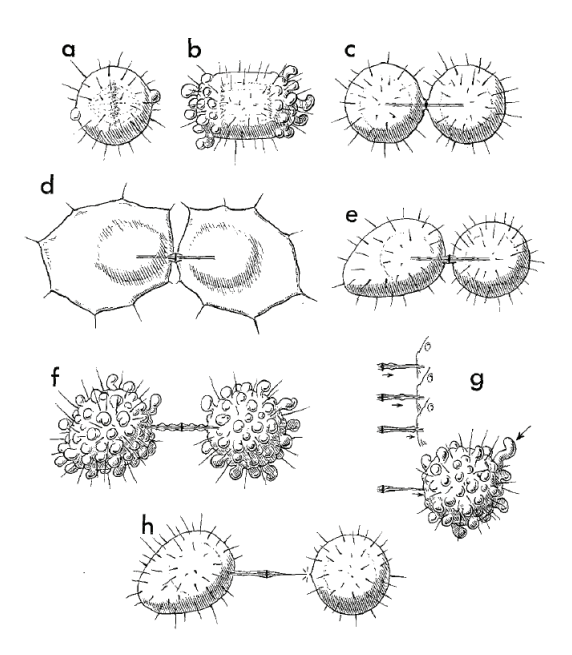


Figure 5.3.2: Mitosis description with details of the midbody movement $(g)^{177}$.

References

- [1] K. Brandenburg and O. Holst. Glycolipids: Distribution and biological function. *eLS*, 2015.
- [2] RD. Marshall. Glycoproteins. Annual review of biochemistry, 41(1):673-702, 1972.
- [3] Donald J. Voet; Judith G. Voet; Charlotte W. Pratt. *Principles of Biochemistry, Third edition.* Wiley, 2008.
- [4] O. Cremona, G. Di Paolo, MR. Wenk, A. Lüthi, WT. Kim, K. Takei, L. Daniell, Y. Nemoto, SB. Shears, RA. Flavell, DA McCormick, and P. De Camilli. Essential role of phosphoinositide metabolism in synaptic vesicle recycling. *Cell*, 99(2):179–188, 1999.
- [5] W. Helfrich. Elastic properties of lipid bilayers: theory and possible experiments. *Zeitschrift für Naturforschung C*, 28(11-12):693-703, 1973.
- [6] PB. Canham. The minimum energy of bending as a possible explanation of the biconcave shape of the human red blood cell. *Journal of theoretical biology*, 26(1):61–81, 1970.
- [7] W. Helfrich and RM. Servuss. Undulations, steric interaction and cohesion of fluid membranes. Il Nuovo Cimento D, 3(1):137-151, 1984.
- [8] E. Evans and W. Rawicz. Entropy-driven tension and bending elasticity in condensed-fluid membranes. *Physical Review Letters*, 64(17):2094, 1990.
- [9] W. Rawicz, KC. Olbrich, T. McIntosh, D. Needham, and E. Evans. Effect of chain length and unsaturation on elasticity of lipid bilayers. *Biophysical journal*, 79(1):328–339, 2000.
- [10] V. Heinrich and RE. Waugh. A piconewton force transducer and its application to measurement of the bending stiffness of phospholipid membranes. *Annals of biomedical engineering*, 24(5): 595–605, 1996.
- [11] FM. Hochmuth, JY. Shao, J. Dai, and MP. Sheetz. Deformation and flow of membrane into tethers extracted from neuronal growth cones. *Biophysical journal*, 70(1):358, 1996.

- [12] M. Bou Khalil, W. Hou, H. Zhou, F. Elisma, LA. Swayne, AP. Blanchard, Z. Yao, SAL. Bennett, and D. Figeys. Lipidomics era: accomplishments and challenges. *Mass spectrometry reviews*, 29 (6):877–929, 2010.
- [13] M. Xavier, P. Rosendahl, M. Herbig, M. Kräter, D. Spencer, M. Bornhäuser, ROC. Oreffo, H. Morgan, J. Guck, and O. Otto. Mechanical phenotyping of primary human skeletal stem cells in heterogeneous populations by real-time deformability cytometry. *Integrative Biology*, 8(5):616–623, 2016.
- [14] AD. Lieber, S. Yehudai-Resheff, EL. Barnhart, JA Theriot, and K. Keren. Membrane tension in rapidly moving cells is determined by cytoskeletal forces. *Current Biology*, 23(15):1409–1417, 2013.
- [15] D. Raucher, T. Stauffer, W. Chen, K. Shen, S. Guo, JD. York, MP. Sheetz, and T. Meyer. Phosphatidylinositol 4, 5-bisphosphate functions as a second messenger that regulates cytoskeleton–plasma membrane adhesion. *Cell*, 100(2):221–228, 2000.
- [16] B. Pontes, NB. Viana, LT. Salgado, M. Farina, VM. Neto, and HM. Nussenzveig. Cell cytoskeleton and tether extraction. *Biophysical journal*, 101(1):43–52, 2011.
- [17] B. Pontes, NB. Viana, L. Campanati, M. Farina, VM. Neto, and HM. Nussenzveig. Structure and elastic properties of tunneling nanotubes. *European Biophysics Journal*, 37(2):121–129, 2008.
- [18] AKC. Yeung. *Mechanics of inter-monolayer coupling in fluid surfactant bilayers*. PhD thesis, University of British Columbia, 1994.
- [19] RE. Waugh and RM. Hochmuth. Mechanics and deformability of hematocytes. *The biomedical engineering handbook*, 35:474–486, 1995.
- [20] J. Song and RE. Waugh. Bending rigidity of SOPC membranes containing cholesterol. *Biophysical journal*, 64(6):1967, 1993.
- [21] EA. Evans. Bending elastic modulus of red blood cell membrane derived from buckling instability in micropipet aspiration tests. *Biophysical Journal*, 43(1):27, 1983.
- [22] EL. Batchelder, G. Hollopeter, C. Campillo, X. Mezanges, EM. Jorgensen, P. Nassoy, P. Sens, and J. Plastino. Membrane tension regulates motility by controlling lamellipodium organization. *Proceedings of the National Academy of Sciences*, 108(28):11429–11434, 2011.
- [23] J. Dai, MP. Sheetz, X. Wan, and CE. Morris. Membrane tension in swelling and shrinking molluscan neurons. *The Journal of neuroscience*, 18(17):6681–6692, 1998.

- [24] J. Wolfe, MF. Dowgert, and PL. Steponkus. Dynamics of membrane exchange of the plasma membrane and the lysis of isolated protoplasts during rapid expansions in area. *The Journal of Membrane Biology*, 86(2):127–138, 1985.
- [25] A. Diz-Muñoz, K. Thurley, S. Chintamen, SJ. Altschuler, LF. Wu, DA. Fletcher, and OD. Weiner. Membrane tension acts through PLD2 and mTORC2 to limit actin network assembly during neutrophil migration. *PLoS Biol*, 14(6):e1002474, 2016.
- [26] J. Dai and MP. Sheetz. Membrane tether formation from blebbing cells. *Biophysical journal*, 77 (6):3363–3370, 1999.
- [27] J. Peukes and T. Betz. Direct measurement of the cortical tension during the growth of membrane blebs. *Biophysical journal*, 107(8):1810–1820, 2014.
- [28] Z. Li, B. Anvari, M. Takashima, P. Brecht, JH. Torres, and WE. Brownell. Membrane tether formation from outer hair cells with optical tweezers. *Biophysical journal*, 82(3):1386–1395, 2002.
- [29] E. Fischer-Friedrich, AA. Hyman, F. Jülicher, DJ. Müller, and J. Helenius. Quantification of surface tension and internal pressure generated by single mitotic cells. *Scientific reports*, 4, 2014.
- [30] NR. Pallas and Y. Harrison. An automated drop shape apparatus and the surface tension of pure water. *Colloids and Surfaces*, 43(2):169–194, 1990.
- [31] B. Sinha, D. Koster, R. Ruez, P. Gonnord, M. Bastiani, D. Abankwa, R. V. Stan, G. Butler-Browne, B. Vedie, L. Johannes, N. Morone, R. G. Parton, G. Raposo, P. Sens, C. Lamaze, and P. Nassoy. Cells respond to mechanical stress by rapid disassembly of caveolae. *Cell*, 144(3): 402–413, Feb 2011.
- [32] A. Pietuch, BR. Brückner, and A. Janshoff. Membrane tension homeostasis of epithelial cells through surface area regulation in response to osmotic stress. *Biochimica et Biophysica Acta* (BBA)-Molecular Cell Research, 1833(3):712–722, 2013.
- [33] K. Alleva, O. Chara, and G. Amodeo. Aquaporins: another piece in the osmotic puzzle. *FEBS letters*, 586(19):2991–2999, 2012.
- [34] AG. Clark and E. Paluch. Mechanics and regulation of cell shape during the cell cycle. pages 31-73, 2011.
- [35] N. Barkai and D. Ben-Zvi. 'Big frog, small frog'-maintaining proportions in embryonic development. *Febs Journal*, 276(5):1196–1207, 2009.

- [36] MP. Stewart, J. Helenius, Y. Toyoda, SP. Ramanathan, DJ. Muller, and AA. Hyman. Hydrostatic pressure and the actomyosin cortex drive mitotic cell rounding. *Nature*, 469(7329):226–230, 2011.
- [37] JY. Tinevez, U. Schulze, G. Salbreux, J. Roensch, J. Joanny, and E. Paluch. Role of cortical tension in bleb growth. *Proceedings of the National Academy of Sciences*, 106(44):18581–18586, 2009.
- [38] AG. Clark, O. Wartlick, G. Salbreux, and EK. Paluch. Stresses at the cell surface during animal cell morphogenesis. *Current Biology*, 24(10):R484–R494, 2014.
- [39] NC. Gauthier, TA. Masters, and MP. Sheetz. Mechanical feedback between membrane tension and dynamics. *Trends in cell biology*, 22(10):527–535, 2012.
- [40] D. Raucher and MP. Sheetz. Characteristics of a membrane reservoir buffering membrane tension. *Biophysical journal*, 77(4):1992–2002, 1999.
- [41] MP. Sheetz and J. Dai. Modulation of membrane dynamics and cell motility by membrane tension. *Trends in cell biology*, 6(3):85–89, 1996.
- [42] AF. Dulhunty and C. Franzini. Caveolae as specialized structural components of surface membrane of skeletal-muscle. In *Federation Proceedings*, volume 33, pages 401–401. Federation Amer. Soc. Exp. Biol., 1974.
- [43] J. Sedzinski, M. Biro, A. Oswald, J. Tinevez, G. Salbreux, and E. Paluch. Polar actomyosin contractility destabilizes the position of the cytokinetic furrow. *Nature*, 476(7361):462–466, 2011.
- [44] LL. Norman, J. Brugés, K. Sengupta, P. Sens, and H. Aranda-Espinoza. Cell blebbing and membrane area homeostasis in spreading and retracting cells. *Biophysical journal*, 99(6):1726–1733, 2010.
- [45] CA. Erickson and JP. Trinkaus. Microvilli and blebs as sources of reserve surface membrane during cell spreading. *Experimental cell research*, 99(2):375–384, 1976.
- [46] SR. Kinn and TD. Allen. Conversion of blebs to microvilli: cell surface reorganisation after trypsin. *Differentiation*, 20(1-3):168–173, 1981.
- [47] TN. Darling, CM. Burrows, and JJ. Blum. Rapid shape change and release of Ninhydrin-Positive substances by Leishmania major promastigotes in response to hypo-osmotic stress. *The Journal of protozoology*, 37(6):493–499, 1990.

- [48] Ian H Lambert and Francisco V Sepúlveda. Swelling-induced taurine efflux from Hela cells: Cell volume regulation. In *Taurine 4*, pages 487–495. Springer, 2002.
- [49] G. Salbreux, G. Charras, and E. Paluch. Actin cortex mechanics and cellular morphogenesis. *Trends in cell biology*, 22(10):536–545, 2012.
- [50] F. Rivero, B. Koppel, B. Peracino, S. Bozzaro, Cornelis J. Siegert, FW., M. Schleicher, R. Albrecht, and AA. Noegel. The role of the cortical cytoskeleton: F-actin crosslinking proteins protect against osmotic stress, ensure cell size, cell shape and motility, and contribute to phagocytosis and development. *Journal of Cell Science*, 109(11):2679–2691, 1996.
- [51] TJ. Jentsch. VRACs and other ion channels and transporters in the regulation of cell volume and beyond. *Nature Reviews Molecular Cell Biology*, 17(5):293–307, 2016.
- [52] VL. Lew and RM. Bookchin. Osmotic effects of protein polymerization: Analysis of volume changes in sickle cell anemia red cells following deoxy-hemoglobin s polymerization. *The Journal of membrane biology*, 122(1):55-67, 1991.
- [53] S. Cayley and MT. Record. Large changes in cytoplasmic biopolymer concentration with osmolality indicate that macromolecular crowding may regulate protein–DNA interactions and growth rate in osmotically stressed Escherichia coli K-12. *Journal of Molecular Recognition*, 17 (5):488–496, 2004.
- [54] CE. Morris and U. Homann. Cell surface area regulation and membrane tension. *The Journal of membrane biology*, 179(2):79–102, 2001.
- [55] P. Sens and J. Plastino. Membrane tension and cytoskeleton organization in cell motility. *Journal of Physics: Condensed Matter*, 27(27):273103, 2015.
- [56] C. Gabella, E. Bertseva, C. Bottier, N. Piacentini, A. Bornert, S. Jeney, L. Forró, IF. Sbalzarini, JJ. Meister, and AB. Verkhovsky. Contact angle at the leading edge controls cell protrusion rate. *Current Biology*, 24(10):1126–1132, 2014.
- [57] JS. Bonifacino and BS. Glick. The mechanisms of vesicle budding and fusion. *Cell*, 116(2): 153–166, 2004.
- [58] C. Barlowe. COPII: a membrane coat that forms endoplasmic reticulum-derived vesicles. *FEBS letters*, 369(1):93-96, 1995.
- [59] V. Popoff, F. Adolf, B. Brügger, and F. Wieland. COPI budding within the Golgi stack. *Cold Spring Harbor perspectives in biology*, 3(11):a005231, 2011.

- [60] BM. Pearse. Clathrin: a unique protein associated with intracellular transfer of membrane by coated vesicles. *Proceedings of the National Academy of Sciences*, 73(4):1255–1259, 1976.
- [61] S. Morlot, V. Galli, M. Klein, N. Chiaruttini, J. Manzi, F. Humbert, L. Dinis, M. Lenz, G. Cappello, and A. Roux. Membrane shape at the edge of the dynamin helix sets location and duration of the fission reaction. *Cell*, 151(3):619–629, 2012.
- [62] B. Antonny, C. Burd, P. De Camilli, E. Chen, O. Daumke, K. Faelber, M. Ford, VA. Frolov, A. Frost, JE. Hinshaw, T Kirchhausen, MM Kozlov, M. Lenz, HH. Low, C. McMahon, H. Merrifield, TD. Pollard, PJ. Robinson, A. Roux, and S Schmid. Membrane fission by dynamin: what we know and what we need to know. *The EMBO Journal*, page e201694613, 2016.
- [63] A. Roux, D. Cuvelier, P. Nassoy, J. Prost, P. Bassereau, and B. Goud. Role of curvature and phase transition in lipid sorting and fission of membrane tubules. *The EMBO journal*, 24(8): 1537–1545, 2005.
- [64] HG. Döbereiner, J. Käs, D. Noppl, I. Sprenger, and E. Sackmann. Budding and fission of vesicles. *Biophysical journal*, 65(4):1396, 1993.
- [65] JM. Allain, C. Storm, A. Roux, MB. Amar, and JF. Joanny. Fission of a multiphase membrane tube. *Physical review letters*, 93(15):158104, 2004.
- [66] C. Bissig, M. Lenoir, MC. Velluz, I. Kufareva, R. Abagyan, M. Overduin, and J. Gruenberg. Viral infection controlled by a calcium-dependent lipid-binding module in alix. *Developmental cell*, 25(4):364–373, 2013.
- [67] HW. Shin, C. Shinotsuka, S. Torii, K. Murakami, and K. Nakayama. Identification and subcellular localization of a novel mammalian dynamin-related protein homologous to yeast Vps1p and Dnm1p. *Journal of Biochemistry*, 122(3):525–530, 1997.
- [68] M. Osawa and HP. Erickson. Liposome division by a simple bacterial division machinery. *Proceedings of the National Academy of Sciences*, 110(27):11000–11004, 2013.
- [69] MK. Bonner and AR. Skop. Cell division screens and dynamin. *Biochemical Society Transactions*, 36(3):431–435, 2008.
- [70] VA. Bankaitis, LM. Johnson, and SD. Emr. Isolation of yeast mutants defective in protein targeting to the vacuole. *Proceedings of the national academy of sciences*, 83(23):9075–9079, 1986.
- [71] RY. Samson, T. Obita, B. Hodgson, MK. Shaw, PLG. Chong, RL. Williams, and SD. Bell. Molecular and structural basis of ESCRT-III recruitment to membranes during archaeal cell division. *Molecular cell*, 41(2):186–196, 2011.

- [72] C. Spitzer, S. Schellmann, A. Sabovljevic, M. Shahriari, C. Keshavaiah, N. Bechtold, M. Herzog, S. Müller, F. Hanisch, and M. Hülskamp. The arabidopsis elch mutant reveals functions of an ESCRT component in cytokinesis. *Development*, 133(23):4679–4689, 2006.
- [73] JG. Carlton and J. Martin-Serrano. Parallels between cytokinesis and retroviral budding: a role for the ESCRT machinery. *Science*, 316(5833):1908–1912, 2007.
- [74] MAY. Adell, GF. Vogel, M. Pakdel, M. Müller, H. Lindner, MW. Hess, and D. Teis. Coordinated binding of Vps4 to ESCRT-III drives membrane neck constriction during MVB vesicle formation. *The Journal of cell biology*, 205(1):33–49, 2014.
- [75] AJ. Jimenez, P. Maiuri, J. Lafaurie-Janvore, S. Divoux, M. Piel, and F. Perez. ESCRT machinery is required for plasma membrane repair. *Science*, 343(6174):1247136, 2014.
- [76] J. Lee, A. Beigneux, ST. Ahmad, SG. Young, and FB. Gao. ESCRT-III dysfunction causes autophagosome accumulation and neurodegeneration. *Current biology*, 17(18):1561–1567, 2007.
- [77] TE. Rusten, T. Vaccari, K. Lindmo, LMW. Rodahl, IP. Nezis, C. Sem-Jacobsen, F. Wendler, J. Vincent, A. Brech, D. Bilder, and H. Stenmark. ESCRTs and Fab1 regulate distinct steps of autophagy. *Current biology*, 17(20):1817–1825, 2007.
- [78] M. Vietri, KO. Schink, C. Campsteijn, CS. Wegner, SW. Schultz, L. Christ, SB. Thoresen, A. Brech, C. Raiborg, and H. Stenmark. Spastin and ESCRT-III coordinate mitotic spindle disassembly and nuclear envelope sealing. *Nature*, 522(7555):231–235, 2015.
- [79] Y. Olmos, L. Hodgson, J. Mantell, P. Verkade, and JG. Carlton. ESCRT-III controls nuclear envelope reformation. *Nature*, 522(7555):236–239, 2015.
- [80] N. Loncle, M. Agromayor, J. Martin-Serrano, and DW. Williams. An ESCRT module is required for neuron pruning. *Scientific reports*, 5, 2015.
- [81] BM. Webster, P. Colombi, J. Jäger, and CP. Lusk. Surveillance of nuclear pore complex assembly by escrt-iii/vps4. *Cell*, 159(2):388–401, 2014.
- [82] E. Morita, V. Sandrin, J. McCullough, A. Katsuyama, IB. Hamilton, and WI. Sundquist. ESCRT-III protein requirements for HIV-1 budding. *Cell host & microbe*, 9(3):235–242, 2011.
- [83] N. Jouvenet, M. Zhadina, PD. Bieniasz, and SM. Simon. Dynamics of ESCRT protein recruitment during retroviral assembly. *Nature cell biology*, 13(4):394–401, 2011.
- [84] WM. Henne, NJ. Buchkovich, Y. Zhao, and SD. Emr. The endosomal sorting complex ESCRT-II mediates the assembly and architecture of ESCRT-III helices. *Cell*, 151(2):356–371, 2012.

- [85] S. Saksena, J. Wahlman, D. Teis, AE. Johnson, and SD. Emr. Functional reconstitution of ESCRT-III assembly and disassembly. *Cell*, 136(1):97–109, 2009.
- [86] M. Babst, DJ. Katzmann, EJ. Estepa-Sabal, T. Meerloo, and SD. Emr. ESCRT-III: an endosome-associated heterooligomeric protein complex required for MVB sorting. *Developmental cell*, 3 (2):271–282, 2002.
- [87] EM. Coonrod and TH. Stevens. The yeast vps class E mutants: the beginning of the molecular genetic analysis of multivesicular body biogenesis. *Molecular biology of the cell*, 21(23):4057–4060, 2010.
- [88] V. Nähse, L. Christ, H. Stenmark, and C. Campsteijn. The abscission checkpoint: Making it to the final cut. *Trends in Cell Biology*, 2016.
- [89] M. Chivet, F. Hemming, S. Fraboulet, R. Sadoul, et al. Emerging role of neuronal exosomes in the central nervous system. *Frontiers in physiology*, 3:145, 2012.
- [90] J. Lafaurie-Janvore, P. Maiuri, I. Wang, M. Pinot, JB. Manneville, T. Betz, M. Balland, and M. Piel. ESCRT-III assembly and cytokinetic abscission are induced by tension release in the intercellular bridge. *Science*, 339(6127):1625–1629, 2013.
- [91] JG. Carlton, A. Caballe, M. Agromayor, M. Kloc, and J. Martin-Serrano. ESCRT-III governs the Aurora B-mediated abscission checkpoint through CHMP4C. *Science*, 336(6078), 2012.
- [92] A. Caballe, DM. Wenzel, M. Agromayor, SL. Alam, JJ. Skalicky, M. Kloc, JG. Carlton, L. Labrador, WI. Sundquist, and J. Martin-Serrano. ULK3 regulates cytokinetic abscission by phosphorylating ESCRT-III proteins. *Elife*, 4:e06547, 2015.
- [93] PP. D'Avino, MG. Giansanti, and M. Petronczki. Cytokinesis in animal cells. *Cold Spring Harbor perspectives in biology*, 7(4):a015834, 2015.
- [94] B. Lacroix and AS. Maddox. Cytokinesis, ploidy and aneuploidy. *The Journal of pathology*, 226 (2):338–351, 2012.
- [95] A. Rustom, R. Saffrich, I. Markovic, P. Walther, and HH. Gerdes. Nanotubular highways for intercellular organelle transport. *Science*, 303(5660):1007–1010, 2004.
- [96] L. Caneparo, P. Pantazis, W. Dempsey, and SE. Fraser. Intercellular bridges in vertebrate gastrulation. *PLoS One*, 6(5):e20230, 2011.
- [97] M. Lenz, S. Morlot, and A. Roux. Mechanical requirements for membrane fission: common facts from various examples. *FEBS letters*, 583(23):3839–3846, 2009.

- [98] G. Fabrikant, S. Lata, JD. Riches, JAG. Briggs, W. Weissenhorn, and MM. Kozlov. Computational model of membrane fission catalyzed by ESCRT-III. *PLoS Comput Biol*, 5(11): e1000575, 2009.
- [99] N. Chiaruttini, L. Redondo-Morata, A. Colom, F. Humbert, M. Lenz, S. Scheuring, and A. Roux. Relaxation of loaded ESCRT-III spiral springs drives membrane deformation. *Cell*, 163(4):866–879, 2015.
- [100] JA. Schiel and R. Prekeris. Membrane dynamics during cytokinesis. *Current opinion in cell biology*, 25(1):92–98, 2013.
- [101] BG. Hosu, M. Sun, F. Marga, M. Grandbois, and G. Forgacs. Eukaryotic membrane tethers revisited using magnetic tweezers. *Physical biology*, 4(2):67, 2007.
- [102] A. Ashkin. Acceleration and trapping of particles by radiation pressure. *Physical Review Letters*, 24(4):156, 1970.
- [103] A. Ashkin and JM. Dziedzic. Optical trapping and manipulation of viruses and bacteria. *Science*, 235(4795):1517–1520, 1987.
- [104] G. Galileo. Discorsi e Dimostrazioni Matematiche Intorno a Due Nuove Scienze. Elzevir, L., 1638.
- [105] E. Zlotek-Zlotkiewicz, S. Monnier, G. Cappello, M. Le Berre, and M. Piel. Optical volume and mass measurements show that mammalian cells swell during mitosis. *The Journal of cell biology*, 211(4):765–774, 2015.
- [106] S. Son, JH. Kang, S. Oh, MW. Kirschner, TJ. Mitchison, and S. Manalis. Resonant microchannel volume and mass measurements show that suspended cells swell during mitosis. *The Journal of cell biology*, 211(4):757–763, 2015.
- [107] SZ. Hua, PA. Gottlieb, J. Heo, and F. Sachs. A mechanosensitive ion channel regulating cell volume. *American Journal of Physiology-Cell Physiology*, 298(6):C1424–C1430, 2010.
- [108] SZ. Hua and T. Pennell. A microfluidic chip for real-time studies of the volume of single cells. *Lab on a Chip*, 9(2):251–256, 2009.
- [109] EC. Gregg and KD. Steidley. Electrical counting and sizing of mammalian cells in suspension. *Biophysical journal*, 5(4):393, 1965.
- [110] P. Dierkes, P. Coulon, S. Neumann, and WR. Schlue. Potentiometric measurement of cell volume changes and intracellular ion concentrations under voltage-clamp conditions in invertebrate nerve cells. *Analytical and bioanalytical chemistry*, 373(8):762–766, 2002.

- [111] K. Kawahara, M. Onodera, and Y. Fukuda. A simple method for continuous measurement of cell height during a volume change in a single A6 cell. *The Japanese journal of physiology*, 44(4): 411–419, 1994.
- [112] M. McManus, J. Fischbarg, A. Sun, S. Hebert, and K. Strange. Laser light-scattering system for studying cell volume regulation and membrane transport processes. *American Journal of Physiology-Cell Physiology*, 265(2):C562–C570, 1993.
- [113] J. Rodríguez-Fernández, J. Perez-Juste, LM. Liz-Marzan, and PR. Lang. Dynamic light scattering of short au rods with low aspect ratios. *The Journal of Physical Chemistry C*, 111(13): 5020–5025, 2007.
- [114] R. Strohmeier and J. Bereiter-Hahn. Hydrostatic pressure in epidermal cells is dependent on Ca-mediated contractions. *Journal of cell science*, 88(5):631–640, 1987.
- [115] M. Zelenina and H. Brismar. Osmotic water permeability measurements using confocal laser scanning microscopy. *European Biophysics Journal*, 29(3):165–171, 2000.
- [116] NB. Grover and CL. Woldringh. Dimensional regulation of cell-cycle events in Escherichia coli during steady-state growth. *Microbiology*, 147(1):171–181, 2001.
- [117] MS. Droste, SS. Biel, . Terstegen, KP. Wittern, H. Wenck, and R. Wepf. Noninvasive measurement of cell volume changes by negative staining. *Journal of biomedical optics*, 10(6):064017–064017, 2005.
- [118] P. Morris and JF. Thain. Improved methods for the measurement of total cell surface area in leaf mesophyll tissue. *Journal of Experimental Botany*, 34(1):95–98, 1983.
- [119] AC. Brumback, JL. Lieber, JK. Angleson, and WJ. Betz. Using FM1-43 to study neuropeptide granule dynamics and exocytosis. *Methods*, 33(4):287–294, 2004.
- [120] MG. Honig and RI. Hume. Carbocyanine dyes. Novel markers for labelling neurons. *Trends in neurosciences*, 12(9):336, 1989.
- [121] F. Aguet, S. Upadhyayula, R. Gaudin, Y. Chou, E. Cocucci, K. He, BC. Chen, K. Mosaliganti, M. Pasham, W. Skillern, WR. Legant, TL. Liu, G. Findlay, E. Marino, G. Danuser, S. Megason, E. Betzig, and T. Kirchhausen. Membrane dynamics of dividing cells imaged by lattice light-sheet microscopy. *Molecular Biology of the Cell*, 27(22):3418–3435, 2016.
- [122] H. Wadell. Volume, shape, and roundness of rock particles. *The Journal of Geology*, pages 443–451, 1932.

- [123] I. Poser, M. Sarov, JRA. Hutchins, JK. Hériché, Y. Toyoda, A. Pozniakovsky, D. Weigl, A. Nitzsche, B. Hegemann, AW. Bird, L. Pelletier, R Kittler, S. Hua, R. Naumann, M. Augsburg, MM. Sykora, H. Hofemeister, Y. Zhang, K. Nasmyth, KP. White, S. Dietzel, K. Mechtler, R Durbin, Stewart AF., JM. Peters, F. Buchholz, and AA. Hyman. BAC TransgeneOmics: a high-throughput method for exploration of protein function in mammals. *Nature methods*, 5 (5):409–415, 2008.
- [124] M. Saleem, S. Morlot, A. Hohendahl, J. Manzi, M. Lenz, and A. Roux. A balance between membrane elasticity and polymerization energy sets the shape of spherical clathrin coats. *Nature communications*, 6, 2015.
- [125] J. Guizetti, L. Schermelleh, J. Mäntler, S. Maar, I. Poser, H. Leonhardt, T. Müller-Reichert, and DW. Gerlich. Cortical constriction during abscission involves helices of ESCRT-III-dependent filaments. *Science*, 331(6024):1616–1620, 2011.
- [126] IH. Lee, H. Kai, LA. Carlson, JT. Groves, and JH. Hurley. Negative membrane curvature catalyzes nucleation of endosomal sorting complex required for transport ESCRT-III assembly. *Proceedings of the National Academy of Sciences*, 112(52):15892–15897, 2015.
- [127] I. Fyfe, AL. Schuh, JM. Edwardson, and A. Audhya. Association of the endosomal sorting complex ESCRT-II with the Vps20 subunit of ESCRT-III generates a curvature-sensitive complex capable of nucleating ESCRT-III filaments. *Journal of Biological Chemistry*, 286(39):34262–34270, 2011.
- [128] M. Simunovic, GA. Voth, A. Callan-Jones, and P. Bassereau. When physics takes over: BAR proteins and membrane curvature. *Trends in cell biology*, 25(12):780–792, 2015.
- [129] M. Babst, B. Wendland, EJ. Estepa, and SD. Emr. The Vps4p AAA ATPase regulates membrane association of a Vps protein complex required for normal endosome function. *The EMBO journal*, 17(11):2982–2993, 1998.
- [130] MAY. Adell, SM. Migliano, and D. Teis. ESCRT-III and Vps4: a dynamic multipurpose tool for membrane budding and scission. *The FEBS journal*, 2016.
- [131] Johannes Schöneberg, Il-Hyung Lee, Janet H Iwasa, and James H Hurley. Reverse-topology membrane scission by the escrt proteins. *Nature Reviews Molecular Cell Biology*, 2016.
- [132] N. Karpova, Y. Bobinnec, S. Fouix, P. Huitorel, and A. Debec. Jupiter, a new Drosophila protein associated with microtubules. *Cell motility and the cytoskeleton*, 63(5):301–312, 2006.

- [133] N. Elad, S. Abramovitch, H. Sabanay, and O. Medalia. Microtubule organization in the final stages of cytokinesis as revealed by cryo-electron tomography. *J Cell Sci*, 124(2):207–215, 2011.
- [134] T. Young. A course of lectures on natural philosophy and the mechanical arts, volume 2. Johnson, 1807.
- [135] G. Lukinavičius, L. Reymond, E. D'Este, A. Masharina, F. Göttfert, H. Ta, A. Güther, M. Fournier, S. Rizzo, H. Waldmann, C. Blaukopf, S. Christoph Sommer, DW. Gerlich, HS. Arndt, SW. Hell, and K. Johnsson. Fluorogenic probes for live-cell imaging of the cytoskeleton. *Nature methods*, 11(7):731–733, 2014.
- [136] D. Berchtold, Ma. Piccolis, N. Chiaruttini, I. Riezman, H. Riezman, A. Roux, TC. Walther, and R. Loewith. Plasma membrane stress induces relocalization of Slm proteins and activation of TORC2 to promote sphingolipid synthesis. *Nature cell biology*, 14(5):542–547, 2012.
- [137] RM. Hochmuth. Micropipette aspiration of living cells. *Journal of biomechanics*, 33(1):15–22, 2000.
- [138] A. Oesterle. *Pipette Cookbook*. Sutter Instrument Company, 2015.
- [139] WM. Zhao, A. Seki, and G. Fang. Cep55, a microtubule-bundling protein, associates with centralspindlin to control the midbody integrity and cell abscission during cytokinesis. *Molecular biology of the cell*, 17(9):3881–3896, 2006.
- [140] M. Fabbro, BB. Zhou, M. Takahashi, B. Sarcevic, P. Lal, ME. Graham, BG. Gabrielli, PJ. Robinson, EA. Nigg, Y. Ono, and KK. Khanna. Cdk1/Erk2-and Plk1-dependent phosphorylation of a centrosome protein, Cep55, is required for its recruitment to midbody and cytokinesis. *Developmental cell*, 9(4):477–488, 2005.
- [141] A. van der Horst, J. Simmons, and KK. Khanna. Cep55 stabilization is required for normal execution of cytokinesis. *Cell Cycle*, 8(22):3742–3749, 2009.
- [142] M. Rosner, K. Schipany, and M. Hengstschläger. Merging high-quality biochemical fractionation with a refined flow cytometry approach to monitor nucleocytoplasmic protein expression throughout the unperturbed mammalian cell cycle. *Nature protocols*, 8(3):602–626, 2013.
- [143] E. Derivery, C. Seum, A. Daeden, S. Loubéry, L. Holtzer, F. Jülicher, and M. Gonzalez-Gaitan. Polarized endosome dynamics by spindle asymmetry during asymmetric cell division. *Nature*, 528(7581):280–285, 2015.

- [144] EK. Hoffmann, IH. Lambert, and SF. Pedersen. Physiology of cell volume regulation in vertebrates. *Physiological reviews*, 89(1):193–277, 2009.
- [145] JR. Blinks. Influence of osmotic strength on cross-section and volume of isolated single muscle fibres. *The Journal of physiology*, 177(1):42–57, 1965.
- [146] M. Dydyńska, DR. Wilkie, HE. Huxley, S. Page, and DR. Wilkie. The osmotic properties of striated muscle fibres in hypertonic solutions. *The Journal of physiology*, 169(2):312, 1963.
- [147] JP. Reuben, E. Lopez, PW. Brandt, and H. Grundfest. Muscle: Volume changes in isolated single fibers. *Science*, 142(3589):246–248, 1963.
- [148] SF. Pedersen, JW. Mills, and EK. Hoffmann. Role of the F-actin cytoskeleton in the RVD and RVI processes in Ehrlich ascites tumor cells. *Experimental cell research*, 252(1):63-74, 1999.
- [149] M. Rasmussen, RT. Alexander, BV. Darborg, N. Møbjerg, EK. Hoffmann, A. Kapus, and SF. Pedersen. Osmotic cell shrinkage activates ezrin/radixin/moesin (ERM) proteins: activation mechanisms and physiological implications. *American Journal of Physiology-Cell Physiology*, 294 (1):C197–C212, 2008.
- [150] C. Stock, RD. Allen, and Y. Naitoh. How external osmolarity affects the activity of the contractile vacuole complex, the cytosolic osmolarity and the water permeability of the plasma membrane in Paramecium multimicronucleatum. *Journal of Experimental Biology*, 204(2):291–304, 2001.
- [151] SF. Pedersen, A. Poulsen, and IH. Lambert. Roles of phospholipase A2 isoforms in swelling-and melittin-induced arachidonic acid release and taurine efflux in NIH3T3 fibroblasts. *American Journal of Physiology-Cell Physiology*, 291(6):C1286–C1296, 2006.
- [152] MP. Sheetz. Cell control by membrane-cytoskeleton adhesion. *Nature Reviews Molecular Cell Biology*, 2(5):392–396, 2001.
- [153] D. Heinrich, M. Ecke, M. Jasnin, U. Engel, and G. Gerisch. Reversible membrane pearling in live cells upon destruction of the actin cortex. *Biophysical journal*, 106(5):1079–1091, 2014.
- [154] R. Bar-Ziv, T. Tlusty, E. Moses, SA. Safran, and A. Bershadsky. Pearling in cells: a clue to understanding cell shape. *Proceedings of the National Academy of Sciences*, 96(18):10140–10145, 1999.
- [155] TM. Suchyna, JH. Johnson, K. Hamer, JF. Leykam, DA. Gage, HF. Clemo, CM. Baumgarten, and F. Sachs. Identification of a peptide toxin from Grammostola spatulata spider venom that blocks cation-selective stretch-activated channels. *The Journal of general physiology*, 115(5): 583–598, 2000.

- [156] VL. Singleton, N. Bohonos, and AJ. Ullstrup. Decumbin, a new compound from a species of Penicillium. *Nature*, 1958.
- [157] W. Pfeiffer. Über aufnahme und ausgabe ungelöster körper: Zur kenntnis der plasmahaut und der vacuolen. Abhandlung der mathematisch-physikalischen Klasse der Sächsischen Akademie der Wissenschaften, 16(2):264–266, 1891.
- [158] F. Vlès. Les Tensions de surface et les déformations de l'oeuf d'Oursin. Archives de physique biologique. Vigot, 1926.
- [159] KS. Cole. Surface forces of the arbacia egg. *Journal of Cellular and Comparative Physiology*, 1 (1):1-9, 1932.
- [160] JM. Mitchison and MM. Swann. The mechanical properties of the cell surface. *Journal of Experimental Biology*, 31(3):461-472, 1954.
- [161] SUA. Shibly, C. Ghatak, MAS. Karal, M. Moniruzzaman, and M. Yamazaki. Experimental estimation of membrane tension induced by osmotic pressure. *Biophysical Journal*, 111(10): 2190–2201, 2016.
- [162] E. Karatekin, O. Sandre, H. Guitouni, N. Borghi, PH. Puech, and F. Brochard-Wyart. Cascades of transient pores in giant vesicles: line tension and transport. *Biophysical journal*, 84(3):1734–1749, 2003.
- [163] E. Evans, V. Heinrich, F. Ludwig, and W. Rawicz. Dynamic tension spectroscopy and strength of biomembranes. *Biophysical journal*, 85(4):2342–2350, 2003.
- [164] N. Levina, S. Tötemeyer, NR. Stokes, P. Louis, MA. Jones, and IR. Booth. Protection of Escherichia coli cells against extreme turgor by activation of MscS and MscL mechanosensitive channels: identification of genes required for MscS activity. *The EMBO journal*, 18(7):1730–1737, 1999.
- [165] SI. Sukharev, P. Blount, B. Martinac, FR. Blattner, and C. Kung. A large-conductance mechanosensitive channel in E. coli encoded by MscL alone. *Nature*, 368(6468):265–268, 1994.
- [166] J. Genova, A. Zheliaskova, and MD. Mitov. The influence of sucrose on the elasticity of SOPC lipid membrane studied by the analysis of thermally induced shape fluctuations. *Colloids and Surfaces A: Physicochemical and Engineering Aspects*, 282:420–422, 2006.
- [167] Q. Verolet, M. Dal Molin, A. Colom, A. Roux, L. Guénée, N. Sakai, and S. Matile. Twisted push-pull probes with turn-on sulfide donors. *Helvetica Chimica Acta*, 2016.

- [168] KD. Entian, T. Schuster, JH. Hegemann, D. Becher, H. Feldmann, U. Güldener, R Götz, M. Hansen, CP. Hollenberg, G. Jansen, W. Kramer, S. Klein, P. Kötter, J. Kricke, H. Launhardt, G. Mannhaupt, A. Maierl, P. Meyer, W. Mewes, T. Munder, RK. Niedenthal, M. Ramezani Rad, A. Röhmer, M. Rose, B. Schäfer, ML. Siegler, J. Vetter, N. Wilhelm, Wolf K., FK. Zimmermann, A. Zollner, and A. Hinnen. Functional analysis of 150 deletion mutants in Saccharomyces cerevisiae by a systematic approach. *Molecular and General Genetics MGG*, 262(4-5):683–702, 1999.
- [169] C. Dimaano, CB. Jones, A. Hanono, M. Curtiss, and M. Babst. Ist1 regulates Vps4 localization and assembly. *Molecular biology of the cell*, 19(2):465–474, 2008.
- [170] P. Steigemann, C. Wurzenberger, MHA. Schmitz, M. Held, J. Guizetti, S. Maar, and DW. Gerlich. Aurora B-mediated abscission checkpoint protects against tetraploidization. *Cell*, 136(3): 473–484, 2009.
- [171] T. Wollert, C. Wunder, J. Lippincott-Schwartz, and JH. Hurley. Membrane scission by the ESCRT-III complex. *Nature*, 458(7235):172–177, 2009.
- [172] JA. Schiel, GC. Simon, C. Zaharris, J. Weisz, D. Castle, CC. Wu, and R. Prekeris. FIP3-endosome-dependent formation of the secondary ingression mediates ESCRT-III recruitment during cytokinesis. *Nature cell biology*, 14(10):1068–1078, 2012.
- [173] J. Janvore. Régulation temporelle de l'abscission, la dernière étape de la division cellulaire : rôle des forces exercées au niveau du pont intercellulaire. PhD thesis, 2012.
- [174] TQP. Uyeda and A. Nagasaki. Variations on a theme: the many modes of cytokinesis. *Current opinion in cell biology*, 16(1):55–60, 2004.
- [175] BM. Discher, YY. Won, DS. Ege, JCM. Lee, FS. Bates, DE. Discher, and DA. Hammer. Polymersomes: tough vesicles made from diblock copolymers. *Science*, 284(5417):1143–1146, 1999.
- [176] IA. Chen, RW. Roberts, and JW. Szostak. The emergence of competition between model protocells. *Science*, 305(5689):1474–1476, 2004.
- [177] B. Byers and DH. Abramson. Cytokinesis in HeLa: post-telophase delay and microtubule-associated motility. *Protoplasma*, 66(4):413–435, 1968.

Materials and method

Cell culture:

HeLa Kyoto cells were cultured in Minimum Essential Media supplemented with 10% Fetal Bovine Serum and 1% Penicillin Streptomycin (Life Technologies, Carlsbad, CA, USA). 5% CO₂ incubator (Thermo Scientific, Waltham, MA, USA)

Microscopy: Two setup were used for imaging.

- The first is composed of an inverted Nikon Ti-E system, a Yokogawa CSU-X1 Confocal Scanner Unit, a iXon camera (Andor, Belfast, NIR, UK), a Laser stack by Intelligent Imaging Innovatios, Inc (Denver, CO, USA), a 37°C incubator (Life Imaging service, Basel, Switzerland), 2 micromanipulator MP-285 (Sutter, Novato, CA, USA) and a home-made optical tweezer with a 1A Manlight laser
- The second is composed of an inverted Nikon T*i*-E system, a Yokogawa CSU-W₁ Confocal Scanner Unit, an Evolve camera (Photometrics, Tucson, AZ, USA) a Laser stack by Intelligent Imaging Innovations, Inc (Denver, CO, USA), a 37°C incubator (Life Imaging service, Basel, Switzerland), a 37°C incubator (Life Imaging service, Basel, Switzerland), an H₃01 CO₂ incubator (Okolab, Pozzuoli, NA, Italy) and MP-285 (Sutter, Novato, CA, USA).

All images were acquired Slidebook software (Denver, CO, USA) and processed using ImageJ software (Public Domain).

Cell were imaged depending on the purpose on :

- 35mm Matek plate dish (Ashland, MA, USA)
- Ibidi *u*-Slide VI^{0.4} (Martinsried, Germany)
- Circular 25mm glass slide in Attofluor cell chamber (ThermoFisher, Waltham, MA, USA).

Live Staining:

Actin and microtubule were stained using SiR-Actin and SiR-tubulin (Spirochrome, Lausanne, Switzerland) following Cellmask Deep red (C10046) or Cell mask Orange (C10045) from ThermoFisher-Scientific, Waltham, MA, USA

Membrane integrity measurement:

HeLa Kyoto cells were incubated for 5 min with Propidium Iodide 160 μ g/mL then observed. 1% Saponin was used as a positive control.

Micropipette:

Borosilicate glass rods of 1 mm outer diamter (OD) and capillaries 1 mm OD- 0.58 mm interior diameter (ID) were used to forge micropipette (Harvard Apparatus, Hollisaton, MA, USA) they were first pulled into two with a puller (Sutter, Novato, CA, USA)(Heat:350, FIL:4, VEL:60, DEL:180, PUL, 100). They were then forged according to the need (MF-900, Narishige, Setagaya-ku, TKY, Japan).

Pipette were hold in HI-7 pipette holder (Narishige, Setagaya-ku,TKY, Japan) and displaced with micromanipulator MP-285 (Sutter, Novato, CA, USA). Pipette aspiration was achieved by Fluigent (Villejuif, France)

MTT assay: The cell proliferation assay was done following ATCC protocol, using Thiazolyl Blue Tetrazolium Bromide (M5655, Sigma)

Publications

The followings are 2 paper published during the course of my thesis. These are the results of collaboration with chemist from the University of Geneva in the context of the National Center of Competency in Research Chemical Biology.

Bang, E. K., Gasparini, G., Molinard, G., Roux, A., Sakai, N., and Matile, S. (2013). Substrate-initiated synthesis of cell-penetrating poly(disulfide)s. Journal of the American Chemical Society, 135(6), 2088-2091. ISO 690

Gasparini, G., Bang, E. K., Molinard, G., Tulumello, D. V., Ward, S., Kelley, S. O., Roux, A. Sakai, N. and Matile, S. (2014). Cellular uptake of substrate-initiated cell-penetrating poly (disulfide) s. Journal of the American Chemical Society, 136(16), 6069-6074. ISO 690



Substrate-Initiated Synthesis of Cell-Penetrating Poly(disulfide)s

Eun-Kyoung Bang,† Giulio Gasparini,† Guillaume Molinard, Aurélien Roux, Naomi Sakai, and Stefan Matile*

School of Chemistry and Biochemistry, University of Geneva, Geneva, Switzerland

Supporting Information

ABSTRACT: Lessons from surface-initiated polymerization are applied to grow cell-penetrating poly(disulfide)s directly on substrates of free choice. Reductive depolymerization after cellular uptake should then release the native substrates and minimize toxicity. In the presence of thiolated substrates, propagators containing a strained disulfide from asparagusic or, preferably, lipoic acid and a guanidinium cation polymerize into poly(disulfide)s in less than 5 min at room temperature at pH 7. Substrateinitiated polymerization of cationic poly(disulfide)s and their depolymerization with dithiothreitol causes the appearance and disappearance of transport activity in fluorogenic vesicles. The same process is further characterized by gel-permeation chromatography and fluorescence resonance energy transfer.

ell-penetrating peptides (CPPs) are short, polycationic peptides or protein domains that are used by viruses to enter cells. 1,2 Their unique ability to transport linked substrates across lipid bilayer membranes has attracted great interest in biomedical applications. Substrates of varying sizes and properties, e.g., small fluorophores to proteins and quantum dots, have been successfully transported into cells using CPPs. The mechanism of cellular uptake is under debate, currently favored are endocytosxis (i.e., macropinocytosis) or passive diffusion across the membrane, depending on conditions. Multiple, moderately hydrophobic cations seem to be all that is needed. Guanidinium cations, as in arginine, are most common, alternatives include ammonium or phosphonium cations. The originally peptidic oligomer backbone has been extensively varied, covering oligocarbamates, β -peptides and several variations of synthetic polymers.¹ Currently, cell-penetrating poly(disulfide)s are emerging as the cell-penetrating molecules of the future because their cytosolic degradation liberates the substrate and eliminates toxicity, one of the key disadvantages associated with CPPs.^{3–5} However, cell-penetrating poly-(disulfide)s have so far been used mainly in noncovalent polyplexes for gene transfection, and covalent attachment of substrates would be difficult with their preparation methods. We have found recently that poly(disulfide)s can be grown directly on solid substrates by surface-initiated ring-opening disulfide-exchange polymerization.⁶ Therefore, we wondered whether the same methodology could be used to prepare cellpenetrating poly(disulfide)s with covalently attached substrates in solution (Figure 1). Probes or drugs that contain thiol group but cannot penetrate cells without assistance are the ideal substrates, which could serve as an initiator to be appended

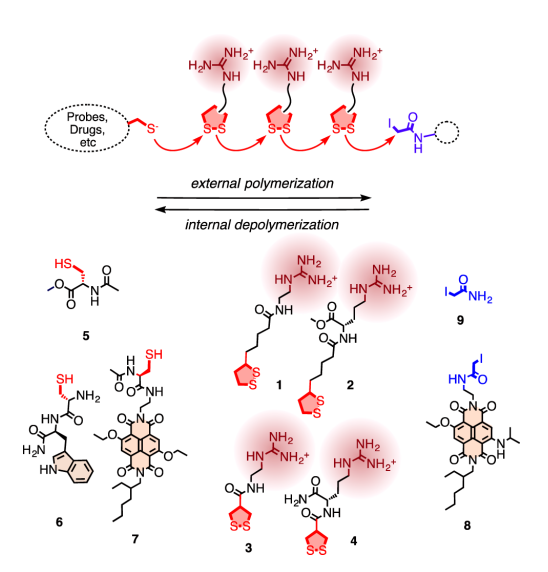


Figure 1. For the covalent delivery of unmodified probes, guanidinium-containing propagators (e.g., 1-4) are polymerized on thiolated substrates (e.g., 5-7) and terminated with iodoacetamides (e.g., 8, 9). After uptake, cell-penetrating poly(disulfide)s are degraded by reductive depolymerization to eliminate toxicity and release the unmodified substrate.

with a membrane-active poly(disulfide). Thiolated siRNA, for instance, is commercially available. The generality of this approach promises a conceptually innovative solution for a central current challenge, i.e., the noninvasive, nontoxic delivery of unmodified substrates in well-defined, covalent systems rather than complex, noncovalent formulations. In this initial report on the topic, we describe the design, synthesis and evaluation of propagators for the substrate-initiated synthesis of cell-penetrating poly(disulfide)s. Their formation in less than $5\,$ min at pH 7 and their depolymerization with 10 mM dithiothreitol (DTT) can be followed directly as appearance and disappearance of transport activity in fluorogenic vesicles.

To ultimately combine surface-initiated polymerization⁶ with cellular uptake, 1-5 we prepared the strained disulfides 1-4 as possible propagators, thiols 5-7 as initiators, and the iodoacetamides 8 and 9 as terminators (Figure 1). The

Received: December 7, 2012 Published: January 30, 2013



2088

dx.doi.org/10.1021/ja311961k | J. Am. Chem. Soc. 2013, 135, 2088-2091

synthesis of all new compounds was straightforward and is described in detail in the Supporting Information (SI Schemes S1–S7, Figures S10–S23). Only freshly prepared material was used.

Fluorogenic vesicles are convenient analytical tools to follow reactions with minimal effort and maximal speed. Here, EYPC-LUVs⊃CF, i.e., large unilamellar vesicles (LUVs) composed of egg yolk phosphatidylcholine (EYPC) and loaded with 5(6)-carboxyfluorescein (CF), were used. EYPC-LUVs⊃CF report CF release as fluorescence recovery because local dilution reduces self-quenching.

The addition of propagator 1 to EYPC-LUVs \supset CF caused CF release only above a relatively high EC₅₀ = 129.9 \pm 0.7 μ M (Figures 2A, B, \bigcirc , S1–S3, S6). Ring-opening disulfide

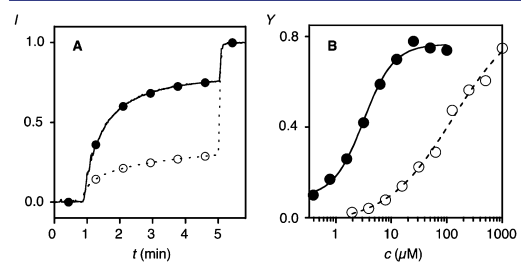


Figure 2. Activity of monomers (\bigcirc) and polymers (\bigcirc). (A) Change in CF emission intensity I during the addition of reaction mixtures with and without initiator 5 (50 s, $75 \mu M$ final guanidinium (monomer 1) concentration) and excess Triton X100 (300 s) to EYPC-LUVs \bigcirc CF. Reaction mixtures: 100 mM 1, 0 (\bigcirc) or 5 mM 5 (\bigcirc), 1 M TEOA, pH 7, 10 min; termination: 5 mM 9. (B) Transport activity Y of 1 before (\bigcirc) and after polymerization (\bigcirc , 5 mM 5) with increasing concentration of guanidinium cations (Y = I before lysis in A (\sim 5 min)).

exchange polymerization³ of 1 (100 mM, pH 7, 1 M triethanolamine (TEOA) buffer), initiated with thiol 5 (5 mM), was followed by adding aliquots of the reaction mixture to EYPC-LUVs \supset CF after termination with iodoacetamide 9. Rapid fluorescence recovery was observed with increasing reaction time (Figure 3A, \bigcirc). At saturation, dose response curves were recorded for the obtained polymers (Figures 2A, B, \bigcirc , S1–S4). An EC₅₀ = 3.2 \pm 1.6 μ M calculated to a 40-fold

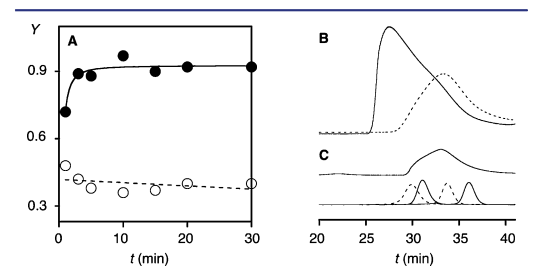


Figure 3. Polymers of 1 made with (♠, solid) and without (O, dashed) initiator 5. (A) Y during polymerization of 1 (100 mM) with (♠) and without 5 (O, 5 mM, pH 7). (B) GPC of 1 (100 mM) polymerized with (solid) and without 5 (dashed, 5 mM, pH 7), compared to (C) polyarginine (top) and standards (bottom, $M_{\rm W}$ 43, 25, 13.7, and 6.5 kDa); Superdex 75, 30% acetonitrile in acetate buffer, pH 6.5.

increase in activity upon substrate-initiated polymerization of propagator 1 with initiator 5 and terminator 9 (Figures 2B, \bigoplus , S2-S4).

According to activity in EYPC-LUVs CF, substrate-initiated polymerization of propagator 1 was accomplished in less than 5 min (Figure 3A, ●). Polymerization was better in the presence than in the absence of initiator 5 (Figures 3A, S2-S4). This conclusion was supported by gel-permeation chromatography (GPC). Polymers obtained from propagator 1 in the presence of initiator 5 were of high molecular weight ($M_w = 62.7 \text{ kDa}$) and dispersity (PDI = 1.83, Figure 3B, solid). Considering increasing transport activity with polymer length but less predictable length-dependence of cellular uptake of CPPs, high molecular weight and dispersity compared to commercially available polyarginine ($M_{\rm w}$ = 16.7 kDa, PDI = 1.7, Figure 3C, solid) were both very desirable characteristics. The same was true for the disappearance of all activity in EYPC-LUVs CF within minutes of incubation with 10 mM DTT (Figure S7).7 This is in the range of cytosolic glutathione (~5 mM) and thus confirms the previously reported biodegradability of cellpenetrating poly(disulfide)s.3,4 Without initiator, weaker absorbance, i.e., lower yield of polymer, at lower $M_w \sim 16.2$ kDa was observed (PDI = 2.1, Figure 3B, dashed).

The polymerization of propagator 1 was analyzed systematically from pH 5 to pH 9 and concentrations from 25 to 200 mM in the presence and the absence of 5 mM initiator 5 (p $K_{\rm a}$ ~ 9.5, Figure 4A, B). Best results were obtained with 100 mM 1 in 1 M TEOA, pH 7 (Figure 4A, B, dotted lines). At lower pH and concentrations, the substrate-initiate polymerization was

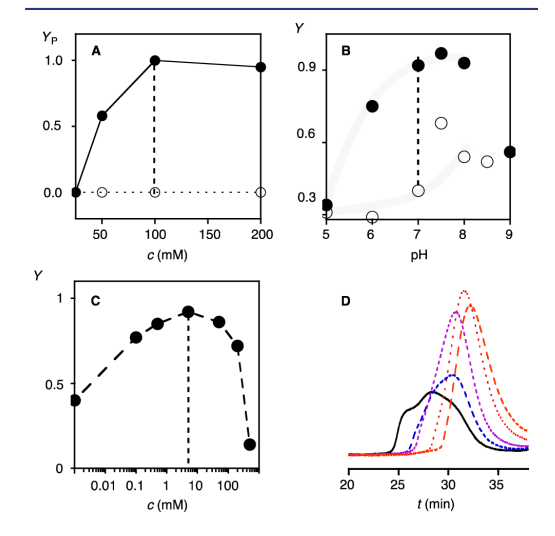


Figure 4. Dependence on propagator concentration (A), pH (B) and initiator concentration (C, D). (A) $Y_{\rm P}$ after polymerization of increasing concentration c of 1 with (\bullet) and without 5 (O, 5 mM, 1 M TEOA, pH 7, 10 min; assay: 75 μ M guanidinium each, $Y_{\rm P} = Y$ normalized to Y=0 before polymerization and Y=1 for maximal activity). (B) Y after polymerization with increasing pH (5 mM 5 (\bullet), 0 mM 5 (O), 100 mM 1, 1 M buffer). (C) Y after polymerization with increasing concentration of 5 (100 mM 1, pH 7). (D) GPC after polymerization with 5 (with increasing $t_{\rm R}$: 0.5, 1, 2, 5, 10 mM; 200 mM 2, pH 7.5).

2089

dx.doi.org/10.1021/ja311961k | J. Am. Chem. Soc. 2013, 135, 2088-2091

incomplete, at higher pH, random polymerization without initiator as well as precipitation started to interfere.

The bell-shaped dependence on initiator concentration was in agreement with the formation of fewer polymers at low and more but shorter and thus less active ones at high initiator concentrations (Figure 4C). Corroborative evidence for the incorporation of the initiators into the polymers was obtained by GPC. Polymers obtained from propagator 2 and increasing concentrations of initiator 5 gave polymers with decreasing molecular weight and dispersity (Figure 4D). Moreover, polymers obtained with Cys-Trp initiator 6 showed the tryptophan emission in the GPC peak. The relative Trp emission increased with decreasing molecular weight, that is decreasing polymer/initiator ratio (Figure S8).

The substrate-initiated polymerization of propagators 1 and 2 with the strained disulfides from lipoic acid was straightforward to control and optimize. The disulfides from asparagusic acid are ideal for surface-initiated polymerization but turned out to be too reactive for substrate-initiated polymerization in solution. Independent of their backbone, propagators 3 and 4 more easily polymerized with less difference between substrate-initiated and random polymerization without initiator (Figure S6). Moreover, cell-penetrating poly(disulfide)s obtained from lipoyl propagators 1 and 2 were active in EYPC LUVs, whereas the less lipophilic polymers from asparagusyl propagators 3 and 4 were poorly active. However, like arginine-rich CPPs, all polymers could be activated in EYPC LUVs by counterions such as pyrenebutyrate (Figures S5, S6).

To probe for substrate-initiated polymerization also with the less perfect asparagusyl propagators, fluorescence resonance energy transfer (FRET) was considered as a method complementary to the functional studies with fluorogenic LUVs and GPC described above for the preferable lipoyl propagators. Polymerization of propagator 4 in CHCl₃/DMF 3:1 was initiated with the yellow, green-fluorescent naphthalenediimide (NDI)⁶ fluorophore 7 ($\lambda_{\rm ex} = 469$ nm, $\lambda_{\rm em} = 484$ nm) and 0.25% Hünig base (DIEA) as base, and terminated with the red NDI 8 ($\lambda_{\rm ex} = 552$ nm, $\lambda_{\rm em} = 582$ nm, Figure 5). With

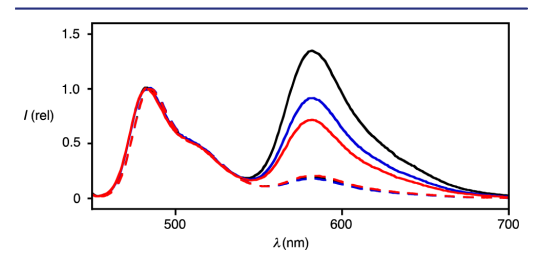


Figure 5. FRET from initiator 7 to terminator 8. Emission spectra (λ_{ex} = 445 nm, CHCl₃) after polymerization of 4 (25 mM) with 7 (1 mM) for 5 s (black), 30 s (blue) and 60 s (red) in CHCl₃/DMF 3:1 (0.25% DIEA), terminated with 8 (2 mM, solid) and depolymerized with DTT (10 mM, dashed).

increasing polymerization time, the FRET emission at $\lambda_{\rm em} = 582$ nm in CHCl₃ decreased (Figure 5). This decrease was consistent with increasing distance between initiator and terminator with increasing reaction time. Depolymerization with DTT caused nearly complete disappearance of FRET (Figure 5, dotted). These results further demonstrated the incorporation of the terminator in the polymer.

In summary, substrate-initiated polymerization of cellpenetrating poly(disulfide)s is introduced as a conceptually new approach to cellular uptake. Two types of propagators and four unrelated methods to prove direct growth of polymers on substrates are described. Namely, (a) polymers obtained with and without initiators are different, (b) the dependence on initiator concentration is bell-shaped, (c) labeled initiators are eluted with polymers in GPC, and (d) FRET between donating initiators and accepting terminators decreases with polymerization time. Ring-opening disulfide exchange polymerization with propagators derived from lipoic acid is facile to control (pH, concentration of initiators, propagators, etc.) and gives polymers with high, stimuli-responsive transport activity in neutral lipid bilayers, whereas propagators derived from asparagusic acid are too reactive and give polymers that require counterion activation for function. With these complete, clear and consistent results, the newly introduced system is ready for cellular uptake experiments ¹⁰ and copolymerization studies^{1a,6b,f} to modulate the properties of the cell-penetrating poly(disulfide)s.

ASSOCIATED CONTENT

S Supporting Information

Details on experimental procedures. This material is available free of charge via the Internet at http://pubs.acs.org.

AUTHOR INFORMATION

Corresponding Author

Stefan.Matile@unige.ch

Author Contributions

[†]These authors contributed equally.

Notes

The authors declare no competing financial interest.

ACKNOWLEDGMENTS

We thank D. Jeannerat, A. Pinto and S. Grass for NMR measurements, the Sciences Mass Spectrometry (SMS) platform for mass spectrometry services, and the University of Geneva, the European Research Council (ERC Advanced Investigator), the National Centre of Competence in Research (NCCR) in Chemical Biology and the Swiss NSF for financial support.

■ REFERENCES

(1) (a) Tezgel, A. O.; Gonzalez-Perez, G.; Telfer, J. C.; Osborne, B. A.; Minter, L. M.; Tew, G. N. Mol. Ther. 2013, 21, 201-209. (b) Som, A.; Reuter, A.; Tew, G. N. Angew. Chem., Int. Ed. 2012, 51, 980-983. (c) Appelbaum, J. S.; LaRochelle, J. R.; Smith, B. A.; Balkin, D. M.; Holub, J. M.; Schepartz, A. Chem. Biol. 2012, 19, 819-830. (d) Ornelas-Megiatto, C.; Wich, P. R.; Fréchet, J. M. J. Am. Chem. Soc. 2012, 134, 1902-1905. (e) Treat, N. J.; Smith, D.; Teng, C.; Flores, J. D.; Abel, B. A.; York, A. W.; Huang, F.; McCormick, C. L. ACS Macro Lett. 2012, 1, 100-104. (f) Budhathoki-Uprety, J.; Peng, L.; Melander, C.; Novak, B. M. ACS Macro Lett. 2012, 1, 370-374. (g) Song, A.; Walker, S. G.; Parker, K. A.; Sampson, N. S. ACS Chem. Biol. 2011, 6, 590-599. (h) Tezgel, A. O.; Telfer, J. C.; Tew, G. N. Biomacromolecules 2011, 12, 3078-3083. (i) Gorska, K.; Manicardi, A.; Barluenga, S.; Winssinger, N. Chem. Commun. 2011, 47, 4364-4366. (k) Dix. A. V.; Fischer, L.; Sarrazin, S.; Redgate, C. P. H.; Esko, I. D.; Tor, Y. ChemBioChem 2010, 11, 2302-2310. (1) Inomata, K.; Ohno, A.; Tochio, H.; Isogai, S.; Tenno, T.; Nakase, I.; Takeuchi, T.; Futaki, S.; Ito, Y.; Hiroaki, H.; Shirakawa, M. Nature 2009, 458, 106-109. (m) McNaughton, B. R.; Cronican, J. J.; Thompson, D. B.; Liu, D. R. Proc. Natl. Acad. Sci. U.S.A. 2009, 106, 6111-6116. (n) Trantow, B.

M.; Cooley, C. B.; Nederberg, F.; Kiesewetter, M. K.; Hedrick, J. L.; Waymouth, R. M.; Wender, P. A. J. Am. Chem. Soc. 2009, 131, 16401-16403. (o) Kolonko, E. M.; Pontrello, J. K.; Mangold, S. L.; Kiessling, L. L. J. Am. Chem. Soc. 2009, 131, 7327-7333. (p) Wender, P. A.; Galliher, W. C.; Goun, E. A.; Jones, L. R.; Pillow, T. H. Adv. Drug Delivery Rev. 2008, 60, 452-472. (q) Esbjorner, E. K.; Lincoln, P.; Norden, B. Biochem. Biophys. Acta 2007, 1768, 1550-1558. (r) Shimanouchi, T.; Walde, P.; Gardiner, J.; Mahajan, Y. R.; Seebach, D.; Thomae, A.; Kraemer, S. D.; Voser, M.; R. Kuboi, R. Biochem. Biophys. Acta 2007, 1768, 2726-2736. (s) Kale, A. A.; Torchilin, V. P. Bioconjugate Chem. 2007, 18, 363-370. Martinell, M.; Salvatella, X.; Fernández-Carneado, J.; Gordo, S.; Feliz, M.; Menéndez, M.; Giralt, E. ChemBioChem 2006, 7, 1105-1113. (t) Schmidt, D.; Jiang, Q. X.; MacKinnon, R. Nature 2006, 444, 775-779. (u) Fischer, R.; Fotin-Mleczek, M.; Hufnagel, H.; Brock, R. ChemBioChem 2005, 6, 2126-2142. (v) Pantarotto, D.; Briand, J.-P.; Prato, M.; Bianco, A. Chem. Commun. 2004, 16-17. (w) Jiang, T.; Olson, E. S.; Nguyen, Q. T.; Roy, M.; Jennings, P. A.; Tsien, R. Y. Proc. Natl. Acad. Sci. U.S.A. 2004, 101, 17867-17872. (x) Umezawa, N.; Gelman, M. A.; Haigis, M. C.; Raines, R. T.; Gellman, S. H. J. Am. Chem. Soc. 2002, 124, 368-

- (2) (a) Sakai, N.; Matile, S. J. Am. Chem. Soc. 2003, 125, 14348–14356. (b) Takeuchi, T.; Kosuge, M.; Tadokoro, A.; Sugiura, Y.; Nishi, M.; Kawata, M.; Sakai, N.; Matile, S.; Futaki, S. ACS Chem. Biol. 2006, 1, 299–303.
- (3) Bang, E.-K.; Lista, M.; Sforazzini, G.; Sakai, N.; Matile, S. Chem. Sci. 2012, 3, 1752–1763.
- (4) (a) Kim, T. I.; Rothmund, T.; Kissel, T.; Kim, S. W. J. Controlled Release 2011, 152, 110–119. (b) Kim, T.; Kim, S. W. React. Funct. Polym. 2011, 71, 344–349. (c) Lin, C.; Engbersen, J. F. J. Expert Opin. Drug Delivery 2009, 6, 421–439. (d) Son, S.; Namgung, R.; Kim, J.; Singha, K.; Kim, W. J. Acc. Chem. Res. 2011, 152, 110–119. (e) Meng, F.; Hennink, W. E.; Zhong, Z. Biomaterials 2009, 30, 2180–2198.
- (5) Thiols at the cell surface have been proposed to further contribute to the uptake of disulfide-containing systems. Torres, A. G.; Gait, M. J. Trends Biotechnol. 2012, 30, 185–190.
- (6) (a) Sakai, N.; Lista, M.; Kel, O.; Sakurai, S.; Emery, D.; Mareda, J.; Vauthey, E.; Mattle, S. J. Am. Chem. Soc. 2011, 133, 15224–15227.
 (b) Lista, M.; Areephong, J.; Sakai, N.; Matile, S. J. Am. Chem. Soc. 2011, 133, 15228–15230. (c) Sakai, N.; Matile, S. J. Am. Chem. Soc. 2011, 133, 18542–18545. (d) Charbonnaz, P.; Sakai, N.; Matile, S. Chem. Sci. 2012, 3, 1492–1496. (e) Areephong, J.; Orentas, E.; Sakai, N.; Matile, S. Chem. Commun. 2012, 48, 10618–10620. (f) Orentas, E.; Lista, M.; Lin, N.-T.; Sakai, N.; Matile, S. Nat. Chem. 2012, 4, 746–750
- (7) See SI
- (8) (a) Takeuchi, T.; Matile, S. Chem. Commun. 2013, 49, 19–29. (b) Litvinchuk, S.; Tanaka, H.; Miyatake, T.; Pasini, D.; Tanaka, T.; Bollot, G.; Mareda, J.; Matile, S. Nat. Mater. 2007, 6, 576–580. (c) Sakai, N.; Sordé, N.; Matile, S. J. Am. Chem. Soc. 2003, 125, 7776–7777. (d) Sordé, N.; Das, G.; Matile, S. Proc. Natl. Acad. Sci. U.S.A. 2003, 100, 11964–11969. (e) Das, G.; Talukdar, P.; Matile, S. Science 2002, 298, 1600–1602.
- (9) Burns, J. A.; Whitesides, G. M. J. Am. Chem. Soc. 1990, 112, 6296-6303.
- (10) Preliminary results with cell-penetrating poly(disulfide)s grown with 1 and 2 on fluorescent probes as initiators revealed efficient uptake into HeLa cells. These ongoing studies will be reported in due course.



Cellular Uptake of Substrate-Initiated Cell-Penetrating Poly(disulfide)s

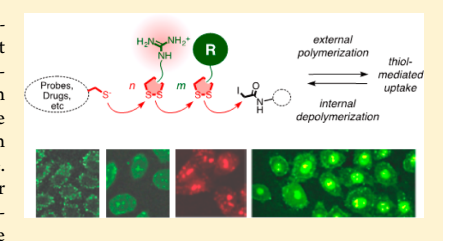
Giulio Gasparini, Eun-Kyoung Bang, Suillaume Molinard, David V. Tulumello, Sandra Ward, Shana O. Kelley, Aurelien Roux, Naomi Sakai, and Stefan Matile*,

[†]School of Chemistry and Biochemistry, National Centre of Competence in Research (NCCR) Chemical Biology, University of Geneva, Geneva 1211, Switzerland

[‡]Department of Pharmaceutical Sciences and Department of Biochemistry, University of Toronto, Toronto, Ontario M5S 3M2,

Supporting Information

ABSTRACT: Substrate-initiated, self-inactivating, cell-penetrating poly-(disulfide)s (siCPDs) are introduced as general transporters for the covalent delivery of unmodified substrates of free choice. With ring-opening disulfideexchange polymerization, we show that guanidinium-rich siCPDs grow on fluorescent substrates within minutes under the mildest conditions. The most active siCPD transporters reach the cytosol of HeLa cells within 5 min and depolymerize in less than 1 min to release the native substrate. Depolymerized right after use, the best siCPDs are nontoxic under conditions where cell-penetrating peptides (CPPs) are cytotoxic. Intracellular localization (cytosol, nucleoli, endosomes) is independent of the



substrate and can be varied on demand, through choice of polymer composition. Insensitivity to endocytosis inhibitors and classical structural variations (hydrophobicity, aromaticity, branching, boronic acids) suggest that the best siCPDs act differently. Supported by experimental evidence, a unique combination of the counterion-mediated translocation of CPPs with the underexplored, thiol-mediated covalent translocation is considered to account for this decisive difference.

■ INTRODUCTION

Efficient cellular delivery is one of the key problems that hampers discovery and development of novel drugs and probes. The problem is most pronounced for but not limited to larger substrates, including oligonucleotides, proteins, and nanoparticles. Since the discovery of the TAT peptide more than 20 years ago,2 a broad variety of arginine-rich cellpenetrating peptides (CPPs) and CPP mimics have been introduced for this purpose.3 Attached or complexed to CPPs, otherwise undeliverable molecules such as drugs, fluorophores, proteins, siRNA, plasmid DNA, or quantum dots are able to cross the cellular barrier. However, CPPs can be cytotoxic, are often trapped in the endosomes, and do not always work reliably. Counterion-mediated translocation has been introduced to improve direct cytosolic delivery and bypass endosomal capture. 4 To reduce toxicity, the sequence as well as the peptidic backbone of CPPs have been varied extensively.³ One of the most promising modifications is represented by cell-penetrating poly(disulfide)s (CPDs). 5,6 Despite the growing interest in CPDs, synthetic methods to produce them are mainly focused on the postmodification of existing polymers (such as polyethylenimine, PEI) or the reaction of monomers already containing a disulfide, and their use has been mainly limited to noncovalent gene transfection.

Inspired by the robustness of the recently discovered ringopening disulfide-exchange polymerization to grow complex functional architectures directly on solid surfaces, we have

proposed to grow CPD transporters directly on molecular substrates in solution, in situ, right before delivery (Figure 1). The term "substrate" is used here to designate any object in need of assistance to enter cells (e.g., drugs, probes, peptides, proteins, DNA, RNA, etc.). Reductive depolymerization of the obtained substrate-initiated (si) CPDs by endogenous glutathione (GSH) in the cytosol would then eliminate toxicity and liberate the native substrate. The siCPD concept promises access to a general, fast, and noninvasive method for the covalent delivery of unmodified substrates, nontoxic, traceless, avoiding noncovalent formulations, and applicable to any substrate of free choice.

The growth of the CPD transporter on the molecular substrate in solution is initiated by a thiol (or a complementary functional group converter) that acts as an initiator I of the disulfide-exchange polymerization (Figure 1). Nucleophilic disulfide exchange opens the strained disulfide in the otherwise freely variable monomer M. forms a covalent disulfide bond between \boldsymbol{I} and \boldsymbol{M} , and regenerates a reactive thiol to attack the next M. The polymerization is terminated with an iodoacetamide T. The simplest possible terminator T is used in this study, but the introduction of additional drugs or probes with the freely variable T is of course inviting for the future. In this study, siCPDs are grown on fluorescent substrates to monitor,

Received: February 14, 2014 Published: April 15, 2014



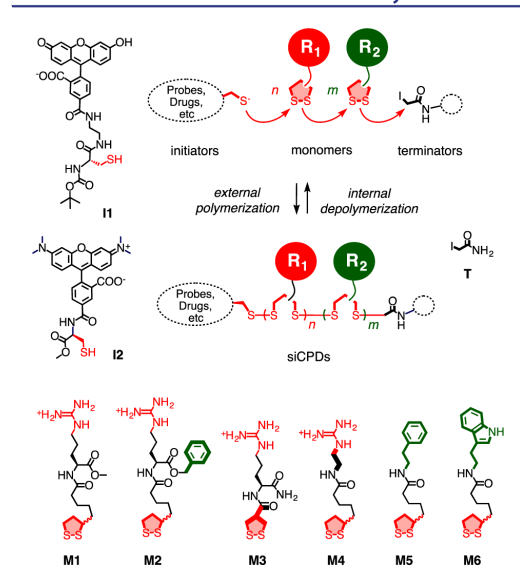


Figure 1. Concept of substrate-initiated, self-inactivating CPD transporters. Fluorescent initiators (I1 derived from carboxyfluorescein and I2 derived from rhodamine) were used to generate polymers through ring-opening disulfide-exchange polymerization or copolymerization of monomers M1–M6. The polymerization process was controlled using iodoacetamide T as the terminator.

for the first time, their entry into HeLa cells. Experimental evidence is provided that siCPDs (1) enter cells within 5 min, (2) can depolymerize in less than 1 min after uptake, (3) are much less toxic than CPPs, (4) operate independent of the attached substrate, (5) can target different organelles on demand, and (6) can enter cells by endocytosis or direct translocation across the membrane barrier, depending on their structure. Presumably, their uptake is mediated by a so far underexploited disulfide exchange with endogenous thiols at

the membrane surface, ^{1,6} i.e., a conceptually innovative, dynamic-covalent ⁹ way to enter cells.

RESULTS AND DISCUSSION

Design and Synthesis. To study the capability of siCPDs to enter cells, fluorescent initiators I1 derived from carboxyfluorescein (CF) and I2 from 5-carboxytetramethylrhodamine (TAMRA) and monomers M1-M6 were envisioned first (Figure 1). In M1, racemic lipoic acid offers the strained disulfide needed for ring-opening disulfide-exchange polymerization initiated by the fluorescent thiols I1 and I2, whereas Larginine offers the guanidinium cation needed to obtain polymers that can cross bilayer membranes like CPPs. In M2, the methyl ester of M1 is replaced by a benzyl ester to increase hydrophobicity and add π -basicity to the polymer. In M3, the lipoic acid of M1 is replaced by a more reactive asparagusic acid. In M4, the spacer between the guanidinium cation and lipoic acid is as short as possible. The new M5 and M6 contain the essence of phenylalanine (Phe) and tryptophan (Trp) with similarly minimalist spacers for copolymerization with the cationic M4. The synthesis of all initiators and monomers was very straightforward (Scheme S1, Supporting Information).

Substrate-initiated polymerization⁸ and copolymerization¹¹ with M1-M6 were best in buffer at pH 7.0-7.5 in 5-30 min at room temperature, depending significantly on the nature of the monomer. The formation of siCPDs was routinely followed by the appearance of transport activity in fluorogenic vesicles (see below). 8,10,11 All new siCPDs were characterized by gel permeation chromatography (GPC; Figure S1, Supporting Information) to determine molecular weight and polydispersity and MALDI MS to also confirm the composition of the copolymers (Figures S2-S4, Supporting Information). Under these conditions, 200 mM M1-M4 polymerized with 5 mM I1, a thiolated derivative of CF, for example, afforded fluorescent siCPDs 1-4 with an average molecular weight (M_w) of 6000-10000 and a polydispersity index (PDI) of ~1.5 (Table S2, Supporting Information). The length of the polymers was variable on demand; shorter polymers were obtained with higher initiator concentrations or shorter reaction time. All siCPDs tested were purified by GPC before use to remove

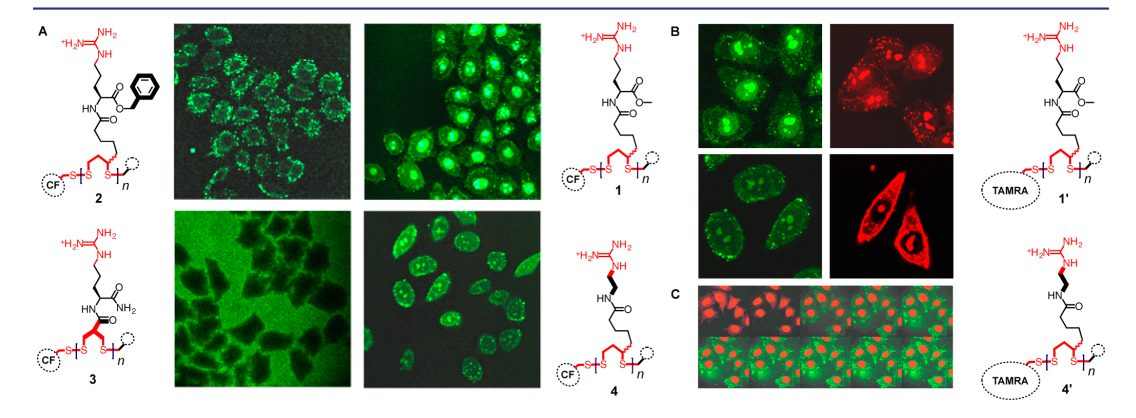


Figure 2. Cellular uptake of fluorescent siCPDs. (A) CLSM images of HeLa cells after 15 min of incubation with CF-labeled polymers 1-4, 500 nM polymer in Leibovitz medium at 37 °C. (B) Same for polymers 1 and 4 prepared from CF (I1) or TAMRA (I2). (C) Spinning disk microscopy kinetics of the uptake of CF-labeled polymer 4 into HeLa cells transfected in the presence of DRAQ5 (500 nM 4 in Leibovitz medium, 37 °C). Images were taken with a time interval of 1 min. The first image corresponds to t=0.

6070

dx.doi.org/10.1021/ja501581b | J. Am. Chem. Soc. 2014, 136, 6069-6074

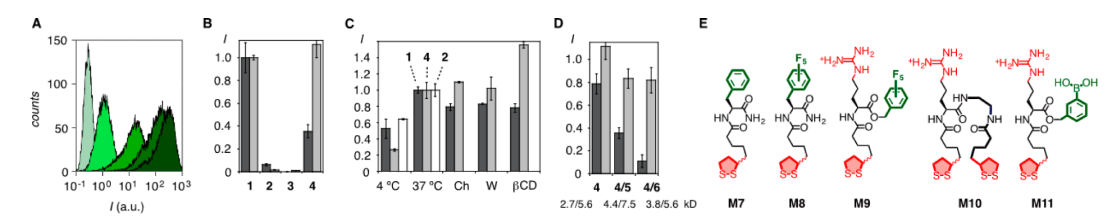


Figure 3. Mechanistic and structural insights into the entry of siCPDs into HeLa cells. (A) Flow cytometry analysis counting fluorescent HeLa cells after incubation with 500 nM initiator I1 (left, light green, overlap with blank) and CF-labeled (co)polymers 1/2 (0:1, 2:1, 8:1, 1:0, with increasing fluorescence instensity I). Surface-bound material was removed by washing three times with heparin-containing PBS. (B) Uptake quantification for CF-labeled polymers 1–4 with CLSM (dark) and flow cytometry (light), normalized to fluorescence intensity I with 1. (C) Flow cytometry data for the uptake of CF-labeled polymers 1 (dark), 4 (light), and 2 (empty) into HeLa cells at 4 and 37 °C and, for 1 and 4 only, also in the presence of chlorpromazine (Ch), wortmannin (W), and methyl- β -cyclodextrin (β CD), normalized to I at 37 °C. (D) Flow cytometry data for the uptake of low (light) and high (dark) molecular weight, CF-labeled polymer 4 and copolymers 4/5 (8:1) and 4/6 (8:1) into HeLa cells, normalized to I with 1 (A). Error bars indicate the mean \pm standard deviation, $n \ge 3$. (E) Structure of additional monomers prepared to grow siCPDs (compare Figure 1).

unused reagents and eventual side products with low molecular weight.

Cellular Uptake. The ability of the siCPDs 1-4 to transport a fluorescent CF substrate into HeLa Kyoto cells was examined using confocal laser scanning microscopy (CLSM). After incubation for 15 min at 37 °C with a 500 nM solution of the desired polymer in Leibovitz medium, the cells were washed with PBS containing heparin (20 U/mL) to remove siCPDs that are bound reversibly at the cell surface (or can exit the cells as easily as they entered). Significant intracellular fluorescent signals were recorded from cells incubated with siCPDs 1, 2, and 4 (Figure 2A). Only polymer 3 grown with asparagusic instead of lipoic acid did not carry CF substrates into HeLa cells. The inactivity of polymer 3 in HeLa cells perfectly reflected the inactivity of polymer 3 as a transporter in fluorogenic vesicles.⁸ This finding thus corroborated the validity of model studies in fluorogenic vesicles to, at least in part, predict the activity of siCPDs as well as CPPs.^{8,11} The CF and TAMRA initiators I1 and I2 alone did not enter HeLa cells under experimental conditions (Figure S7, Supporting Information).

The intracellular distribution of CF-labeled siCPDs 1–4 differed significantly. The original siCPD 1 accumulated mainly inside the nucleus, especially in the nucleoli (Figure 2A, top right, B, top left). The minimalist siCPD 4 localized mainly in the cytoplasm (Figure 2A, bottom right, B, bottom left). The more hydrophobic, π -basic siCPD 2 remained mainly trapped inside the endosomes (Figure 2A, top left). The localization of different siCPDs in different organelles was relatively independent of the concentration and incubation time.

To explore the dependence of siCPD uptake on the attached substrate, polymers 1' and 4' were grown with initiator 12, a thiolated derivative of TAMRA. HeLa Kyoto cells were incubated under the conditions used for the CF-labeled siCPDs 1 and 4. The results demonstrated that siCPDs 1' and 4' grown with the neutral TAMRA 12 behave exactly like siCPDs 1 and 4 grown with the anionic CF 11 (Figure 2B). Namely, siCPDs delivered their substrates reliably to the nucleoli and cytoplasm, respectively, independent of the nature of the substrates.

The kinetics of cellular uptake and localization of CF-labeled siCPD 4 were measured with HeLa Kyoto cells that were treated with DRAQ5 to visualize their nuclei in the far red. Spinning disk microscopy images were recorded immediately after the addition of the polymer solution and with a time interval of 1 min during incubation with 500 nM in Leibovitz

medium at 37 °C (Figure 2C). Already after 2 min of incubation, intracellular fluorescence could be observed. Within 10 min, siCPD 4 accumulated in the cytosol but was unable to significantly enter into the nucleus. Intracellular fluorescence intensity was preserved after removal of the polymer solution used to incubate the cells. This irreversible accumulation of siCPD 4 in the cytosol was in excellent agreement with fast reductive depolymerization of siCPD 4 in the cytosol (see below).

Flow cytometry was used for rapid access to quantitative data (Figure 3A). Comparison with CLSM data for polymers 1–4 revealed comparable trends but clear underestimates with CLSM for cytosolic emission from siCPD 4, which performs the best according to flow cytometry (Figure 3B).

Significant uptake of siCPDs 1, 2, and 4 was observed at 4 °C (Figure 3C). This demonstrated that uptake does not occur exclusively by endocytosis.^{3,4b} Compared to that at 37 °C, reduced activity found at 4 °C could originate simply from less favorable direct translocation across the rigidified membranes, ¹² although losses from missing contributions from endocytosis cannot be excluded.

Comparably high activity was obtained with siCPD 2, although endosomal location at 37 °C demonstrated exclusive uptake by endocytosis, but CLSM images obtained at 4 °C showed the hydrophobic siCPD 2 mainly at the surface, probably too deeply buried in the hydrophobic core of the membrane to be removed by washing with heparin (Figure S6B, Supporting Information).¹³ Preserved localization for siCPDs 1 and 4 in the nucleoli and cytosol, respectively, at 4 °C was in agreement with a preserved uptake mechanism, i.e., dominant direct translocation across the membrane (Figure S6A,C). The validity of this interpretation was further supported by insensitivity of siCPDs 1 and 4 to selective endocytosis inhibitors, i.e., wortmannin for macropinocytosis, chlorpromazine for clathrin-mediated endocytosis, and methyl- β -cyclodextrin (M β CD) for caveolar endocytosis. ¹⁴ The distinct increase in activity of siCPDs 4 with M β CD could originate from facilitated translocation across cholesterol-poor membranes.15

The activity of siCPD 4 increased with increasing length of the polymer (Figure 3D). The same trend, even more pronounced, was found for the more hydrophobic copolymers 4/5 and 4/6. Significant length dependence was as expected because both transport activity in membranes 4a,16 and

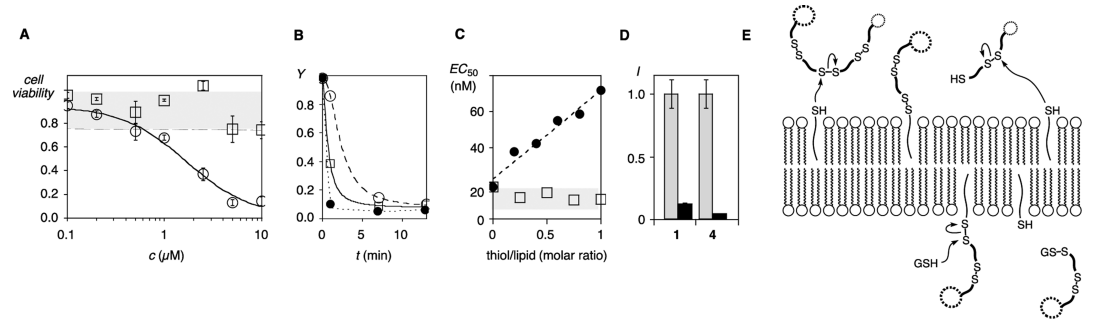


Figure 4. Toxicity, depolymerization, and thiol-mediated translocation of siCPDs. (A) Cell viability measured with the MTT assay for polymer 4 (squares) and poly-L-arginine (circles) at different concentrations. (B) Relative transport activity Y of polymer 4 (filled symbols) and 1 (empty symbols) in fluorogenic vesicles after incubation with 2.5 mM (circles) and 5 mM (squares) glutathione (GSH) for time t. (C) Effective concentration of polymer 4 in fluorogenic vesicles in the presence of increasing amounts of octadecanethiol (circles) and GSH (squares). (D) Flow cytometry data for the uptake of CF-labeled polymers 1 and 4 into HeLa cells with (dark) or without (light) pretreatment with 1.2 mM DTNB for 30 min before addition of siCPDs. Uptake for each polymer is normalized to 1.0 in the absence of DTNB. (E) Proposed mechanism for thiol-mediated uptake of siCPDs.

contributions from endocytosis (and toxicity) generally increase with the length of related polymers, including CPPs.³

However, the introduction of hydrophobic benzyl and indolyl residues in copolymers 4/5 and 4/6 neither increased the activity of siCPD 4 nor changed the preferential accumulation in the cytosol (Figure 3D). Consistently decreasing activity with increasing hydrophobicity, in sharp contrast to many observations with CPPs and the general importance of Phe and Trp for membrane protein function, already provided first indications that siCPDs might be fundamentally different and function by a different mechanism (see below). Similarly decreasing activity with increasing hydrophobicity was found in the amino acid series with π basic copolymers 1/2 (Figure 3A) and 1/7 and, slightly less pronounced, also with superhydrophobic π -acids in copolymers 1/8 and 1/9 (Figure S8, Supporting Information). The branched polymer 10 or copolymers 1/10 obtained with the divalent monomer M10 showed particularly poor activity and high toxicity (Figures S8 and S9, Supporting Information). Also boronic acids in copolymers 1/11 did not increase activity despite the possibility to assist uptake with the formation of dynamic covalent boronic ester bonds with glycosaminoglycans at the cell surface, thus enhancing the local concentration and promoting uptake. Sf,17 Quite the contrary, a less desired increase of copolymers 1/11 permanently located at the cell surface and in the endosomes was noted in CLSM images (Figure S6D, Supporting Information). This general failure to improve performance with fairly standard structural modifications suggested that the cellular uptake of siCPDs 1 and 4 is already near maximum levels for this class of transporters and possibly occurs by a different mechanism compared to that of other CPP mimics, i.e., thiol-mediated uptake.

Toxicity, Internal Depolymerization, and Exofacial Thiols. Why are siCPDs better? What really makes the difference? Toxicity was quantified first. MTT assays were performed with the cytosolic siCPD 4 in comparison with poly-Larginine as a comparable CPP. In this assay, the metabolic activity of the cells was assessed by their ability to enzymatically convert the tetrazolium dye MTT into formazan. The polymers were incubated with HeLa cells for 15 min at a concentration ranging from 0.1 to 10 μ M. Then the polymer

solution was removed, and the cells were washed with heparin sulfate. After addition of culture media, the cells were incubated for 24 h prior to execution of the MTT assay. Under these conditions, siCPD 4 showed negligible cytotoxicity up to 10 μ M, whereas polyarginine (16.4 kDa) exhibited an EC₅₀ below 2 μM (Figure 4A; hexaarginine was also cytotoxic at 10 μM). The nontoxicity of siCPD 4 was in excellent agreement with rapid depolymerization as soon as the cytosol is reached (see below). All siCPDs tested had good cell viability in the concentration used for the cellular uptake measurements (Figure S9, Supporting Information). However, contrary to the nontoxic siCPD 4 in the cytosol, siCPD 1 was increasingly cytotoxic at higher concentrations. This finding was consistent with incomplete depolymerization before leaving the cytosol (see below) and subsequent interference with cellular function after binding to the oligonucleotides in the nucleoli.

Cytosolic depolymerization was quantified next. It is difficult to quantify in cells, so transport studies in fluorogenic vesicles were selected to secure direct evidence. In this firmly validated assay (see above, Figure S5, Supporting Information), 8,11 large unilamellar vesicles (LUVs) composed of egg yolk phosphatidylcholine (EYPC) are loaded with CF at concentrations high enough to ensure self-quenching. Local dilution upon CF export by siCPDs, ^{8,11} CPPs, ^{3,4,15} or other anion transporters is then observed as fluorescence recovery. Consistent with perfect cellular uptake, siCPDs 1 and 4 showed maximal transport activity in the CF assay (without activation by amphiphilic counterions, polyarginine is inactive in EYPC vesicles).4 Incubation with GSH at cytosolic concentrations resulted in rapid loss of activity. The cytosolic siCPDs 4 was completely inactivated within less than 1 min by 2.5 mM GSH (Figure 4B, •). Depolymerization of the nucleolar siCPDs 1 by 2.5 mM GSH was complete within about 5 min (Figure 4B, □). The lifetime of the transporter in 5 mM GSH was clearly shorter (Figure 4B, \bigcirc).

Sensitivity toward exofacial thiols was explored last. The presence of octadecanethiol in the EYPC membrane significantly changed the transport activity of siCPD 4 (Figure 4C, \bullet). At a molar ratio octadecanethiol/lipid of 1:1, the EC₅₀ of 4, i.e., the effective siCPD concentration to reach 50% activity, was weakened by a factor of 4. A similar increase of the EC₅₀

6072

dx.doi.org/10.1021/ja501581b | J. Am. Chem. Soc. 2014, 136, 6069-6074

was not observed in the presence of equivalent concentrations of GSH (Figure 4C, []; these GSH concentrations are far below the ones needed to depolymerize siCPD 4 as in Figure 4B, ●). Activation by thiols at the membrane surface but insensitivity to equimolar thiols in the water indicated that disulfide exchange between siCPD 4 and exofacial thiols occurs. In fluorogenic vesicles, the resulting shortening of siCPD 4 caused a loss in activity. In cells, this covalent binding to the surface is expected to increase the local concentration of the siCPD and thus accelerate direct, counterion-mediated translocation across the membrane (Figure 4E). Experimental evidence for thiol-mediated translocation from fluorogenic vesicles is unprecedented. To evaluate the validity of this implication from fluorogenic vesicles, the inhibition of thiolmediated translocation with Ellman's reagent (i.e., 5,5'dithiobis-2-nitrobenzoic acid, or DTNB) was explored directly in HeLa cells. The cells were incubated with the cellimpermeable DTNB for 30 min to convert all free thiols at the surface into disulfides. According to flow cytometry measurements, cellular uptake of siCPDs 1 and 4 was significantly reduced in the absence of exofacial thiols (Figure 4D). Similarly reduced uptake has been observed previously for other cell-penetrating poly(disulfide)s. 1,6 The inactivation by Ellman's reagent was more pronounced for siCPD 4 than for siCPD 1. Considering that siCPD 4 depolymerizes faster than siCPD 1 (Figure 4C), this difference implied that the efficiency of thiol-mediated translocation is determined by the velocity of disulfide exchange.

CONCLUSIONS

This study introduces substrate-initiated cell-penetrating poly-(disulfide)s as general, nontoxic, self-inactivating transporters for the covalent delivery of native substrates of free choice. We provide experimental evidence that the formation of siCPDs can be initiated by fluorescent probes and occurs within minutes under the mildest conditions (water, room temperature, pH 7) and that the most active siCPDs reach the cytosol of HeLa cells in 5 min, where they depolymerize in less than 1 min. The most active siCPDs are nontoxic at all tested concentrations (up to 10 μ M), whereas comparable CPPs are toxic. Intracellular localization and the uptake mechanism are independent of the substrate and can be varied on demand by varying the hydrophobicity and disulfide-exchange kinetics. Namely, more hydrophobic siCPDs enter mainly by endocytosis and accumulate in endosomes. More hydrophilic siCPDs with fast disulfide-exchange kinetics accumulate in the cytosol because they depolymerize as soon as they arrive. In clear contrast, the lifetime of siCPDs with slow disulfideexchange kinetics is sufficient for them to proceed from the cytosol to the nucleus and accumulate on the anionic oligonucleotides in the nucleoli.

The simplest siCPDs are the best. The most compact siCPD 4 is derived from lipoic acid and a guanidinium cation, the original siCPD 1 simply from lipoic acid and L-arginine. Classical structural modifications (hydrophobicity, aromaticity, branching, boronic acids) do not improve performance. This unresponsiveness suggests that the best siCPDs act differently. Insensitivity toward inhibitors demonstrates that endocytosis is almost irrelevant. Significant dependence on the presence of exofacial thiols suggests that the counterion-mediated translocation known from CPPs⁴ is coupled with thiol-mediated translocation. Namely, siCPDs bind covalently to the membrane surface by disulfide exchange with exofacial thiols,

cross the membrane like CPPs along transient micellar defects, and detach into the cytosol by disulfide exchange with intracellular glutathione (Figure 4E). This fascinating, conceptually innovative thiol/counterion-mediated uptake mechanism drives the concept of covalent delivery of unmodified substrates to the extreme: The self-inactivating transporters not only grow covalently on the molecular substrate in solution, they also bind covalently to the membrane they are crossing. The inability of both initiators I1 and I2 to enter HeLa cells demonstrates that, contrary to predictions, simple thiolation is insufficient to turn on thiol-mediated uptake. Permanent capture at the surface and in endosomes found with boronic acids in copolymers 1/11 confirmed that thiol-mediated translocation requires more than dynamic covalent bonds at the cell surface. For covalent translocation, the simplest siCPDs are then best because they offer disulfide bonds and guanidinium cations at the highest effective concentration for thiol/counterion-mediated translocation.

Once the siCPD has arrived in the cytosol, disulfideexchange kinetics seem to determine its final destination. Whereas the instantaneous depolymerization of transporter 4 liberates the unmodified substrates in the cytosol, a lifetime of less than 5 min is sufficient for transporter 1 to proceed into the nucleus. Rapid self-inactivation right after uptake also explains nicely why transporter 4 is completely nontoxic. Most importantly, it appears that thiol/counterion-mediated translocation is also controlled by disulfide-exchange kinetics. However, the origin of the different depolymerization kinetics is unknown. Differences in polymer length are insufficient to account for their extent. Possibly, the guanidinium cations in 4 are in the best position to activate the thiolate leaving groups by intramolecular ion pairing, but this is just a hypothesis. Apparently essential to fully understand and exploit the unique advantages of siCPDs, the origin, the variability, and the functional consequences of disulfide-exchange kinetics of siCPDs are currently explored in the greatest detail, with particular emphasis on thiol/counterion-mediated transloca-

ASSOCIATED CONTENT

Supporting Information

Experimental details and NMR spectra. This material is available free of charge via the Internet at http://pubs.acs.org.

AUTHOR INFORMATION

Corresponding Author

stefan.matile@unige.ch

Present Address

§E.-K.B.: Korea Institute of Science and Technology (KIST), Seoul 136-791, South Korea.

Notes

The authors declare no competing financial interest.

ACKNOWLEDGMENTS

We thank the NMR, Sciences Mass Spectrometry (SMS), and Bioimaging (BiP) platforms for their services and the University of Geneva, European Research Council (ERC Advanced Investigator), National Centre of Competence in Research (NCCR) Chemical Biology, and Swiss National Science Foundation for financial support.

REFERENCES

Torres, A. G.; Gait, M. J. Trends Biotechnol. 2012, 30, 185–190.
 (a) Green, M.; Lowenstein, P. M. Cell 1988, 55, 1179–1188.
 (b) Frankel, A. O.; Pabo, C. O. Cell 1988, 55, 1189–1193.

(3) (a) Stanzl, E. G.; Trantow, B. M.; Vargas, J. R.; Wender, P. A. Acc. Chem. Res. 2013, 135, 2944-2954. (b) Sgolastra, F.; Deronde, B. M.; Sarapas, J. M.; Som, A.; Tew, G. N. Acc. Chem. Res. 2013, 135, 2977-2987. (c) Futaki, S.; Hirose, H.; Nakase, I. Curr. Pharm. Des. 2013, 19, 2863-2868. (d) Bautista, A. D.; Craig, C. J.; Harker, E. A.; Shepartz, A. Curr. Opin. Chem. Biol. 2007, 11, 685-692. (e) Bechara, C.; Sagan, S. FEBS Lett. 2013, 587, 1693-1702. (f) Torchilin, V. P. Adv. Drug Delivery Rev. 2008, 60, 548-558. (g) Stewart, K. M.; Horton, K. L.; Kelley, S. O. Org. Biomol. Chem. 2008, 6, 2242-2255. (h) Sgolastra, F.; Minter, L. M.; Osborne, B. A.; Tew, G. N. Biomacromolecules 2014, 10, 812-820. (i) Weinstain, R.; Savariar, E. N.; Felsen, C. N.; Tsien, R. Y. J. Am. Chem. Soc. 2014, 136, 874-877. (j) Lei, E. K.; Pereira, M. P.; Kelley, S. O. Angew. Chem., Int. Ed. 2013, 52, 9660-9663. (k) Lnoue, M.; Tong, W.; Esko, J. D.; Tor, Y. ACS Chem. Biol. 2013, 8, 1383-1388. (1) Tang, H.; Yin, L.; Kim, K. H.; Cheng, J. Chem. Sci. 2013, 4, 3839-3844. (m) Ornelas-Megiatto, C.; Wich, P. R.; Fréchet, J. M. J. Am. Chem. Soc. 2012, 134, 1902-1905. (n) Suzuki, Y.; Okuro, K.; Takeuchi, T.; Aida, T. J. Am. Chem. Soc. 2012, 134, 15273-15276. (o) Som, A.; Reuter, A.; Tew, G. N. Angew. Chem., Int. Ed. 2012, 51, 980-983. (p) Appelbaum, J. S.; LaRochelle, J. R.; Smith, B. A.; Balkin, D. M.; Holub, J. M.; Schepartz, A. Chem. Biol. 2012, 19, 819-830. (q) He, J.; Hristova, K.; Wimley, W. C. Angew. Chem., Int. Ed. 2012, 51, 7150-7153. (r) Treat, N. J.; Smith, D.; Teng, C.; Flores, J. D.; Abel, B. A.; York, A. W.; Huang, F.; McCormick, C. L. ACS Macro Lett. 2012, 1, 100–104. (s) Kolonko, E. M.; Pontrello, J. K.; Mangold, S. L.; Kiessling, L. L. J. Am. Chem. Soc. 2009, 131, 7327-7333. (t) McNaughton, B. R.; Cronican, J. J.; Thompson, D. B.; Liu, D. R. Proc. Natl. Acad. Sci. U.S.A. 2009, 106, 6111-6116. (u) Trantow, B. M.; Cooley, C. B.; Nederberg, F.; Kiesewetter, M. K.; Hedrick, J. L.; Waymouth, R. M.; Wender, P. A. J. Am. Chem. Soc. 2009, 131, 16401-16403. (v) Herce, H. D.; Garcia, A. E.; Litt, J.; Kane, R. S.; Martin, P.; Enrique, N.; Rebolledo, A.; Milesi, V. Biophys. J. 2009, 97, 1917-1925. (w) Shimanouchi, T.; Walde, P.; Gardiner, J.; Mahajan, Y. R.; Seebach, D.; Thomae, A.; Kraemer, S. D.; Voser, M.; R. Kuboi, R. Biochim. Biophys. Acta, Biomembr. 2007, 1768, 2726-2736. (x) Fernandez-Carneado, J.; Van Gool, M.; Martos, V.; Castel, S.; Prados, P.; De Mendoza, J.; Giralt, E. J. Am. Chem. Soc. 2005, 127, 869-874. (y) Fillon, Y.; Anderson, J.; Chmielewski, J. J. Am. Chem. Soc. 2005, 127, 11798-11803. (z) Pantarotto, D.; Briand, J.-P.; Prato, M.; Bianco, A. Chem. Commun. 2004, 16-17. (aa) Jiang, T.; Olson, E. S.; Nguyen, Q. T.; Roy, M.; Jennings, P. A.; Tsien, R. Y. Proc. Natl. Acad. Sci. U.S.A. 2004, 101, 17867-17872. (bb) Zhou, P.; Wang, M.; Du, L.; Fisher, G. W.; Waggoner, A.; Ly, D. H. J. Am. Chem. Soc. 2003, 125, 6878-6879. (cc) Luedtke, N. W.; Carmichael, P.; Tor, Y. J. Am. Chem. Soc. 2003, 125, 12374-12375. (dd) Umezawa, N.; Gelman, M. A.; Haigis, M. C.; Raines, R. T.; Gellman, S. H. J. Am. Chem. Soc. 2002, 124, 368-369. (ee) Sakai, N.; Baumeister, B.; Matile, S. ChemBioChem 2000, 1, 123-125. (ff) Schwarze, S. R.; Ho, A.; Vocero-Akbani, A.; Dowdy, S. F. Science 1999, 285, 1569-1572.

(4) (a) Sakai, N.; Matile, S. J. Am. Chem. Soc. 2003, 125, 14348—14356. (b) Takeuchi, T.; Kosuge, M.; Tadokoro, A.; Sugiura, Y.; Nishi, M.; Kawata, M.; Sakai, N.; Matile, S.; Futaki, S. ACS Chem. Biol. 2006, I, 299—303. (c) Schmidt, D.; Jiang, Q. X.; MacKinnon, R. Nature 2006, 444, 775—779. (d) Inomata, K.; Ohno, A.; Tochio, H.; Isogai, S.; Tenno, T.; Nakase, I.; Takeuchi, T.; Futaki, S.; Ito, Y.; Hiroaki, H.; Shirakawa, M. Nature 2009, 458, 106—109. (e) Katayama, S.; Nakase, I.; Yano, Y.; Murayama, T.; Nakata, Y.; Matsuzaki, K.; Futaki, S. Biochim. Biophys. Acta, Biomembr. 2013, 1828, 2134—2142.

(5) (a) Lin, C.; Engbersen, J. F. J. Expert Opin. Drug Delivery 2009, 6, 421–439. (b) Meng, F. H.; Hennink, W. E.; Zhong, Z. Y. Biomaterials 2009, 30, 2180–2198. (c) Kim, T.-I.; Kim, S. W. React. Funct. Polym. 2011, 71, 344–349. (d) Bang, E.-K.; Lista, M.; Sforazzini, G.; Sakai, N.; Matile, S. Chem. Sci. 2012, 3, 1752–1763. (e) Son, S.; Namgung, R.; Kim, J.; Singha, K.; Kim, W. J. Acc. Chem. Res. 2012, 45, 1100–1112. (f) Piest, M.; Engbersen, J. F. J. J. Controlled Release 2011, 155,

331–340. (g) Kim, T.; Rothmund, T.; Kissel, T.; Kim, S. W. J. Controlled Release 2011, 152, 110–119. (h) Wua, C.; Li, J.; Zhua, Y.; Chena, J.; Oupický, D. Biomaterials 2013, 34, 8843–8850. (i) Zeng, H.; Little, H. C.; Tiambeng, T. N.; Williams, G. A.; Guan, Z. J. Am. Chem. Soc. 2013, 135, 4962–4965. (j) Drake, C. A.; Aissaoui, A.; Argyros, O.; Thanou, M.; Steinke, J. H. G.; Miller, A. D. J. Controlled Release 2013, 171, 81–90.

(6) (a) Kang, H. C.; Kang, H.-J.; Bae, Y. H. Biomaterials 2011, 32, 1193–1203. (b) Li, J.; Manickam, D. S.; Chen, J.; Oupicky, D. Eur. J. Pharm. Sci. 2012, 46, 173–180. (c) Brülisauer, L.; Kathriner, N.; Prenrecaj, M.; Gauthier, M. A.; Leroux, J.-C. Angew. Chem., Int. Ed. 2012, 51, 12454–12458.

(7) (a) Sakai, N.; Lista, M.; Kel, O.; Sakurai, S.; Emery, D.; Mareda, J.; Vauthey, E.; Matile, S. J. Am. Chem. Soc. 2011, 133, 15224–15227. (b) Lista, M.; Areephong, J.; Sakai, N.; Matile, S. J. Am. Chem. Soc. 2011, 133, 15228–15231. (c) Sakai, N.; Matile, S. J. Am. Chem. Soc. 2011, 133, 18542–18545. (d) Orentas, E.; Lista, M.; Lin, N.-T.; Sakai, N.; Matile, S. Nat. Chem. 2012, 4, 746–750. (e) Sforazzini, G.; Orentas, E.; Bolag, A.; Sakai, N.; Matile, S. J. Am. Chem. Soc. 2013, 135, 12082–12090.

(8) Bang, E.-K.; Gasparini, G.; Molinard, G.; Roux, A.; Sakai, N.; Matile, S. J. Am. Chem. Soc. 2013, 135, 2088–2091.

(9) (a) Li, J.; Nowak, P.; Otto, S. J. Am. Chem. Soc. 2013, 135, 9222–9239.
 (b) Lehn, J. M. Top. Curr. Chem. 2012, 322, 1–32.
 (c) Black, S. P.; Sanders, J. K. M.; Stefankiewicz, A. R. Chem. Soc. Rev. 2014, 43, 1861–1872.
 (d) Wilson, A.; Gasparini, G.; Matile, S. Chem. Soc. Rev. 2014, 43, 1948–1962.

(10) See the Supporting Information.

- (11) Bang, E.-K.; Ward, S.; Gasparini, G.; Sakai, N.; Matile, S. *Polym. Chem.* **2014**, *5*, 2433–2441.
- (12) van Meer, G.; Voelker, D. R.; Feigenson, G. W. Nat. Rev. Mol. Cell Biol. 2008, 9, 112–124.
- (13) Sakai, N.; Takeuchi, T.; Futaki, S.; Matile, S. ChemBioChem 2005, 6, 114-122.
- (14) Khalil, I. A.; Kogure, K.; Akita, H.; Harashima, H. *Pharmacol. Rev.* **2006**, *58*, 32–45.
- (15) Nishihara, M.; Perret, F.; Takeuchi, T.; Futaki, S.; Lazar, A. N.; Coleman, A. W.; Sakai, N.; Matile, S. Org. Biomol. Chem. 2005, 3, 1659–1669.
- (16) Hennig, A.; Gabriel, G. J.; Tew, G. N.; Matile, S. J. Am. Chem. Soc. 2008, 130, 10338–10344.
- (17) Ellis, G. A.; Palte, M. J.; Raines, R. T. J. Am. Chem. Soc. 2012, 134, 3631–3634.
- (18) Mosmann, T. J. Immunol. Methods 1983, 65, 55-63.